ABSTRACT

BOBOLEA, RUXANDRA. A Study of Continuous Electrochemical Processing Operation Feasibility for Spent Nuclear Fuel. (Under the direction of Dr. Man-Sung Yim.)

Several methods of reprocessing are currently available to separate recyclable materials from spent nuclear fuel. Electrochemical processing, also known as pyroprocessing, represents a non-aqueous method of reprocessing that uses high temperature molten-salt based electrochemical technology. This method provides several advantages over conventional aqueous processing with respect to proliferation resistance. With electrochemical processing there is no pure plutonium separation and the presence of large decay heat and high radiation barriers dissuades diversion attempts. As the current electrochemical processing relies on a batch operation, the total throughput of the system is inherently limited and nuclear materials accounting is difficult due to the nonhomogeneous nature of the process. This results in much larger uncertainties in the total amount of material processed compared to the aqueous UREX+ or PUREX processes. Continuous electrochemical processing was considered as a way to address these concerns. The objective of this research was to investigate the feasibility of a continuous electrochemical processing operation to achieve the desired separation performance by using computer based simulation. The conceptual design of the continuous electrochemical processing includes two separate stages in a molten salt medium. First, a pure uranium deposit is collected at a solid cathode during the uranium extraction stage. When the amount of plutonium in electrorefiner becomes comparable or higher than the amount of uranium in the electrorefiner, a liquid

cathode is employed to extract both uranium and plutonium in the second stage. In this approach, molten salt, as the material carrier, flows through the electrorefiner while chopped spent fuel is continuously fed into the system. Simulations of electrochemical reactions at the electrode surfaces were based on the kinetic modeling capability of a time-dependent code, REFIN. Based on a screening study performed for the most significant process parameters over a broad range of values, a functional combination of initial uranium and plutonium concentrations at the anode and in the molten salt was determined for continuous operation. This dictated the use of a higher concentration of uranium than plutonium at the anode and a lower concentration of uranium than plutonium in the molten salt. Furthermore, using design of experiment technique for computers, a refinement of initial concentrations was performed to maximize the total throughput and minimize the operational time. The flow velocity profiles and chemical concentration distributions of elements in molten salt have been determined through three dimensional Computational Fluid Dynamics simulations using ANSYS CFX. This approach resulted in the need to evaluate the diffusion layer thickness at the cathode – molten salt interface, an important parameter for the electrochemical process. Computer based simulations of the continuous electrochemical processing concept presented in this study have provided an indication that electrochemical processing could be a viable technology for closing the nuclear fuel cycle.

A Study of Continuous Electrochemical Processing Operation Feasibility for Spent Nuclear Fuel

by
Ruxandra Bobolea

A thesis submitted to the Graduate Faculty of
North Carolina State University
in partial fulfillment of the
requirements for the Degree of
Master of Science

Nuclear Engineering

Raleigh, North Carolina

2009

APPROVED BY:

_____	_____
Dr. David N. McNelis	Dr. Jeff Thompson

_____
Dr. Man-Sung Yim
Chair of Advisory Committee

DEDICATION

For my husband Alin and my grandparents.

BIOGRAPHY

Ruxandra Bobolea was born in 1979 in Bucharest, Romania. Science, logic and their experimental verification have always fascinated her, and, after years, this fascination inspired her to choose engineering as her career option. She graduated with a degree in Economic Engineering in Power Engineering at Power Engineering College, POLITEHNICA University of Bucharest first ranked undergraduate of Power Engineering College 2002 class. One year later she earned her Master Degree in Nuclear Safety and Radiation Protection at Nuclear Engineering Department, POLITEHNICA University of Bucharest. Willing to gain experience in nuclear industry, she worked for five years as a Project Coordinator Engineer within the Project Coordination Department at Cernavoda Nuclear Power Plant Unit 1, Romania. The continued quest for professional development through education provided the motivation to join the Nuclear Engineering Department at North Carolina State University in August 2007. As recognition of her academic performance, she received the invitation to join United States oldest, largest and most selective all-disciplines honor society, Phi Kappa Phi, in Fall 2008. She worked with Dr. Man-Sung Yim on investigation of the continuous electrochemical processing of spent nuclear fuel. She will join Reloads Thermal Hydraulic Analysis, PWR Core Engineering Group at AREVA NP in Lynchburg, after her graduation in May 2009.

ACKNOWLEDGMENTS

I would like to thank my adviser Dr. Man-Sung Yim for his constant support and valuable advice throughout the course of my research work. His guidance and encouragement served as a continuous source of inspiration. I would also like to express my gratitude to Dr. David N. McNelis and Dr. Jeff Thompson for their kind support and useful feedback towards the completion of this thesis.

I would like to express special thanks to my family, especially my parents, for their continuous encouragement. Nevertheless, this endeavor would have very little value without my husband Alin being there to share and experience all the joys and sadness along the way, especially because he was a Nuclear Engineering graduate student at the same time.

TABLE OF CONTENTS

LIST OF TABLES

LIST OF FIGURES

LIST OF SYMBOLS

a_i	activity of species i
A	interfacial area density, (m^{-1})
C_i	concentration of species i, (mol/cm^3)
$C_{\varepsilon 1}$	k-ε turbulence model constant, (1.44)
$C_{\varepsilon 2}$	k-ε turbulence model constant, (1.92)
C_{μ}	k-ε turbulence model constant, (0.09)
d	distance or length, (m)
D_i	diffusion coefficient of species i, (cm^2/s)
E	standard electrochemical potential defined by Gibbs free energy, (V)
E°	standard electrode potential, (V)
F	Faraday's constant, (96,487 Coulomb/mol)
ΔG	"standard" Gibbs energy change for a reaction, (kcal/mol)
ΔG_f°	free formation energy of selected compound, (kcal/mol)
h_{tot}	specific total enthalpy, (J/kg)
I	electric current intensity, (A)
J_i	net flux density for species i, ($mol/cm^2 \cdot s$)
$J_{i,convection}$	flux density due to convection of species i, ($mol/cm^2 \cdot s$)
$J_{i,diffusion}$	flux density due to diffusion of species i, ($mol/cm^2 \cdot s$)

$J_{i,migration}$	flux density due to migration of species i, (mol/cm^2·s)
k	turbulent kinetic energy per unit mass, (m^2/s^2)
K_{eq}	equilibrium constant
m	mass of material transported, (kg)
M	molar mass, (mol/kg)
M^D	momentum due to interphase drag force
M^L	momentum due to lift force
M^{LUB}	momentum due to wall lubrication force
M_S	momentum due to solids pressure force
M^{TD}	momentum due to turbulence dispersion force
M^{VM}	momentum due to virtual mass force
n	number of electrons transferred through the external circuit
N	number of components in mixture
p, p_{stat}	static (thermodynamic) pressure, (Pa)
p`	modified pressure, (Pa)
p_{tot}	total pressure, (Pa)
P_k	shear production of turbulence, (kg/m·s^3)
Pr	Prandtl number
Q	amount of electric charge, (Coulomb)
r	volume fraction

R	universal gas constant, (8.3143 J/mol·K)
Re	Reynolds number
R_v	radial vector from the domain axis of rotation to the wall, (m)
S_E	energy source, ($kg/m \cdot s^3$)
S_M	momentum source, ($kg/m^2 \cdot s^2$)
S_{MS}	mass source, ($kg/m^3 \cdot s$)
t	time, (s)
T	static (thermodynamic) temperature, (K)
u_i	mobility of species i, ($cm^2 \cdot mol/J \cdot s$)
U	vector of velocity $U_{x,y,z}$, (m/s)
v	bulk fluid velocity, (cm/s)
v_i	velocity of ions in electrolyte, (cm/s)
V	volume, (m^3)
X_i	mole fraction of species i
z_i	charge number of species i
α	subscript to indicated that the quantity applies to component α
β	subscript to indicated that the quantity applies to component β
ε	turbulence dissipation rate, (m^2/s^3)
Φ	electric potential, (V)
γ_i	activity coefficient of species i

Γ	diffusivity, (m^2/s)
λ	thermal conductivity, (W/m·K)
μ	molecular (dynamic) viscosity, (Pa·s)
μ_{eff}	effective viscosity, (Pa·s)
μ_t	turbulent viscosity, (Pa·s)
ρ	density, (kg/m^3)
σ_k	k-ε turbulence model constant, (1.0)
σ_ε	k-ε turbulence model constant, (1.3)
τ	shear stress, (Pa)
ω	angular velocity, (s^{-1})

LIST OF ABREVIATIONS

ANL	Argonne National Laboratory
CFD	Computational Fluid Dynamics
COEX	Combined Extraction Process
DOE	Department of Energy
ERB-II	Experimental Breeder Reactor II
KAPL	Knolls Atomic Power Laboratory
IMSE	Integrated Mean Squared Error
INL	Idaho National Laboratory
LWR	Light Water Reactor
ORNL	Oak Ridge National Laboratory
PUREX	Plutonium and Uranium Extraction Process
TRUEX	Transuranic Extraction Process
UREX	Uranium Extraction Process

Chapter 1 Introduction

A unique feature of nuclear energy is the availability in spent nuclear fuel of recyclable fissile and fertile materials able to provide new fuel to generate power. When we recycle paper, glass, plastic or metal we separate useful materials from waste, mainly to reduce the consumption of fresh raw materials and also to diminish the air and water pollution. Spent nuclear fuel contains considerable amounts of useful materials. To illustrate this, the composition of used nuclear fuel is presented in the first section of this chapter. Furthermore, an overview of reprocessing is given to bring this thesis into context. A comparison of reprocessing methods, underlining the advantages and disadvantages of current electrochemical processing technology, is provided for a better understanding of the motivation of using and improving this technology.

1.1 Nuclear Energy and Spent Nuclear Fuel

One of the most critical topics in today's society is energy. Major concerns include resource depletion, impact on air and water pollution, security and cost. Energy generation affects all aspects of life, from every day tasks to industrial productivity and feeding the population. During the last fifty years nuclear energy production has been expanded worldwide.

Conventional nuclear power is based on the nuclear fission reaction to generate energy. When the fissile uranium-235 isotope absorbs a neutron, the intermediate nuclide uranium-236 becomes immediately unstable and fissions. The products of this reaction typically include two fission products, 200 MeV of energy and an average of 2.5 neutrons. More uranium is bombarded by some of these neutrons to produce energy whereas others are used to create fissionable plutonium-239 from uranium-238.

Table 1.1 illustrates the composition of the LWR spent nuclear fuel.

Table 1.1 – Composition of LWR spent nuclear fuel [1]

Element or group of elements	**Percent, by weight**
Actinides	
Uranium	95.6
Plutonium	0.9
Minor Actinides	0.1
Fission products	
Stable / Short Lived	3.0
Cesium / Strontium	0.3
Iodine / Technetium	0.1

As it can be seen, the bulk of spent nuclear fuel is reusable material. This represents the motivation for reprocessing used nuclear fuel.

By separating uranium and plutonium from waste, the volume of material to be disposed of as high-level waste is reduced and also allows uranium and plutonium to be used as reactor fuel. The spent nuclear fuel is highly toxic because it contains very large inventory of radioactive isotopes with high radiation energy whose half-lives can be extremely long. Also, due to its high fissile plutonium content, the proliferation issue becomes important specifically if any further partitioning is involved.

1.2 Overview of Reprocessing

Reprocessing of spent nuclear fuel refers to the separation process of useful material from waste. Separation is usually achieved by utilizing the differences in chemical and physical properties of the substances through the mean of a separating agent. The main goals for conducting spent fuel separation are to recover useful materials, uranium, plutonium, and thorium, if present, and to reuse them as fuel, to remove radioactive fission products from them and to obtain a suitable form for safe and long-term storage. Reprocessing technologies can be grouped into two main categories: technologies based on aqueous chemistry and those based on molten salts and molten metals.

1.2.1 History of Reprocessing

Initially, Oak Ridge National Laboratory (ORNL) developed a bismuth phosphate method of reprocessing spent fuel which was used at Hanford, Washington site beginning in 1944. The process, operating in batches, required several stages including dissolution of cladding material. Uranium and most of the fission products were discarded as heavy metal waste whereas plutonium was further purified. Large amounts of waste and chemicals were generated and no uranium was separated.

Argonne National Laboratory (ANL) developed a new reprocessing method based on aluminum nitrate in aqueous phase using hexone as solvent for extraction. The process was continuous but required large amounts of aluminum nitrate.

This method was replaced by plutonium and uranium extraction process (PUREX) developed by Knolls Atomic Power Laboratory (KAPL) and tested at ORNL in 1950-52 and used worldwide today. PUREX is a solvent-extraction technique used to extract uranium and plutonium, independent of each other, from fission products. The method uses nitric acid and tri-butyl phosphate dissolved in an organic liquid [2]. Adaptations to PUREX have been applied to become more suitable for treatment of waste and civilian use. Uranium extraction process (UREX) can be used to remove uranium, which represents most of the volume and mass of spent nuclear fuel. The PUREX process has been modified to prevent plutonium extraction by adding acetohydroxamic acid to the extraction and scrub sections, and thus developing UREX process.

ANL developed another related process for recovering transuranic metals from waste, called TRUEX. This process added another extraction agent to tri-butyl phosphate to remove transuranic elements from spent fuel and thus to lower alpha activity of the waste. A melt refining process has been developed in the 1960s to process EBR-II metal fuel in which the volatile fission products were removed [3]. This process offered partial separation of actinides and no separate plutonium was recovered. This represents the initial work carried out in electrochemical processing, also known as pyroprocessing.

1.2.2 Reprocessing Today

Generally, there are two main categories of reprocessing technologies of spent nuclear fuel. They are either based on aqueous or non-aqueous processes, as presented in Table 1.2.

Among all these processes, PUREX is the most completely developed and widely used at present. It is based on the selective affinity of tri-butyl phosphate for uranium and plutonium. Combined extraction (COEX) of uranium and plutonium was proposed as a simplification of the PUREX technology. This process, developed in France, leaves plutonium with uranium to fabricate mixed oxide fuel. Other variations of PUREX are developed. These recover initially only uranium and then the residual is treated to recover plutonium with other transuranics (hence UREX+ processes).

Table 1.2 – Main reprocessing technologies of spent nuclear fuel

Aqueous processes	**Non-aqueous processes**
PUREX	Electrochemical Processing (also known as Pyroprocessing)
COEX	Fluoride Volatility
UREX	-
UREX+	-
TRUEX	-
Supercritical CO_2	-

The main difference between variations of UREX+ consists of how plutonium is mixed with various actinides. UREX technology only separates pure uranium and technetium and nothing else. Also, experiments using supercritical CO_2 technology are ongoing and it is considered a promising alternative for liquid-liquid extraction systems [4].

The non-aqueous processes include electrochemical processing and fluoride volatility. Electrochemical processing technologies employ molten salt and molten metal electrorefining process. Fluoride volatility, which uses the volatility of the uranium hexafluoride, neptunium hexafluoride, and plutonium hexafluoride to separate them from other materials as well as each other, represents a physical separation process.

Electrochemical processing techniques to separate actinide elements from waste have been under development in U. S., notably at ANL, as well as in Russia (at Research Institute of Atomic Reactors), Japan (at Central Research Institute of Electric Power Industry), India (at Indira Gandhi Center for Atomic Research), and Republic of Korea (at the Korea Atomic Energy Research Institute). Production of a separate plutonium stream is very difficult for this process, since plutonium is collected together with uranium and other elements.

Studies on the molten salt electrorefining process for metallic fuels and oxide electrowinning process for oxide fuels have been carried out also in India. There, electrochemical processing studies on uranium alloys have been performed in a laboratory-scale argon atmosphere facility for molten salt processes [5].

In Japan, basic electrochemical processing research became very important, especially studies which involved electrochemical and thermodynamic approach. Electrochemical and related experiments for uranium, plutonium, and other minor actinides were performed in a large-sized inert glove box built for molten salt processes. Also, a special attention was given to electrochemical processing of nitride fuels in Japan, due to their good reactor performance for the future fast breeder reactor [6].

Investigation of continuous operation of electrochemical process has started to become more important during the last few years. One of the recent U.S. patents presents a continuous electrorefining process [7]. This approach is focused on uranium separation from spent nuclear fuel and other actinides from used fuel are not considered for separation.

1.3 Reprocessing Technology Comparison

Several attributes applicable to reprocessing technologies can be compared. A brief comparison of the most important features of spent fuel reprocessing methods is provided in the following paragraphs.

Proliferation risk plays a major role in selecting the reprocessing technology. The risk is mainly given by the possibility of separating pure plutonium from spent nuclear fuel. From this point of view, electrochemical processing has an advantage over PUREX technology because it recovers plutonium together with uranium and other transuranic elements (neptunium, americium, and curium). Also, UREX does not separate plutonium.

Waste toxicity is also important in evaluating a spent fuel reprocessing method. A concern about PUREX is that neptunium, americium, and curium are kept in waste. These elements are very toxic and affect the design of geologic repositories. UREX can be an alternative to PUREX since plutonium is not separated and other elements are kept with plutonium. Electrochemical processing recovers all the actinides and therefore the remaining waste is not as long lived as it would otherwise be. Most of these actinides can be consumed by reactors as fuel and thus the long term threat from waste is reduced.

Another advantage of electrochemical processing over aqueous methods is that the desired outcome is achieved in fewer steps and the technology is considerably more compact, allowing on-site reprocessing of reactor waste. This minimizes the burden during spent fuel transportation and due to security concerns.

Also, electrochemical processing can be applied to high burn-up fuel and fuel with little cooling time, as the operation temperature is high. Electrochemical processing does not use water, which is easily contaminated and also tends to serve as a moderator, but uses molten salt and molten metals which are known for their fast kinetics and radiation resistance.

Advanced aqueous methods are best suited to treat spent fuel that is stored and generated today. The PUREX process only dissolves some types of fuel (oxide fuel) but it does not dissolve metal fuels. At the same time, electrochemical processing can be adapted to treat both metal and oxide fuels.

Unlike the PUREX and UREX+ processes, current electrochemical processing technology relies on batch operation and, therefore, the total throughput of the system is limited and the uncertainties in total amount of material processed are significant. This is due to fact that some material remains in the molten salt for several batches until the salt is processed. The estimated uncertainties, per element, for electrochemical processing are presented in Table 1.3.

Table 1.3 – Estimated uncertainties in electrochemical processing material balance [8]

Element	Error [%]
Np	27 %
Pu	6 %
Am	39 %
Cm	12 %
U	13 %

1.4 Electrochemical Processing Modeling Overview

Several models have been developed in order to predict and to keep track of the material balance in electrochemical processing. Simulation represents a useful tool to investigate the performance of the electrochemical process. Also, the capability to calculate the process outcome using modeling saves time and energy.

Models use thermodynamic equilibrium based on the high temperature process operation and fast kinetics. In 1989 Ackerman developed at ANL, based on the theoretical model of Johnson, the code called PYRO to calculate mass flow and compositions in electrochemical processing. The code, written in PASCAL, was based on thermodynamic equilibrium considerations. Furthermore, the code was extended to include mass tracking of isotopes and their radioactive decay [9].

Nawada and Bhat developed in 1995 a thermochemical model for application to a multicomponent system in the electrorefiner [10]. They used a similar principle to PYRO.

Next, in 1996, Ahluwalia and Geyer developed at ANL a computer code, named GC, for flow sheet simulation of electrochemical processing of spent nuclear fuel [9]. The code utilizes an algorithm for analyzing simultaneous chemical reactions between species distributed across many phases. They applied the computer code GC to electrochemical processing flow sheet of LWR oxide fuel.

Researchers at CRIEPI, Japan have developed TRAIL code based on a diffusion model [9]. This code uses diffusion layer theory in the vicinity of the electrodes.

Diffusion layer thickness was determined based on polarization data measured with uranium. They assumed fast kinetics at interface between electrode and electrolyte based on the high temperature of the process. The code assumes a linear concentration profile within the diffusion layer and uniform concentrations in electrolyte and cadmium.

Models presented above are based on thermodynamic equilibrium or simple diffusion kinetics. These models work well at low current densities but their accuracy degrades at high current densities, when kinetic factors become important.

A FORTRAN-based electrorefining model, called REFIN, has been developed based on a new mathematical model formulated to treat the time-dependent behavior of multi-component electrochemical systems [9]. The model is able to predict the current density for each species participating in the electrochemical reactions. The code solves the electrochemical reactions within the diffusion layer. REFIN has a unique advantage over other models due to its capability in considering electromigration in transient phenomena simulation [9].

REFIN code can simulate different types of electrodes, such as liquid anode and liquid / solid cathode. The type of electrode employed in the simulation is defined in the input file, by specifying the diffusion layer thickness. Seven elements of interest are defined in this code. These are: uranium, plutonium, neodymium, cadmium, lithium, potassium, and chlorine.

REFIN code has been benchmarked against Tomczuk et al. experiment performed at ANL [11]. Tomczuk et al. performed several experiments to investigate the electrodeposition of uranium and plutonium to solid cathode as part of the electrochemical processing development. The electrorefiner used in the experiment consisted of a liquid cadmium anode, a molten LiCl-KCl electrolyte, and a rotating solid cathode. During the experiment five tests have been performed. In each test the electrorefiner was operated for a preset time at a selected constant current. The molten salt, liquid anode and solid cathode were analyzed before and after each test for uranium, plutonium, americium, and rare earths (Ce, Nd, and Y). The solid cathode was removed after each test. Also, during these tests, the ratio of plutonium inventory to uranium inventory in the electrorefiner and the $PuCl_3$/ UCl_3 ratio in the electrolyte have been increased by removing pure uranium on the solid cathode.

In the study presented herein, REFIN code was employed to solve mass transfer in the diffusion layer at molten salt – electrode interface.

1.5 Scope of Thesis

The main objective of this thesis was to investigate the feasibility of continuous electrochemical processing operation for spent nuclear fuel to achieve the desired separation performance by using computer based simulations. This study focused on computational simulation of the processes that take place in the electrorefiner, the key equipment of the electrochemical process.

Since the current electrochemical processing technology relies on batch operation, the total throughput of the system is inherently limited. Furthermore, nuclear materials accounting is also difficult because some of the material is held in the molten salt for several batches until the salt is recovered.

Simulation of the electrochemical reactions at the electrode surfaces was based on the kinetic modeling capability of a time-dependent one dimensional code, REFIN [9]. The code was benchmarked against experimental data [11]. REFIN code was used to determine the mass of uranium deposited at solid cathode and also the amount of uranium and plutonium collected at liquid cadmium cathode. In addition, the operation time for the electrochemical process was estimated using REFIN code, based on the operational and geometrical parameters of the electrorefiner. The flow velocity profiles and chemical concentration distribution of elements in the molten salt were determined through 3D CFD simulation using ANSYS CFX-11.0. By solving the mass and momentum transfer in the bulk solution with ANSYS CFX, diffusion layer thickness for the considered design and parameters was calculated.

Moreover, a design of experiment for computers was performed to investigate the separation efficiency of the electrochemical process for the proposed concept, using JMP-7.0 statistical software.

Electrochemical processing of spent nuclear fuel plays an important role in the development of the next generation nuclear reactors and also the technologies that will close the nuclear fuel cycle. Successful demonstration of the continuous electrochemical processing leads to development of a new process of reprocessing for spent nuclear fuel that does not allow pure plutonium separation, which is an important advantage over conventional aqueous processing. Additionally, this approach offers several improvements over current batch electrochemical processing operation including larger throughput and significant safeguards benefit with the reduction of the measurement uncertainties.

Chapter 1 of this thesis presents the motivation for reprocessing spent nuclear fuel and a brief reprocessing history and technology comparison. The uncertainties in material balance for electrochemical processing are given to underline the need for a continuous process development. In Chapter 2, the chemical and physical principles of electrochemical process and the theory behind the CFD simulation are reviewed. Chapter 3 describes the continuous electrochemical processing concept proposed in this study. In Chapter 4, the computational simulation for the continuous concept is presented. The results are shown and discussed in Chapter 5. The conclusions derived from findings and recommendations for future work are given in Chapter 6.

Chapter 2 Theory

In order to embark on our explorations of the continuous electrochemical processing operation concept, we need to understand first the principles that are behind the electrochemical separation. This chapter begins by presenting the technology and equipment involved in electrochemical processing of spent nuclear fuel. Next, it provides a description of the physics and chemistry of the electrochemical processing. Furthermore, a discussion on design of experiment for computers is given. This technique is used in this study to optimize the separation efficiency and operation time of the continuous electrochemical processing concept. Finally, a review of the mathematics of CFD is presented. CFD simulations are employed to determine the hydrodynamic conditions of the electrochemical process and to calculate the diffusion layer thickness.

2.1 Electrochemical Processing

2.1.1 Process Overview

Electrochemical processing of spent nuclear fuel refers to the set of operations required to recover actinide elements from spent fuel and to recycle them back into the reactor. Electrochemical processing consists of several high temperature processes.

Electrorefining is the most important among them because it separates actinide elements from the fission products present in the spent nuclear fuel. Other processes are mainly employed to manage the waste. The electrochemical processing flowchart is presented in Figure 2.1.

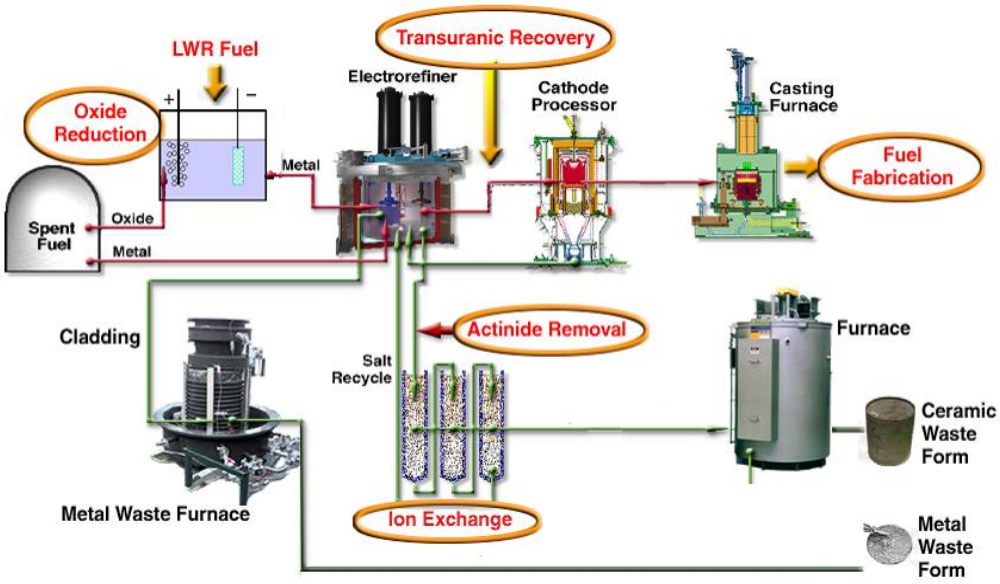

Figure 2.1 – Electrochemical processing flowchart [12]

One of the advantages of the electrochemical processing is the use of molten salts as electrolyte. Besides their fast kinetics, molten salts have a high radiation resistance. Liquid metals, which can be used as anodes or cathodes, have similar advantages. In the electrorefiner, the main equipment in the process, the chemical species are dissolved and

brought into contact. The processing operations begin with decladding and chopping the spent fuel. The chopping operation is performed by a chopper, where the fuel rods are cut into short lengths. The chopped fuel rod segments are placed in a perforated steel basket, which represents the anode during the electrorefining operation. For spent fuel from commercial reactors, which consists of uranium oxide, another step is performed prior to the electrorefiner, in order to convert the oxide fuel into metallic form. The oxide fuel loaded into the cathode basket is reduced to produce oxygen gas or CO_2 at the anode. This operation is known as electrolytic oxide reduction.

The electrorefining of spent nuclear fuel is virtually the same as the electrorefining process used in the minerals industry. During this process an impure metal, which represents the anode, is electrotransported through an electrolyte to the cathode where it is deposited in a condition of greater purity. Electrorefining in chloride salt is mainly used to extract uranium and plutonium. A molten salt medium of LiCl-KCl eutectic is employed and dissolved actinide chlorides, such as UCl_3 and $PuCl_3$, are added to the process. The electrorefiner operating temperature is typically 500 °C.

After the anode basket is loaded with chopped spent fuel, it is lowered into the molten salt and virtually pure uranium is collected at a solid mandrel cathode by means of an applied electric current. It has been observed experimentally that the morphology of the uranium-plutonium mixture deposited on solid cathode has changed from dendritic form that contained only uranium to amorphous form that contained uranium and plutonium.

The amorphous deposit is non-adherent on solid cathode [13]. As a result, liquid cadmium cathode was employed for collecting uranium-plutonium mixture. Other elements, such as americium, neptunium, curium and some rare-earth fission products are also collected at the liquid cadmium cathode. In electrochemical process, actinides are recovered as a group and no pure plutonium is collected at cathode. The fact that the plutonium product contains some highly radioactive material and it is diluted with uranium discourages weapons proliferation and undesirable diversion. This represents a major advantage of this technology.

The remaining fission products accumulate in the salt and in the cadmium pool situated at the bottom of the electrorefiner vessel. The role of the liquid cadmium pool is to collect the uranium dendrites that drop from the solid cathode during electrorefining. Also, it acts as an anode during the deposition mode and as an intermediate electrode during the direct transport mode [14].

The electrorefiner can be operated in three different modes, which can be visualized in Figure 2.2:

- Anodic Dissolution – in this mode the perforated steel basket, called fuel dissolution basket, serves as anode and the liquid cadmium pool from the bottom of the electrorefiner vessel represents the liquid cathode.
- Direct Transport – is the process that takes place when uranium is electrotransported from solid anode to solid cathode through the molten salt. It has been experimentally observed that cadmium pool at the bottom of the electrorefiner acts as an intermediate

electrode during the direct transport operation and only a portion of the applied current passes directly from the anode basket to cathode, through the electrolyte [14].

- Deposition – this is the process of deposition to solid cathode of uranium that has been dissolved in liquid cadmium pool and molten salt during anodic dissolution process.

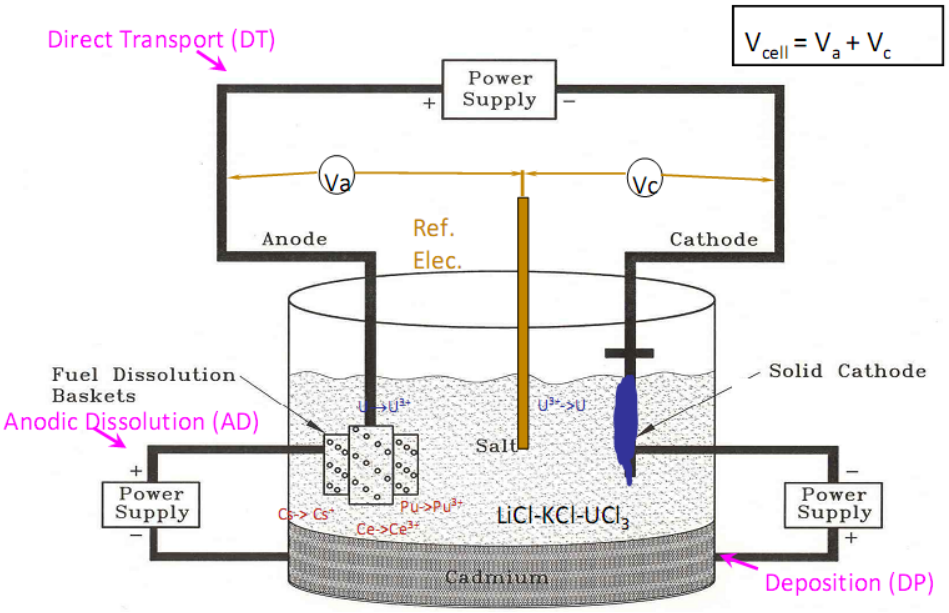

Figure 2.2 – Electrorefining process [12]

The cathode deposit, removed from the electrorefiner, is sent to the cathode processor. Cathode processor is a high-temperature vacuum furnace where cathode deposit is consolidated and any volatile materials are removed by vaporization. These volatile materials

could be salt, in case of a solid uranium deposit, or liquid cadmium, in case of a liquid cadmium cathode deposit. The cathode processor product is sufficiently free of impurities to be used as feed material for the next operational steps, casting furnace and fuel fabrication.

The electrochemical processing of spent nuclear fuel results in two high-level waste forms, the ceramic waste form and the metal waste form. The ceramic waste form has been developed to stabilize the active fission products and transuranic elements of the electrolyte. The ceramic waste form is produced by mixing and blending the waste salt with zeolite. The salt-loaded zeolite is mixed with borosilicate glass and consolidated at high temperature and pressure to make the final ceramic waste form. The metal waste form is used to stabilize noble metal fission products, non-active fuel matrix and cladding materials. The material is placed in the metal waste furnace and the resulting ingot represents the metal waste form.

2.1.2 Principle of Electrorefining

Electrorefining is the most important step in the electrochemical processing operation. This is the process where the actinides are separated and recovered from the fission products in the spent fuel. Electrochemical processing of spent fuel is based on the partition of the spent fuel elements according to the free energies of formation of selected chlorides at 500 °C. The chloride electrolyte system is used because it presents the advantage of an ideal grouping of elements based on the chloride stability.

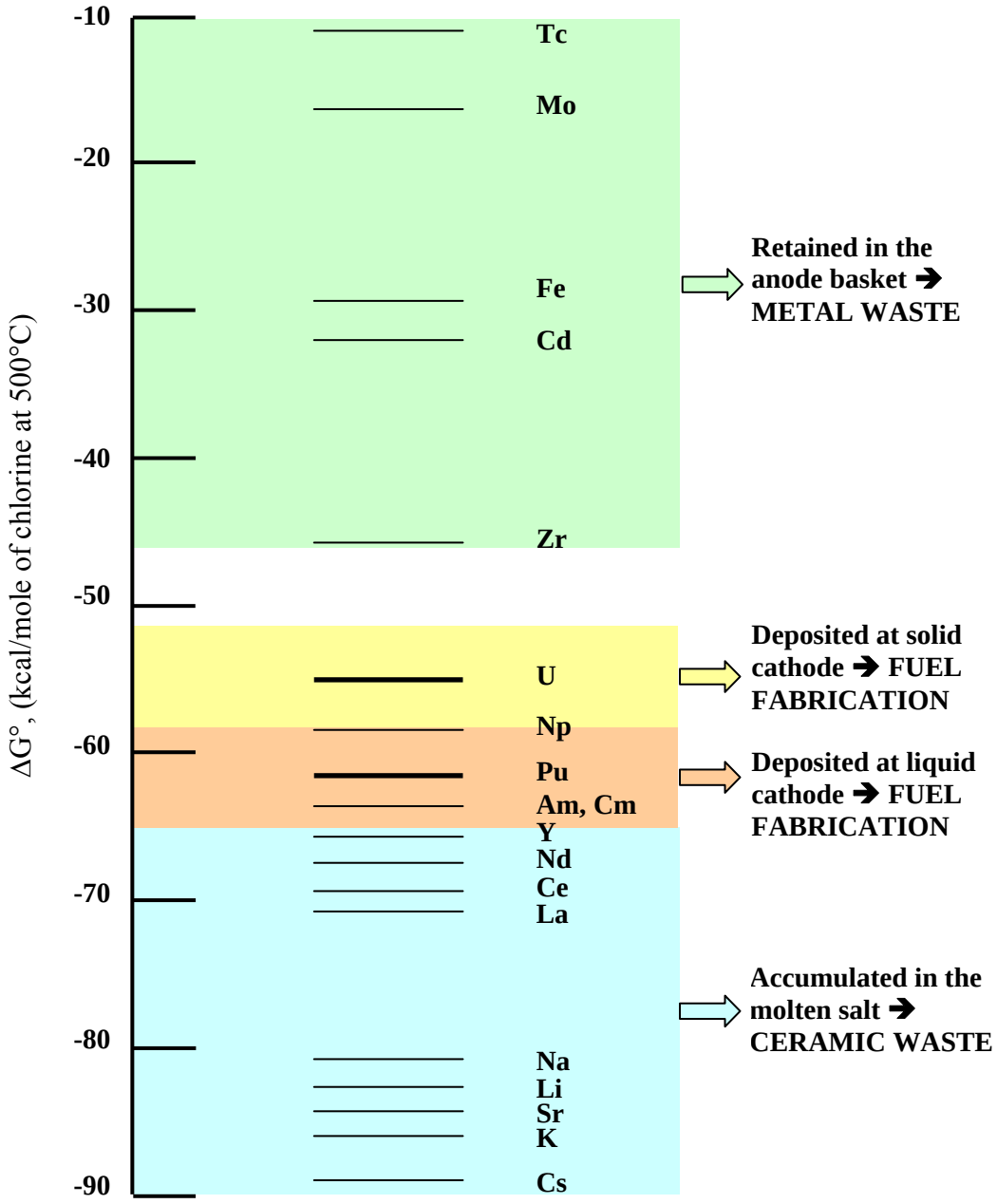

Figure 2.3 – Standard free energies of formation of fission product, actinide element and electrolyte chlorides at 500 °C

Three main thermodynamic classes are observed in Figure 2.3, based on the standard free energies of formation of fission product, actinide element, and electrolyte chlorides at 500 °C. Elements located at the top of Figure 2.3 have relatively unstable chlorides. These elements include cadmium, cladding hull constituents and the transition-metal fission products. As a consequence, during electrorefiner operation, these elements remain in the anode basket and at the end will be part of the metal waste form.

The elements positioned at the bottom of Figure 2.3 have highly stable chlorides. These elements are completely oxidized to chlorides and accumulate in the molten salt during the electrorefiner operation. They are periodically removed from the molten salt into the ceramic waste form by means of ion exchange.

The middle group consists of elements that are electrotransportable to solid or liquid cathode by means of an externally applied electric current. These elements are those of interest in the electrochemical processing of spent fuel. Table 2.1 presents an ordered list of the stabilities of the element chlorides involved in electrochemical processing at 500 °C.

At anode, electric current is used to oxidize metal into the salt phase and to simultaneously reduce the same amount of chloride from the salt phase to the cathode phase. By controlling electrotransport phenomenon, a pure uranium deposit can be collected at solid cathode and a mixed uranium-plutonium-rare-earth metal product can be obtained at liquid cadmium cathode. During the operation of the electrorefiner, the elements of this group are in equilibrium both as metals and as chlorides. The distribution of each of the possible element

pairs between salt and metal phases can be determined based on the equilibrium constants for the reactions between each pair of elements in this group.

Table 2.1 – Free energies of formation of selected chlorides at 500 °C [3, 15]

Element Chloride	**Free Energy [kcal/mole of chlorine]**
CsCl	-87.8
KCl	-86.7
$SrCl_2$	-84.7
LiCl	-82.5
NaCl	-81.2
$LaCl_3$	-70.2
$PrCl_3$	-69.0
$CeCl_3$	-68.6
$NdCl_3$	-67.9
YCl_3	-65.1
$PuCl_3$	-62.4
$NpCl_3$	-58.1
UCl_3	-55.2
$ZrCl_4$	-46.6
$CdCl_2$	-32.3
$FeCl_2$	-29.2
$NbCl_5$	-26.7
$MoCl_2$	-16.8

The exchange reaction between any two different metallic elements, M and N, in this class is given by:

$$\frac{x}{3}MCl_x + \frac{y}{3}N \leftrightarrow \frac{x}{3}M + \frac{y}{3}NCl_y \tag{2.1}$$

For the exchange reaction, the free energy change is given by the following formula:

$$\Delta G = \frac{y}{3}\Delta G_f^{\circ}(NCl_y) - \frac{x}{3}\Delta G_f^{\circ}(MCl_x) \tag{2.2}$$

where $\Delta G_f^{\circ}(\cdot)$ represents the free energy of formation of that compound.

The equilibrium constant for the exchange reaction is determined using the free energy change:

$$K_{eq} = \exp(-\Delta G / RT) \tag{2.3}$$

Also, the equilibrium constant can be written using the activity coefficients of the reactants and products of the exchange reaction, as follows:

$$K_{eq} = \frac{(a_{NCl_y})^{y/3}(a_M)^{x/3}}{(a_{MCl_x})^{x/3}(a_N)^{y/3}} \tag{2.4}$$

where a_i represents the activity of species i.

Expressing the activity of species i as the product between the activity coefficient γ_i and the mole fraction X_i, Equation (2.4) becomes:

$$K_{eq} = \left(\frac{\gamma_{NCl_y}}{\gamma_N}\right)^{y/3}\left(\frac{\gamma_M}{\gamma_{MCl_x}}\right)^{x/3}\left(\frac{X_{NCl_y}}{X_N}\right)^{y/3}\left(\frac{X_M}{X_{MCl_x}}\right)^{x/3} \tag{2.5}$$

The equilibrium condition given by Equation (2.5) is satisfied at each interface by the element distribution in the salt and metal phases. The amount of electric charge passed gives the amount of material in the anode and cathode metal phases.

The Nernst equation, which relates the potential generated by an electrochemical cell to the standard potential E^0 and the activities of the species involved in the cell reaction, is then given by:

$$E = E^{\circ} - \frac{RT}{nF} \ln \frac{(a_{NCl_y})^{y/3} (a_M)^{x/3}}{(a_{MCl_x})^{x/3} (a_N)^{y/3}} \tag{2.6}$$

where R is the universal gas constant, F is the Faraday's constant, T is the absolute temperature and n represents the number of electrons transferred through the external circuit for the reaction.

Table 2.2 shows the activity coefficients of actinides and rare earths at infinite dilution in liquid cadmium and molten salt.

Table 2.2 – Activity coefficient of actinides and rare earths at infinite dilution [9]

Element	**Coefficient in liquid Cd**	**Chloride**	**Coefficient in LiCl-KCl**
U	75	UCl_3	$5.79 \cdot 10^{-3}$
Np	$8.2 \cdot 10^{-3}$	$NpCl_3$	-
Pu	$1.38 \cdot 10^{-4}$	$PuCl_3$	$6.62 \cdot 10^{-3}$
Am	$\approx 2 \cdot 10^{-6}$	-	-
Cm	$\approx 3 \cdot 10^{-5}$	-	-
Ce	$9.76 \cdot 10^{-9}$	$CeCl_3$	$1.5 \cdot 10^{-3}$
La	$3.58 \cdot 10^{-9}$	$LaCl_3$	$4.7 \cdot 10^{-3}$
Pr	$1.8 \cdot 10^{-8}$	$PrCl_3$	$3.3 \cdot 10^{-3}$
Nd	$\approx 6 \cdot 10^{-9}$	$NdCl_3$	$1.8 \cdot 10^{-2}$
Y	-	YCl_3	$6.3 \cdot 10^{-6}$

2.1.3 Electrode Reactions

The electrode at which positive charge enters the solution and the reactant is said to be oxidized is termed the anode. Similarly, the cathode represents the electrode where the negative charge enters the electrolyte solution or the positive charge leaves the solution. In this case, the reactant is reduced. General anode and cathode reactions are:

$$M^0\,(\text{metal}) \rightarrow M^{z_i}\,(\text{molten salt}) + z_i\, e^- \text{ (Anode process)} \quad (2.7)$$

$$M^{z_i}\,(\text{molten salt}) + z_i\, e^- \rightarrow M^0\,(\text{metal}) \text{ (Cathode process)} \quad (2.8)$$

where z_i is the charge number of species i.

The reaction at the anode involves removal of z_i electrons per atom and, therefore, the M^{z_i} ions are formed in the salt phase. The removed electrons are conducted through an external circuit to the cathode, where the metal is formed. The amount of material being electrotransported from the anode to the cathode is proportional to the electric charge passed in the electric circuit. The electric charge is given by the product of the electric current and time, thus the mass of material transported is given by:

$$m = \frac{M \cdot Q}{n \cdot F} \tag{2.9}$$

where M is the molar mass of the element, Q represents the amount of charge passed and n is the number of electrons involved in the reaction.

Equation (2.9) is known as the Faraday's first law and is used to determine the amount of material deposited at the cathode. Expressing the electric charge as the product of the electric current and time, the mass of material electrodeposited at the electrode is given by:

$$m = \frac{M \cdot I \cdot t}{n \cdot F} = const \cdot I \cdot t \tag{2.10}$$

where I is the value of the applied electric current and t represents the operation time.

Equation (2.10) shows that the amount of material collected at the cathode is directly proportional to the molar mass of the element, the applied electric current, and time of operation.

2.1.4 Mass Transport Mechanisms

Similarly to the movement of electrons in a conductor in response to an electric field, ions move in an electrolyte in response to an electric field, and also concentration gradients and bulk fluid motion. The movement of ions due to the electric field is called migration. In this case, the electric field represents the driving force for the motion of the charged particles. The process of progression of ions from an area with high concentration to an area of lower concentration represents diffusion. The bulk movement of a fluid is convection. The sum of all these processes gives the net flux of ions.

The velocity of ions in the electrolyte as a consequence of the electric field represents the migration velocity, which can be expressed as:

$$v_i = -z_i u_i F \nabla \Phi \tag{2.11}$$

where u_i represents the mobility of species i and Φ is the potential in solution. Mobility is the proportionality factor that indicates how fast the ions move as a result of the electric current.

Using Equation (2.11), the flux density due to migration is given by:

$$J_{i,migration} = v_i C_i = -z_i u_i F C_i \nabla \Phi \tag{2.12}$$

where C_i represents the concentration of the species i.

The application of an electric current creates the movement of all ions in molten salt by migration. As a result, a change in concentration is observed across the molten salt. These concentration gradients drive mass transport by process of diffusion, in addition to electromigration.

The flux density due to diffusion is:

$$J_{i,diffusion} = -D_i \nabla C_i \tag{2.13}$$

where D_i is the diffusion coefficient of species i.

Convection refers to the movement of ions in the bulk solution. It can be caused by density gradients (natural convection) or by mechanical stirring (forced convection). Also, convection can be turbulent, when the motion is chaotic, or laminar, described by smooth, constant fluid motion. The Reynolds number characterizes whether the flow conditions lead to laminar (low Reynolds numbers) or turbulent flow (high Reynolds numbers).

The flux density by convection of a species i is expressed as:

$$J_{i,convection} = C_i v \tag{2.14}$$

where v represents the bulk fluid velocity.

Combining the Equations (2.12), (2.13), and (2.14) the net flux density is obtained:

$$J_i = -z_i u_i F C_i \nabla \Phi - D_i \nabla C_i + C_i v \tag{2.15}$$

Equation (2.15) shows that mass transport mechanisms in an electrochemical cell are migration, diffusion and convection [16].

The mobility of chemical species can be expressed using the Nernst – Einstein relation, as:

$$D_i = RTu_i \tag{2.16}$$

Inserting Equation (2.16) in Equation (2.15), the net flux density is given by:

$$J_i = -\frac{F}{RT} z_i D_i C_i \nabla \Phi - D_i \nabla C_i + C_i v \tag{2.17}$$

From Equation (2.17), the current in solution can be obtained from the flux density of charged species:

$$I = \sum_i z_i F J_i \qquad (2.18)$$

where J_i represents the flux density of species i.

2.1.5 Diffusion Layer

Although there is fluid motion in the bulk solution, there is a thin layer adjacent to the electrode where the molten salt is stationary. In the bulk solution, the governing mass transport mechanisms are convection and migration. Diffusion is almost negligible in the bulk solution because the concentration is approximately constant. The ions travel by convection and migration from the bulk up to the stationary layer and then cross the layer by diffusion. This thin layer adjacent to the electrode surface is called diffusion layer.

The diffusion layer represents the region in the vicinity of an electrode where the concentrations are different from the values in the bulk solution [17]. The exact value of the diffusion layer thickness is hard to obtain since it represents an approximate property. The diffusion layer thickness depends strongly on the effectiveness of the forced convection, being smaller when the convection is more intense [18]. The method of determining the diffusion layer thickness is presented below. Figure 2.4 shows the concentration profile near the electrode surface. The concentration profile would be constant, equal to C_0, if no electric current passes.

When the electric current is applied the electrode surface concentration decreases to C_e. The thickness of diffusion layer is given by the distance from the electrode surface to the intersection of the tangent to the true concentration profile at interface and the straight line extension of the concentration in the bulk solution [17, 19].

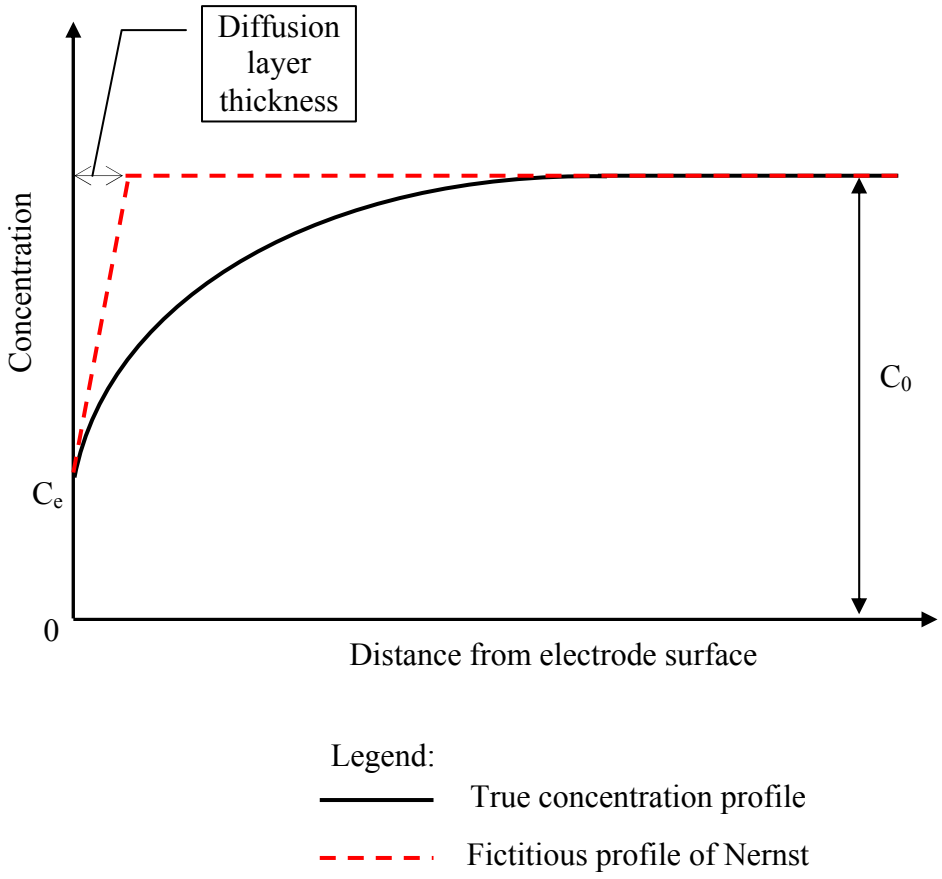

Figure 2.4 – Concentration profile and diffusion layer thickness

2.2 Design of Experiment for Computers

Nowadays, experiments are used widely to study and optimize processes and systems. Usually, the goals of experiments performed in modern industry and engineering are to improve the quality of products, to reduce the operation time and overall costs of the process. Experiments are categorized as physical or computer experiments. Typically, an experiment is performed in a laboratory. This type of experiment is called a physical experiment. During the past years, conducting an experiment with appropriate computer hardware and software became increasingly popular. In most of the cases a computer experiment is feasible when physical experiments are impossible to implement. Such examples may include experiments that are time consuming, have a number of factors that is too large to perform a physical experiment or are too expensive to run on the scale needed for answering a particular research question. Whereas physical experiments measure a stochastic response, computer experiments yield a deterministic answer for a given set of input conditions. Therefore, most of the traditional tools of design of experiment (blocking, replication and randomization) are not used in solving computer experiments [20].

2.2.1 Factors and Experimental Domain

A factor represents a variable that can be controllable and is of interest in the experiment. Usually, a factor is called an input variable in a computer experiment [21]. Those variables that are not considered in an experiment are regarded as variables with fixed values.

Factors can be quantitative or qualitative. A quantitative factor is one that has a numerical value and can vary in a range or interval whereas qualitative or categorical factors are those defined as categories of different materials, operators, etc. Most of the factors employed in a computer experiment are quantitative.

The space where the factors take values is defined as the experimental domain [21]. There may be several specific values within the experimental domain where the factor is tested. An experimental domain can be defined by two (low and high) or more specific values. These particular values represent the levels of that factor. In computer experiment, the experimental domain is also defined as the input variable space. A run is described by the implementation of one of the possible combinations of levels of the factors. The result of a run represents the response or the output, for computer experiments. Like factors, the response of an experiment can be quantitative or qualitative, based on the objective of the experiment.

2.2.2 Experimental Designs for Computers

Selection of an experimental design is a key issue in performing a computer experiment. Classical designs are abandoned when performing computer experiments in favor of others that treat all the regions of the design space equally. The type of design that fills the space of experiment by spreading the points evenly throughout the experimental domain is called space-filling design.

There are several space-filling designs that can be employed when performing a computer experiment [22], such as:

- Sphere Packing Design;
- Uniform Design;
- Latin Hypercube Design;
- Minimum Potential Design;
- Maximum Entropy Design;
- Gaussian Process IMSE Optimal Design.

Sphere Packing design tries to spread the points as much as possible in the input variable space by maximizing the minimum distance between pairs of design points. This operation is done without any constrains. Uniform design minimizes the discrepancy between the design points. This does not always result in an even spacing of the factor levels. Latin Hypercube design assigns for each factor a number of levels equal to the number of runs performed in the experimental design. The levels are spaced evenly throughout the variable domain. Compared to the sphere packing design, Latin Hypercube design maximizes the minimum distance between points maintaining the even spacing between factor levels. Minimum Potential design spreads points out inside a sphere. This type of design has spherical symmetry and uniform spacing. Maximum Entropy design optimizes a measure of the amount of information contained in an experiment. Gaussian Process IMSE Optimal design minimizes the integrated mean squared error of the Gaussian process model over the experimental domain.

2.3 Three dimensional CFD Modeling

Computational Fluid Dynamics, a computer based tool, is used to simulate the behavior of systems involving fluid flow, multiphase and multicomponent interactions, heat transfer and other physical processes. Current advances in computer power and performance allow saving time and effort in creating a CFD model. Nowadays, CFD represents a recognized tool for research and industry. Performing a CFD simulation assumes several steps. First of all, the geometry is created and the required mesh is generated, depending on the objective of the simulation. The next step is to specify the physics of the problem that has to be investigated by creating the input file for solver. After that, the CFD problem is solved and the results are processed.

The CFD tool used in this study to solve the mass and momentum transfer in bulk solution is ANSYS CFX-11.0. This represents a finite element analysis tool developed by ANSYS, Inc.

2.3.1 Basic Equations

The set of equation solved by ANSYS CFX are the unsteady Navier-Stokes equations in their conservation form [23]. The instantaneous equations of mass, momentum and energy conservation are averaged, for turbulent flows, leading to additional terms.

Before presenting the equations, several mathematical notations are given.

Gradient operator

The gradient of a general scalar function $\phi(x, y, z)$ is defined as:

$$\nabla\phi = \frac{\partial\phi}{\partial x}\mathrm{i} + \frac{\partial\phi}{\partial y}\mathrm{j} + \frac{\partial\phi}{\partial z}\mathrm{k} \tag{2.19}$$

Divergence operator

For a vector function $U(x, y, z)$, the divergence is given by:

$$\nabla \bullet U = \frac{\partial U_x}{\partial x} + \frac{\partial U_y}{\partial y} + \frac{\partial U_z}{\partial z} \tag{2.20}$$

Dyadic operator

The dyadic operator of two vectors, U and V, is given by:

$$U \otimes V = \begin{bmatrix} U_x V_x & U_x V_y & U_x V_z \\ U_y V_x & U_y V_y & U_y V_z \\ U_z V_x & U_z V_y & U_z V_z \end{bmatrix} \tag{2.21}$$

The instantaneous equation of mass is:

$$\frac{\partial\rho}{\partial t} + \nabla \bullet (\rho U) = 0 \tag{2.22}$$

where ρ is the density and U is the velocity vector.

The momentum equation is given by:

$$\frac{\partial(\rho U)}{\partial t} + \nabla \bullet (\rho U \otimes U) = -\nabla p + \nabla \bullet \tau + S_M \tag{2.23}$$

where p is the static pressure, τ is the shear stress and S_M is the momentum source.

The term $\nabla \bullet (\rho U \otimes U)$ in Equation (2.23) can be expressed in the specific tensor notation, as:

$$\nabla \bullet (\rho U \otimes U) = \begin{bmatrix} \frac{\partial}{\partial x}(\rho U_x U_x) + \frac{\partial}{\partial y}(\rho U_y U_x) + \frac{\partial}{\partial z}(\rho U_z U_x) \\ \frac{\partial}{\partial x}(\rho U_x U_y) + \frac{\partial}{\partial y}(\rho U_y U_y) + \frac{\partial}{\partial z}(\rho U_z U_y) \\ \frac{\partial}{\partial x}(\rho U_x U_z) + \frac{\partial}{\partial y}(\rho U_y U_z) + \frac{\partial}{\partial z}(\rho U_z U_z) \end{bmatrix} \quad (2.24)$$

The total energy equation can be written as:

$$\frac{\partial(\rho h_{tot})}{\partial t} - \frac{\partial p}{\partial t} + \nabla \bullet (\rho U h_{tot}) = \nabla \bullet (\lambda \nabla T) + \nabla \bullet (U \bullet \tau) + U \bullet S_M + S_E \quad (2.25)$$

where h_{tot} is the total enthalpy, λ represents thermal conductivity, T is temperature, and S_E is the energy source. The term $U \bullet S_M$ represents the work due to external momentum sources. This term is currently neglected in ANSYS-CFX. The term $\nabla \bullet (U \bullet \tau)$ represents the work due to viscous stresses.

2.3.2 Boundary Conditions

To be able to solve a CFD problem, we have to specify boundary conditions. The type of boundary condition employed in the investigation of the diffusion layer thickness is wall. There are several types of boundary conditions for wall that can be specified in ANSYS-CFX. Those used herein are No Slip (Not Moving, no Wall Velocity) and No Slip (Moving, with Wall Velocity). A short discussion is provided below.

Wall - No Slip (Not Moving, no Wall Velocity) Boundary Condition

This type of boundary condition is used for the molten salt domain boundary. In this case, the velocity of the electrolyte at the wall boundary is set to zero, and, therefore, the boundary condition for the velocity is:

$$U_{Wall} = 0 \tag{2.26}$$

Wall - No Slip (Moving, with Wall Velocity) Boundary Condition

As mentioned in a previous section, the thickness of the diffusion layer strongly depends on the forced convection. In an electrochemical cell, both the cathodes and the stirrer are used to mix the molten salt and to create suitable conditions for the electrochemical process.

For this type of boundary condition, the molten salt at the wall boundary moves with the same velocity as the wall. Three options are available in ANSYS-CFX for the wall velocity:

- Cartesian Components:

In this case, the user can specify Cartesian components in a local or global coordinate frame:

$$U_{Wall} = U_{spec}\,i + V_{spec}\,j + W_{spec}\,k \tag{2.27}$$

- Cylindrical Components:

Cylindrical components are specified in a local cylindrical coordinate system and these are transformed by ANSYS-CFX into the global Cartesian coordinate system:

$$U_{Wall} = U_{r,spec}\,\hat{r} + U_{\theta,spec}\,\hat{\theta} + U_{z,spec}\,\hat{z} \tag{2.28}$$

- Rotating Wall:

A rotating wall is specified in rotating frames. The velocity of the wall is given by:

$$U_{Wall} = -\omega R_v \tag{2.29}$$

where ω is the angular velocity of the domain and R_v is the radial vector from the domain axis of rotation to the wall.

The rotating wall boundary condition has been used for the cathodes and stirrer in this thesis. Different values and directions can be specified for each of them. The ANSYS solver transforms the wall velocity specified by user into Cartesian components.

2.3.3 Turbulence Model

Fluctuations in time and space of the fluid represent turbulence. Turbulence occurs when the inertia forces in the fluid are more significant compared to the viscous forces. Turbulence modeling is an important issue in CFD simulations. The turbulence model used in CFD simulation of electrochemical cell is the k-epsilon model. The k-epsilon model is one of the most common models in turbulence. It is a two-equation model in which transport equations are solved for the turbulent kinetic energy k and its dissipation rate ε. The turbulence kinetic energy k is defined as the variance of fluctuations in velocity.

The continuity equation for k-ε model is given by:

$$\frac{\partial \rho}{\partial t} + \nabla \bullet (\rho U) = 0 \tag{2.30}$$

The momentum equation is expressed as:

$$\frac{\partial \rho U}{\partial t} + \nabla \bullet (\rho U \otimes U) - \nabla \bullet (\mu_{eff} \nabla U) = -\nabla p' + \nabla \bullet (\mu_{eff} \nabla U)^T + B \tag{2.31}$$

where B is the body forces, μ_{eff} is the effective viscosity, p' is the modified pressure, equal to p in ANSYS, by default.

In the k-ε model, the effective viscosity accounting for turbulence is expressed as:

$$\mu_{eff} = \mu + \mu_t = \mu + C_\mu \rho \frac{k^2}{\varepsilon} \tag{2.32}$$

where C_μ is a constant and μ_t is the turbulence viscosity.

Writing the differential transport equations for the turbulence kinetic energy:

$$\frac{\partial(\rho k)}{\partial t} + \nabla \bullet (\rho U k) = \nabla \bullet \left[\left(\mu + \frac{\mu_t}{\sigma_k} \right) \nabla k \right] + P_k - \rho\varepsilon \tag{2.33}$$

and for the turbulence dissipation rate:

$$\frac{\partial(\rho\varepsilon)}{\partial t} + \nabla \bullet (\rho U \varepsilon) = \nabla \bullet \left[\left(\mu + \frac{\mu_t}{\sigma_\varepsilon} \right) \nabla \varepsilon \right] + \frac{\varepsilon}{k} (C_{\varepsilon 1} P_k - C_{\varepsilon 2} \rho\varepsilon) \tag{2.34}$$

the values of k and ε are determined.

In Equations (2.33) and (2.34) $C_{\varepsilon 1}, C_{\varepsilon 2,}\, \sigma_k, \sigma_\varepsilon$ are constants and P_k represents the turbulence production due to viscous forces.

2.3.4 Component Model

In ANSYS CFX two separate flow models are available, an Eulerian-Eulerian multiphase model and a Lagrangian Particle Tracking multiphase model [23]. For Eulerian-Eulerian model two distinct sub-models can be used, the homogeneous model and the inter-fluid transfer (inhomogeneous) model. In this study, the inhomogeneous model has been employed.

Several notations are given before presenting the model. First, the volume fraction of component α is denoted r_α. The volume occupied by component α in a small volume V around a point where the volume fraction is r_α is given by:

$$V_\alpha = r_\alpha V \tag{2.35}$$

The mixture density ρ_m is defined as:

$$\rho_m = \sum_\alpha \rho_\alpha r_\alpha \tag{2.36}$$

The total pressure is given by:

$$p_{tot} = p_{stat} + \sum_\alpha \frac{1}{2} r_\alpha \rho_\alpha U_\alpha^2 \tag{2.37}$$

where p_{stat} represents the static (thermodynamic) pressure, r_α is the volume fraction for component α, ρ_α is the density of component α and U_α is the velocity magnitude for component α.

In the inhomogeneous model the momentum, heat and mass interfacial transfer depends on the contact surface area of the two components α and β. This is described by the

interfacial area per unit volume, denoted as the interfacial area density $A_{\alpha\beta}$. Interfacial transfer can be modeled using particle or mixture models. Mixture model has been used in this thesis to model the uranium and molten salt solution in the electrorefiner. The surface area per unit volume is determined as:

$$A_{\alpha\beta} = \frac{r_\alpha r_\beta}{d_{\alpha\beta}} \tag{2.38}$$

where $d_{\alpha\beta}$ is the interfacial length scale.

Interphase transfer coefficients can be correlated to give the mixture Reynolds number and Prandtl number, as follows:

$$Re_{\alpha\beta} = \frac{\rho_{\alpha\beta}\left|U_\beta - U_\alpha\right| d_{\alpha\beta}}{\mu_{\alpha\beta}} \tag{2.39}$$

$$Pr_{\alpha\beta} = \frac{\mu C_{p\alpha\beta}}{\lambda_{\alpha\beta}} \tag{2.40}$$

where $\rho_{\alpha\beta}$, $\mu_{\alpha\beta}$, $C_{p\alpha\beta}$, and $\lambda_{\alpha\beta}$ are the density, viscosity, specific heat capacity and thermal conductivity of the mixture. These are defined as:

$$\rho_{\alpha\beta} = r_\alpha \rho_\alpha + r_\beta \rho_\beta \tag{2.41}$$

$$\mu_{\alpha\beta} = r_\alpha \mu_\alpha + r_\beta \mu_\beta \tag{2.42}$$

The momentum and mass transfer equations for the inhomogeneous model in ANSYS CFX are presented in the following paragraphs.

First, the momentum equation is given by:

$$\frac{\partial}{\partial t}\left(r_\alpha \rho_\alpha U_\alpha\right) + \nabla \bullet \left(r_\alpha \left(\rho_\alpha U_\alpha \otimes U_\alpha\right)\right) = -r_\alpha \nabla p_\alpha + \nabla \bullet \left(r_\alpha \mu_\alpha \left(\nabla U_\alpha + \left(\nabla U_\alpha\right)^T\right)\right) + \sum_{\beta=1}^{N}\left(\Gamma^+_{\alpha\beta} U_\beta - \Gamma^+_{\beta\alpha} U_\alpha\right) + S_{M\alpha} + M_\alpha \tag{2.43}$$

where N is the number of components in mixture, $S_{M\alpha}$ represents the momentum sources generated by external body forces, and M_α describes the interfacial forces on α given by the presence of other components. The term $\Gamma^+_{\alpha\beta} U_\beta - \Gamma^+_{\beta\alpha} U_\alpha$ gives the momentum transfer due to interphase mass transfer.

The continuity equation is as follows:

$$\frac{\partial}{\partial t}\left(r_\alpha \rho_\alpha\right) + \nabla \bullet \left(r_\alpha \rho_\alpha U_\alpha\right) = S_{MS\alpha} + \sum_{\beta=1}^{N} \Gamma_{\alpha\beta} \tag{2.44}$$

where $S_{MS\alpha}$ is the mass source and $\Gamma_{\alpha\beta}$ describes the mass flow rate per unit volume from component β to α.

The volume conservation equation, which shows that the volume fractions sum to unity, is:

$$\sum_{\alpha=1}^{N} r_\alpha = 1 \tag{2.45}$$

Additional N-1 equations are needed to be able to solve the set of 4N+1 hydrodynamic equations presented above for the 5N unknowns: U_α the velocity of component α, V_α the volume of component α, W_α the fluid viscous and body force work term for component α, r_α the volume fraction of component α, and p_α the pressure of component α.

These equations are provided by pressure constraints, given that all components share the same pressure field:

$$p_\alpha = p \text{ for all } \alpha = 1,\ldots, N \tag{2.46}$$

Interphase momentum transfer $M_{\alpha\beta}$ is given by the forces acting on component α due to its interaction with component β. Thus, the total force on component α is given by:

$$M_\alpha = \sum_{\beta \neq \alpha} M_{\alpha\beta} \tag{2.47}$$

The interfacial forces between two components are equal and of opposite sign, such that their sum is zero:

$$\left(M_{\alpha\beta} = -M_{\beta\alpha}\right) \Rightarrow \sum_\alpha M_\alpha = 0 \tag{2.48}$$

Several distinct physical effects may give rise to interfacial force moments acting between two components:

$$M_{\alpha\beta} = M_{\alpha\beta}^{D} + M_{\alpha\beta}^{L} + M_{\alpha\beta}^{LUB} + M_{\alpha\beta}^{VM} + M_{\alpha\beta}^{TD} + M_S + \ldots \tag{2.49}$$

where $M_{\alpha\beta}^{D}$ is the momentum due to interphase drag force, $M_{\alpha\beta}^{L}$ is the momentum given by the lift force, $M_{\alpha\beta}^{LUB}$ is the momentum due to the wall lubrication force, $M_{\alpha\beta}^{VM}$ is the virtual mass force momentum, $M_{\alpha\beta}^{TD}$ is the turbulence dispersion force momentum and M_S represents the momentum due to solids pressure force. For the purpose of this study, the momentum due to interphase drag force is the most significant.

Chapter 3 Continuous Electrochemical Processing Concept

As discussed in the previous chapters, the current electrochemical processing technology relies on batch operation. Consequently, compared to the current aqueous reprocessing technologies, the process has significant uncertainties in determining the total amount of material processed and also the total throughput of the electrochemical system is limited. Therefore, the feasibility of continuous operation of electrochemical process is investigated and analyzed herein. In this chapter a presentation of the main requirements for the continuous electrochemical concept is given. Furthermore, a description of the proposed continuous concept for electrorefining is provided.

3.1 Main Requirements

Based on the understanding of the electrochemical process, there are several requirements that have to be met in order to operate continuously the electrochemical processing at high recovery efficiencies. The most important are presented in the following paragraphs.

First of all, separate stages have to be employed to collect simultaneously a pure uranium deposit at solid cathode and mixed uranium and plutonium deposit at liquid cathode.

Currently, the electrorefiner operation consists of collecting first uranium at solid cathode. Uranium is separated from other less noble elements by imposing a cathode potential larger than plutonium reduction potential. Then, when the amount of plutonium in electrorefiner becomes comparable or higher than the amount of uranium in the electrorefiner, the solid cathode is exchanged with a liquid cadmium cathode. Thus, both uranium and plutonium are collected at the liquid cathode. Other transuranic elements, like neptunium, curium, and americium, may be collected with plutonium at a liquid cadmium cathode, due to their small activity coefficients in cadmium. The continuous electrochemical concept will allow simultaneous operation of solid and liquid cathodes by imposing two different stages of extraction. The first one, called uranium extraction stage, will employ a solid cathode whereas the second one, uranium-plutonium extraction stage, will use liquid cadmium as cathode.

From Faraday's first law, it can be determined that only a limited amount of material can be deposited at cathode, per ampere-hour. This amount is proportional to the molar mass of the metal and also to the quantity of electricity transferred at the electrode. Using Equation (2.10), the mass of uranium that is deposited at cathode per ampere-hour is given by:

$$m_U = \frac{238.03\text{g/mol} \cdot 1\text{A} \cdot 3600\text{s}}{3 \cdot 96487\text{C/mol}} = 2.96\text{g} \qquad (3.1)$$

where 238.03 g/mol represents the uranium molar mass and 96487 C/mol is Faraday's constant. Consequently, to increase the throughput of the electrorefiner a higher electric current has to be applied.

This depends also on several design and operating parameters, like: anode potential, salt resistance, distance between electrodes and area of electrodes. The smaller the salt resistance and distance between electrodes the higher is the electric current. Also, a larger area of electrodes facilitates a higher electric current.

Based on these, a separate circuit will be formed by each anode and cathode during cathode movement in continuous electrochemical processing operation. Moreover, the distance between the anode and cathode should not be increased during cathode movement from the beginning of the stage to the end of the stage.

In addition to these, a compact continuous concept is developed. The area where the anode baskets are continuously loaded with chopped spent fuel is limited to the first stage, the uranium extraction stage. A compact design has the advantage of being easier to build, maintain and model.

3.2 Concept Description

The continuous electrochemical processing concept envisioned in this study consists of two extraction stages. A detailed description of each stage is provided in the following paragraphs. The material flow in the continuous electrochemical process is presented in Figure 3.1.

The first stage of the continuous electrochemical processing operation represents the uranium extraction region. A schematic representation of both stages is shown in Figure 3.2. A solid cathode mandrel is employed in this stage to collect uranium deposit. This stage consists of a channel where a molten chloride salt (LiCl-KCl) is floating on a liquid cadmium pool. A small amount of uranium chloride and plutonium chloride is added into the molten salt, from the beginning of the process. The equipment is operated at 500 °C (773 K). Both molten salt and liquid cadmium continuously flow from the entrance of the stage to the next region of the electrorefining process. Several perforated anode baskets, in which chopped spent fuels are continuously loaded, are situated on both sides of the channel.

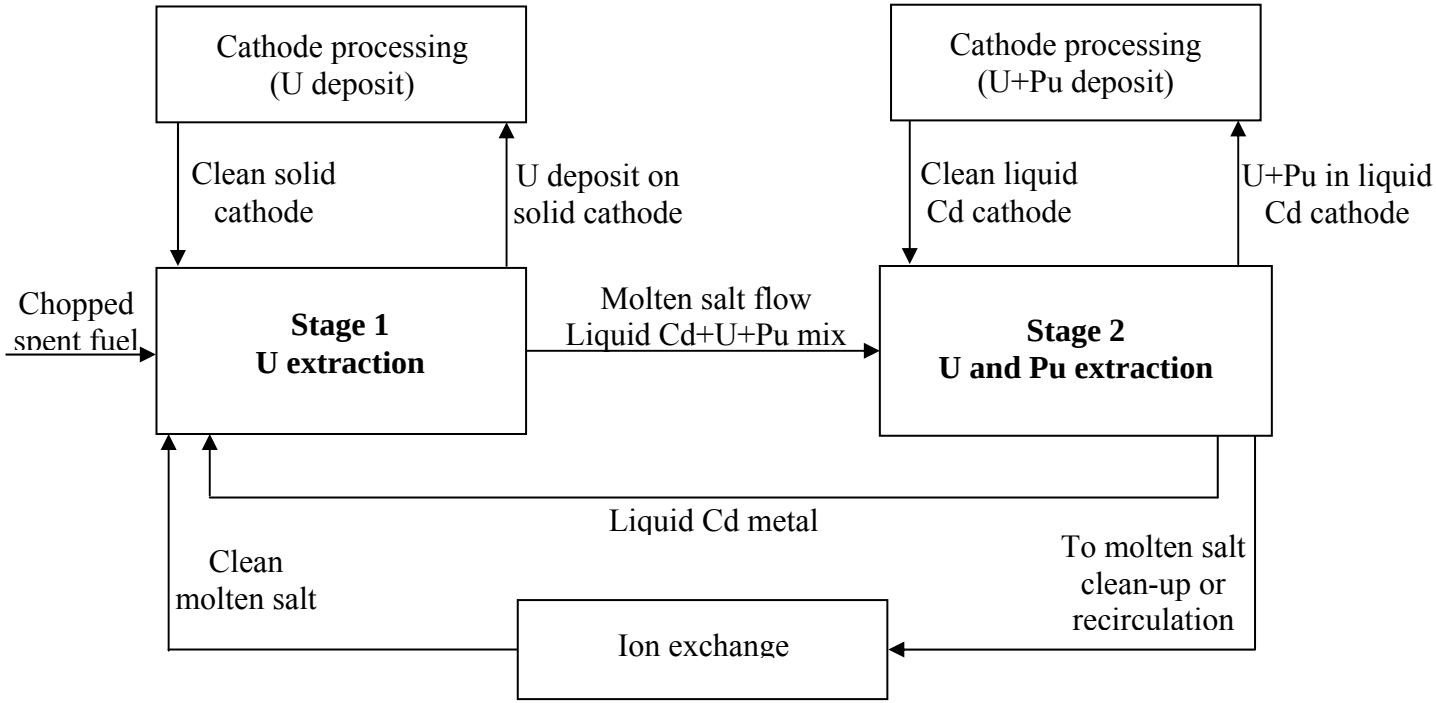

Figure 3.1 – Material flow in the continuous electrochemical process

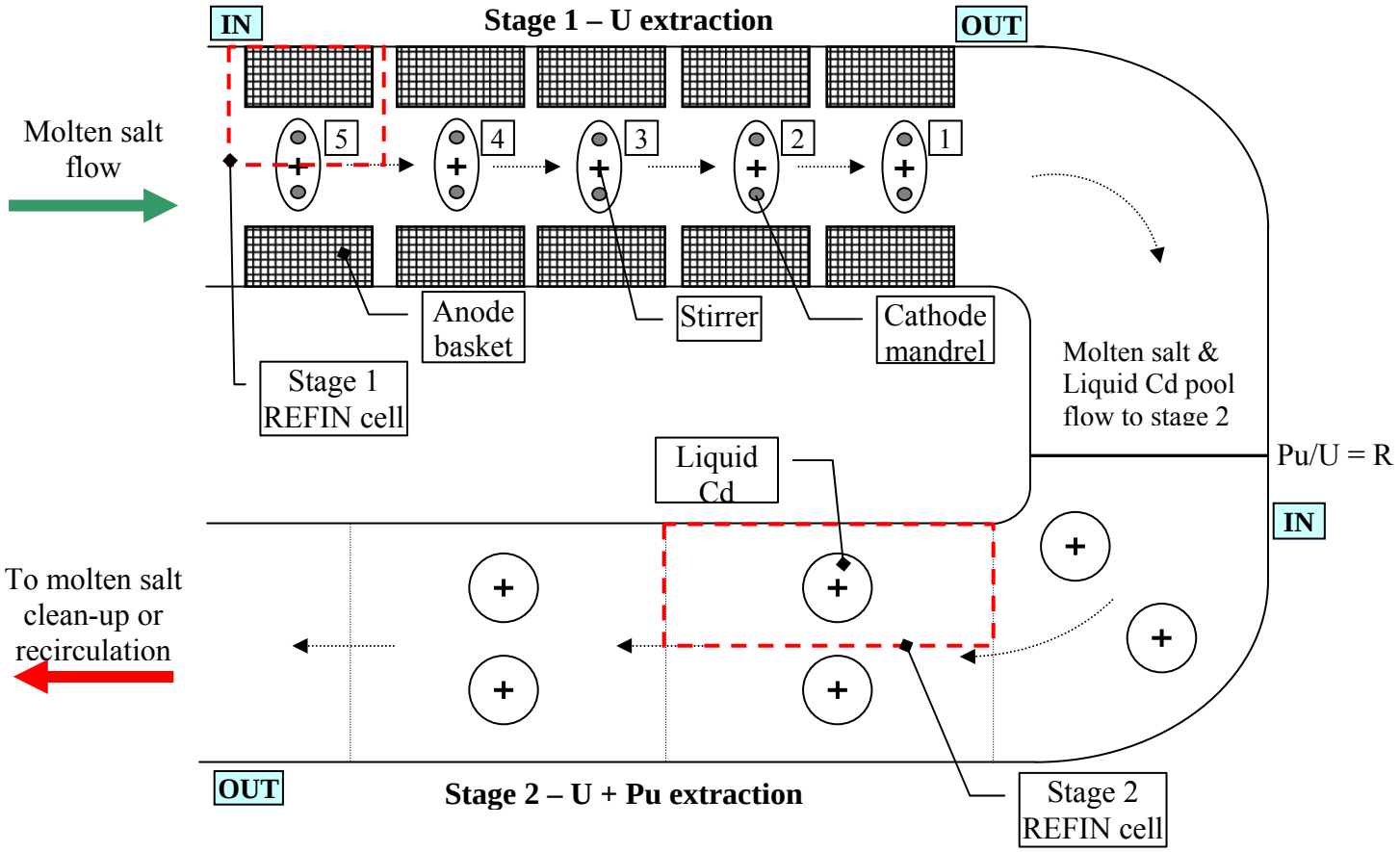

Figure 3.2 – Continuous electrochemical processing concept flowchart

Solid mandrels, arranged as presented in detail in Figure 3.3, represent the cathodes of the first stage of the electrorefiner. A cruciform stirrer located between two cathodes, at equal distance, is used to mix the electrolyte and to create turbulent conditions for the process. In addition, each cathode mandrel is rotating, but with a lower rotational velocity than the stirrer, to assure uniform uranium deposition. The arrangement presented in Figure 3.3 represents a cathode assembly.

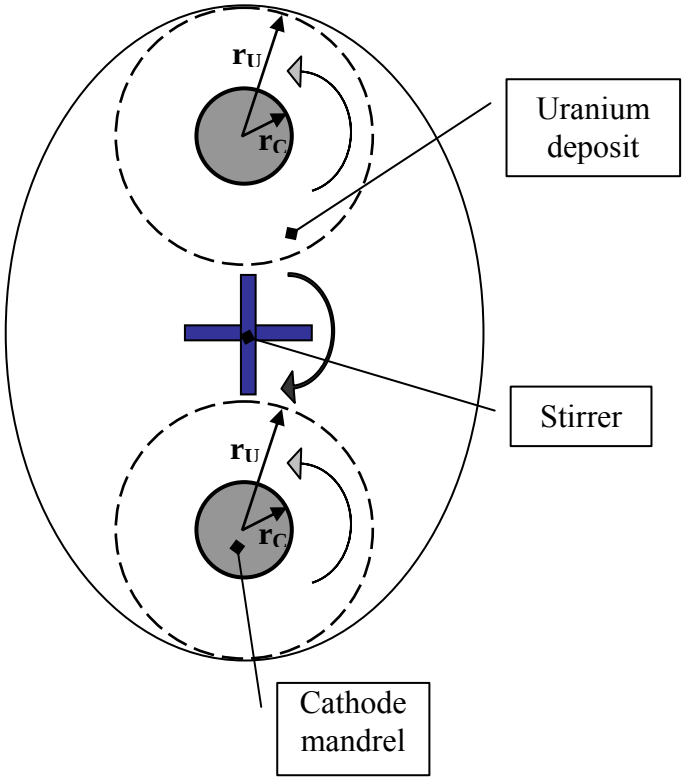

Figure 3.3 – Cathode assembly used for uranium extraction (top view)

The stirrer is also used to limit the uranium deposit on solid cathode to the dimension of the exit port, during the electrorefiner operation. An insulator disc positioned at the bottom of the cathode mandrel can be used to restrain dendritic deposits from growing toward the cadmium pool. This arrangement is illustrated in Figure 3.4.

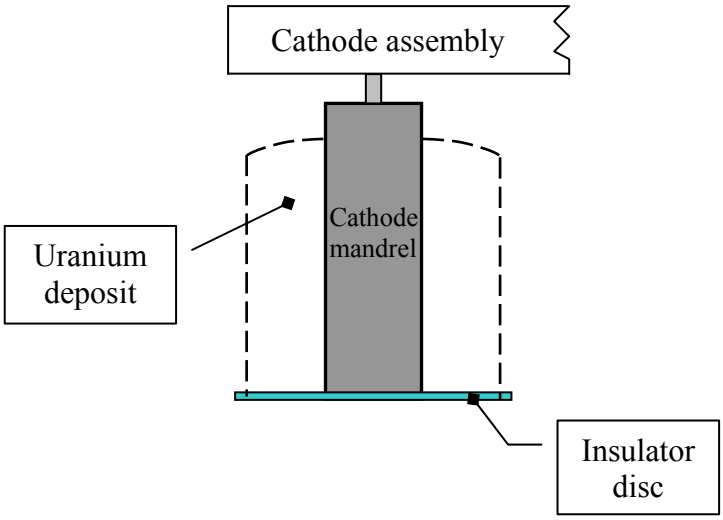

Figure 3.4 – Cathode mandrel with insulator disc (front view)

During the electrorefiner operation, each cathode forms a separate circuit with the perforated anode basket on its side. The electrorefiner channel consists of several anode – cathode circuits distributed along the channel length. This arrangement allows to simultaneously operate several circuits and therefore to save time and increase the electrorefiner productivity.

Moreover, the distance between the electrodes is kept constant during cathode movement. The perforated anode baskets are fed with chopped fuel elements and then are lowered into the molten salt. In this stage, the electrorefiner is operated in direct transport mode. An electric current is applied for each anode – cathode circuit and uranium is electrotransported to the solid cathode. The same value of the electric current is applied for each circuit. Each cathode spends an equal amount of time in each electric circuit and thus collects an equal amount of uranium. Continuously, a clean cathode assembly is introduced at the beginning of the first stage and, as it moves to the end of the first stage, in the direction of the molten salt flow, it collects pure uranium deposit. When the cathode assembly reaches the end of the channel, it is extracted from the electrorefiner and the uranium deposit is removed.

In uranium extraction stage, the role of the cadmium pool is to serve as an intermediate electrode during the direct transport operation. Thus, uranium is electrotransported from anode basket to the cadmium pool at the bottom of the channel, and, at the same time, an equal amount of uranium is transported from the cadmium pool to the solid cathode. Furthermore, another role of the cadmium pool is to collect the uranium dendrites which drop from solid cathode during cathode movement. As a result, a small amount of uranium and plutonium is collected in the cadmium pool during the first stage of operation. This material will be recovered in the second stage, when the cadmium pool represents the anode of the electrorefiner.

During the uranium extraction stage, plutonium chloride accumulates in the molten salt. Only uranium is collected at the solid cathode. Rare-earths metals remain almost entirely in the salt.

The length of the first stage is dictated by the moment when the concentration of plutonium in electrorefiner becomes comparable or higher than the concentration of uranium. When this condition is satisfied, a mixture of uranium, plutonium, neptunium, americium and curium can be recovered at the liquid cadmium cathode. In addition, it is important to mention that a pure uranium deposit must be collected in the first stage. Since plutonium deposition at solid cathode is not desired the electrorefining process in first stage is stopped prior to achieving this condition. It has been explained in a previous chapter the reason for not depositing plutonium to the solid cathode.

The molten salt and the liquid cadmium pool situated at the bottom of vessel flow continuously to the second stage. Here, a liquid cadmium cathode is employed to collect a mixture of uranium, plutonium and other elements. In this stage, the anode is the liquid cadmium pool flowing from the first stage and containing small amounts of uranium and plutonium. Uranium and plutonium from molten salt and anode are electrotransported to the liquid cadmium cathode by means of an applied electric current. A stirrer is used to continuously mix the liquid cadmium cathode. Thus, the formation of dendritic uranium, which would hamper the plutonium deposition at liquid cathode, is inhibited.

In this way, plutonium – uranium mixture is obtained at the liquid cadmium cathode, for further fuel fabrication. This plutonium product is sufficiently diluted with uranium in order to discourage weapons proliferation. After this stage, cadmium pool from the bottom of the vessel flows to the first stage and continues the process. The contaminated molten salt is cleaned using ion exchangers and clean molten salt is fed constantly into the first stage.

Design geometry of the continuous concept of electrochemical process is presented in the following chapter along with the modeling techniques. Compared to the current electrochemical technology, this concept has the advantage of a better estimation of the total amount of material processed because material is not held in the molten salt for several batches, as it is performed presently.

Chapter 4 Computation Modeling and Simulation

This chapter starts by presenting the electrochemical modeling of the continuous concept performed to simulate the reactions at the electrode surfaces. Based on the electrorefiner geometry, the initial element concentrations at anode and molten salt were investigated to achieve a continuous operation for the electrorefiner. Furthermore, a design of experiment was performed to optimize the recovery efficiency and the operation time for the continuous electrorefiner. Next, the chapter describes the three dimensional CFD modeling carried out to determine the thickness of the diffusion layer for the continuous electrochemical design.

4.1 Electrochemical Modeling

The model for the electrochemical reactions at the electrode surfaces was developed based on the kinetic modeling capability of a time-dependent one dimensional code, REFIN [9]. The REFIN code, which simulates the electrochemical reactions within the diffusion layer, was benchmarked against experimental data [11]. The code is capable of simulating an electrorefiner employing different types of electrodes.

Using this tool, the amount of material deposited at solid cathode in the first stage and the mass of plutonium and uranium collected at liquid cathode in the second stage are determined. Element distribution within the molten salt and the liquid cadmium metal is also obtained. Moreover, operation time of the electrorefiner is calculated. The uranium / uranium and plutonium recovery efficiency is evaluated for the continuous electrochemical operation, based on the results obtained from simulation.

4.1.1 Geometry

The geometry of the continuous electrorefiner has been inspired by Mk-IV electrorefiner, located in the Fuel Conditioning Facility at INL. Mk-IV electrorefiner was designed for processing driver fuel and consists of an electrorefiner vessel and four ports used to insert and remove anode baskets and cathode mandrels into electrolyte [24]. The continuous electrorefiner concept proposed in this thesis consists of several electrochemical circuits that operate simultaneously, as illustrated in Figure 4.1. In the first stage, each circuit consists of a perforated anode basket loaded with spent fuel and a solid cathode mandrel. Cadmium pool from the bottom of the vessel becomes the anode in second stage, when liquid cadmium is employed as cathode to collect both uranium and plutonium. The geometrical dimensions of the electrodes and stirrer are given in Table 4.1.

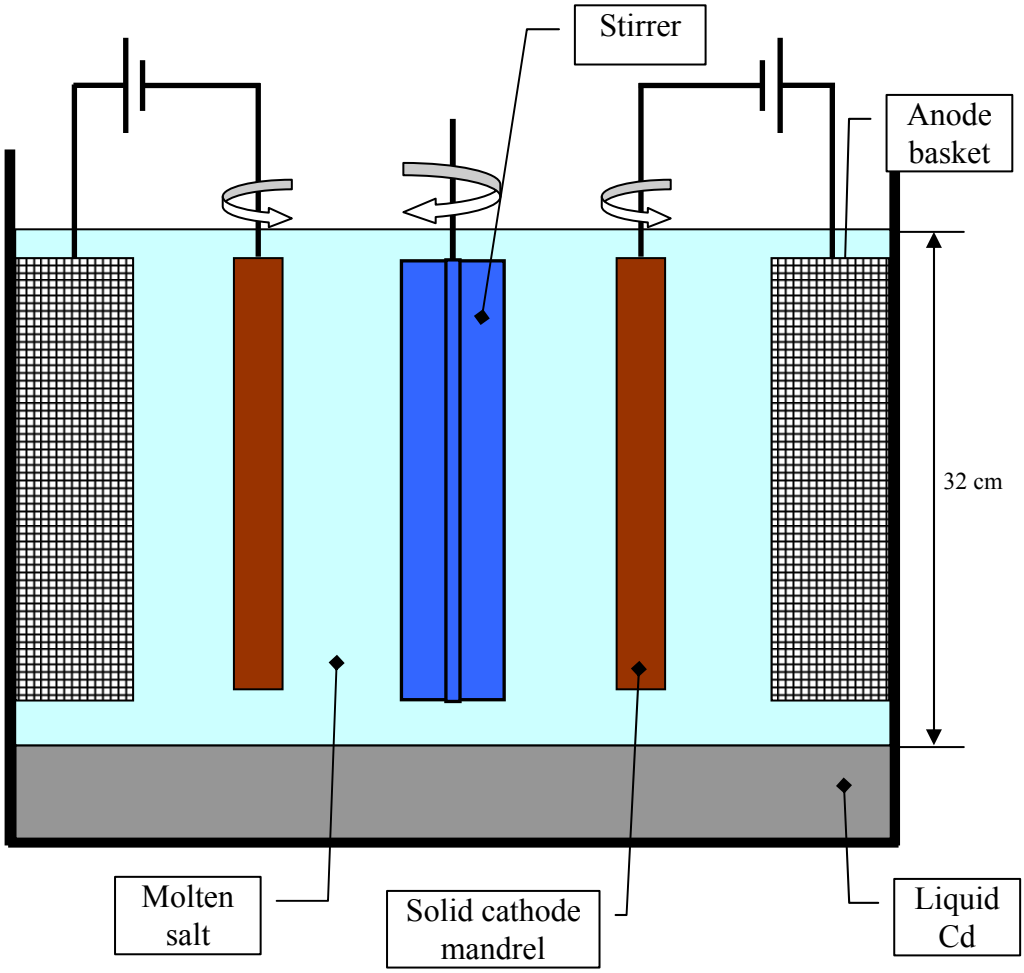

Figure 4.1 – Schematic of electrochemical circuits in continuous operation (front view)

A graphical representation of the electrochemical cell modeled with REFIN is given in Figure 4.2 (red contour). The conceptual continuous electrorefiner investigated in this thesis consists of 10 electrochemical cells as seen in Figure 4.2 (red contour) and described in Table 4.1.

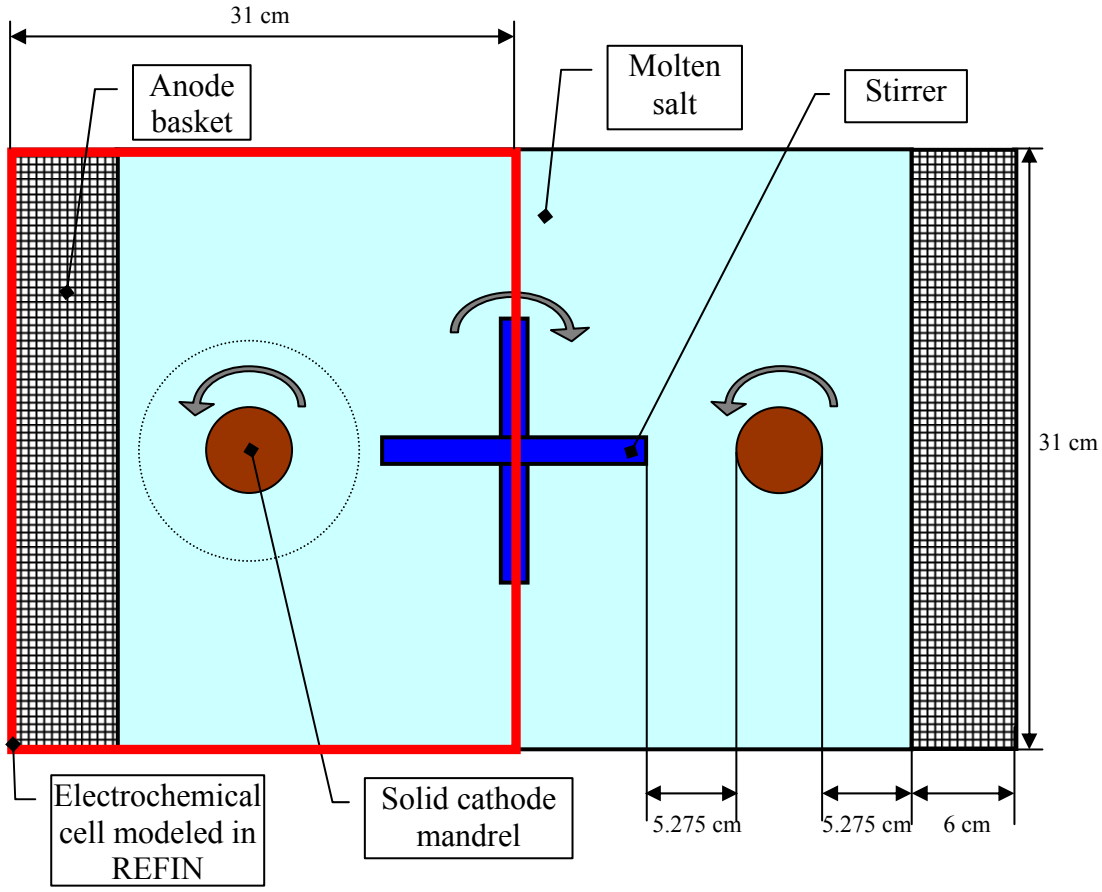

Figure 4.2 – Electrochemical cell modeled with REFIN code (top view)

Table 4.1 – Geometrical features of REFIN cell (red contours in Figures 3.2 and 4.2)

Component	Parameter	Value
Cathode mandrel (Stage 1 REFIN cell)	Diameter [cm]	6.7
	Height [cm]	23
Anode basket (Stage 1 REFIN cell)	Height [cm]	25
	Width [cm]	6
	Length [cm]	31
Molten salt (Stage 1 REFIN cell)	Height [cm]	32
	Width [cm]	31
	Length [cm]	31
Liquid Cd pool (Stage 1 REFIN cell)	Height w/o fuel [cm]	10.0
	Height w/ fuel [cm]	11.09
	Width [cm]	31
	Length [cm]	31
Cruciform stirrer (Stage 1 REFIN cell)	Height [cm]	25
	Side width [cm]	1.5
	Side length [cm]	7
Liquid Cd cathode (Stage 2 REFIN cell)	Height [cm]	2
	Diameter [cm]	35.68
Molten salt (Stage 2 REFIN cell)	Height [cm]	12.09
	Width [cm]	50
	Length [cm]	40
Liquid Cd anode (pool) (Stage 2 REFIN cell)	Height [cm]	5.3
	Width [cm]	50
	Length [cm]	40

Based on these characteristics, the volume of the molten salt and anode, and the area of interface anode – molten salt and molten salt – cathode are determined. These are summarized in Table 4.2. REFIN code offers the possibility of modeling an electrochemical cell employing a liquid cadmium anode and a solid / liquid cathode. Thus, first stage was modeled taking into account the role of intermediate electrode of the cadmium pool, as described in Chapter 2.

Table 4.2 – Volumes and areas of interface of electrochemical cell modeled with REFIN

Component	**Value**
Liquid anode volume [cm^3]	10661.3
Molten salt volume [cm^3]	24179.5
Liquid cathode volume (stage 2) [cm^3]	2000
Uranium extraction stage (stage 1)	
Area of interface anode – molten salt [cm^2]	961
Area of interface cathode – molten salt [cm^2]	484
Uranium and plutonium extraction stage (stage 2)	
Area of interface anode – molten salt [cm^2]	2000
Area of interface cathode – molten salt [cm^2]	1000

4.1.2 Process Parameters of Electrochemical Cell

After setting the geometry for electrorefiner, several process parameters have to be specified. They are summarized in Table 4.3. Among them, standard electrochemical potential of elements and diffusion layer thickness play an important role in electrochemical model development. The elements of interest defined in REFIN code are: uranium, plutonium, neodymium, cadmium, lithium, potassium, and chlorine. For liquid electrodes two diffusion layers are defined, one layer inside the electrode and another one in the molten salt, at the electrolyte – electrode interface. For solid electrodes only the diffusion layer into molten salt at the interface between molten salt and electrode is defined. It was observed that the diffusion layer thickness in molten salt, at the interface with solid cathode, has the most significant influence on the electrochemical process. The value of diffusion layer thickness will be determined using ANSYS CFX based on the geometry and, most important, the initial concentration of elements in molten salt. The initial values of the diffusion layer thickness are presented in Table 4.3 [9].

Table 4.3 – Process parameters for electrochemical modeling [9]

Parameter	**Value**
Operating temperature	773 K
Standard electrode potential E^0 vs. Cl_2/Cl^- [V]	
K/K^+	3.760
Li/Li^+	3.578
Nd/Nd^{3+}	2.944
Pu/Pu^{3+}	2.706
U/U^{3+}	2.394
Cd/Cd^{2+}	1.403
Cl^-/Cl_2	0
Diffusion coefficient in LiCl-KCl [cm^2/s]	
U	$6.8634 \cdot 10^{-6}$
Pu	$1.0829 \cdot 10^{-5}$
Nd	$1.2075 \cdot 10^{-5}$
Cd	$2.2300 \cdot 10^{-5}$
Diffusion layer thickness [cm]	
Liquid metal electrode	$2.0 \cdot 10^{-3}$
Molten salt – liquid metal electrode side	$2.0 \cdot 10^{-2}$
Molten salt – solid electrode side	$2.0 \cdot 10^{-3}$

4.1.3 Initial Element Concentrations at Anode and Molten Salt

The initial uranium and plutonium concentrations at anode and electrolyte play a major role in developing a continuous electrorefiner for processing spent fuel. The optimum combination of initial concentration of elements at anode and molten salt has been determined based on a sensitivity study presented further.

The electrolyte employed in this study is LiCl-KCl eutectic salt containing small amounts of dissolved UCl_3 and $PuCl_3$ [24].

Table 4.4 – Electrolyte parameters

Electrolyte	LiCl-KCl molten salt
Mass [g]	37502.4
Volume [cm^3]	24179.5

The anode charge presented in Table 4.5 is based on the typical composition of an anode basket loaded with EBR-II fuel. Experiments with this fuel have been conducted in the Mk-IV electrorefiner at ANL and INL [24]. The purpose of the sensitivity study is to identify the initial element concentration both at anode and in molten salt suitable for continuous operation of the electrorefiner, based on the element weight percent presented in Table 4.5.

Table 4.5 – Anode parameters

Anode density [g/cm^3] [9]	7.8
Anode mass [g]	83158.2
Anode volume [cm^3]	10661.3
Cd mass [g]	74958
Cd weight percent	90.15
U mass [g] [24]	8065.13
U weight percent	9.7
Pu mass [g] [24]	41.37
Pu weight percent	0.05
Nd mass [g] [24]	93.10
Nd weight percent	0.1

For this investigation, the maximum initial concentration was set to 10 weight percent and the minimum initial element concentration to 0.05 weight percent. This range was divided into three intervals, for a larger set of possible combinations, as follows: from 0.05 weight percent to 3.25 weight percent; from 3.25 weight percent to 7.50 weight percent; from 7.50 weight percent to 10.00 weight percent. The generic categories of initial element concentration at anode and molten salt performed are illustrated in Table 4.6. A total of 256 REFIN simulations have been done for all the combinations of initial element concentrations. For each investigation performed both extraction stages were analyzed.

Table 4.6 – Combinations of initial element concentration at anode and molten salt

Category	Initial element weight percent in molten salt	Initial element weight percent at anode
1	U > Pu	U > Pu
2	U > Pu	U < Pu
3	U < Pu	U < Pu
4	U < Pu	U > Pu
5	U > Pu	U = Pu
6	U < Pu	U = Pu
7	U = Pu	U > Pu
8	U = Pu	U < Pu
9	U = Pu	U = Pu

4.1.4 Design of Experiment

A design of experiment was performed using JMP software to identify the combinations of initial element concentrations at anode and molten salt and electric current that result in optimum recovery efficiency and operation time. The study has been conducted within a short range for the combination listed in Table 4.6 that demonstrated to be functional for continuous electrochemical operation. This combination consists of less uranium than plutonium in molten salt and more uranium than plutonium at anode. Factors of interest and the input variable space are presented in Table 4.7. All factors are quantitative.

Table 4.7 – Input variable space

Factor	Low level	High level
Electric current [A]	25	40
Initial concentration of U in molten salt [wt.%]	1.2	1.5
Initial concentration of Pu in molten salt [wt.%]	1.5	2.0
Initial concentration of U at anode [wt.%]	9.1	9.7
Initial concentration of Pu at anode [wt.%]	0.1	0.5

A Latin Hypercube design with optimal spacing has been employed for this experiment. A number of 30 runs have been performed, and therefore 30 levels have been considered for each input variable. These are illustrated in Table 4.8. Latin Hypercube design represents a healthy compromise between uniform design and sphere packing design. It is preferable because all its projections onto the coordinate axes are uniform and it also has a lower discrepancy over other designs, which indicates a better uniformity of the design points.

Table 4.8 – Latin Hypercube design with optimal spacing for electrorefiner

Run	Electric current [A]	Initial concentration of U at anode [wt.%]	Initial concentration of Pu at anode [wt.%]	Initial concentration of U in molten salt [wt.%]	Initial concentration of Pu in molten salt [wt.%]
1	35.34	9.37	0.43	1.23	1.91
2	38.97	9.24	0.21	1.26	1.72
3	33.79	9.66	0.50	1.38	1.52
4	25.00	9.29	0.32	1.44	1.83
5	32.24	9.18	0.42	1.22	1.53
6	27.07	9.64	0.28	1.48	1.67
7	31.72	9.10	0.22	1.39	1.74
8	40.00	9.53	0.25	1.29	1.93
9	28.10	9.62	0.18	1.37	1.95
10	25.52	9.49	0.14	1.32	1.66
11	34.83	9.70	0.40	1.33	1.81
12	37.41	9.12	0.33	1.42	1.55
13	37.93	9.31	0.16	1.43	1.86
14	32.76	9.27	0.44	1.49	1.76
15	26.55	9.39	0.39	1.28	1.97
16	33.28	9.33	0.35	1.40	2.00
17	29.66	9.14	0.46	1.31	1.79

Table 4.8 (continued)

Run	Electric current [A]	Initial concentration of U at anode [wt.%]	Initial concentration of Pu at anode [wt.%]	Initial concentration of U in molten salt [wt.%]	Initial concentration of Pu in molten salt [wt.%]
18	35.86	9.58	0.29	1.50	1.90
19	39.48	9.45	0.49	1.41	1.71
20	30.69	9.68	0.31	1.20	1.62
21	29.14	9.35	0.10	1.47	1.78
22	38.45	9.47	0.38	1.25	1.57
23	36.38	9.51	0.24	1.46	1.60
24	34.31	9.22	0.13	1.36	1.50
25	36.90	9.60	0.11	1.27	1.59
26	31.21	9.43	0.17	1.21	1.84
27	28.62	9.56	0.47	1.45	1.88
28	27.59	9.16	0.20	1.30	1.98
29	30.17	9.41	0.36	1.34	1.64
30	26.03	9.20	0.27	1.24	1.69

A graphical representation of the Latin Hypercube design with 30 runs is provided in Figure 4.3. For each run performed, the following responses were analyzed: U recovery efficiency for stage 1, operation time for stage 1, U recovery efficiency for stage 1 + 2, total U+Pu recovery efficiency for stage 1 + 2, and total operation time.

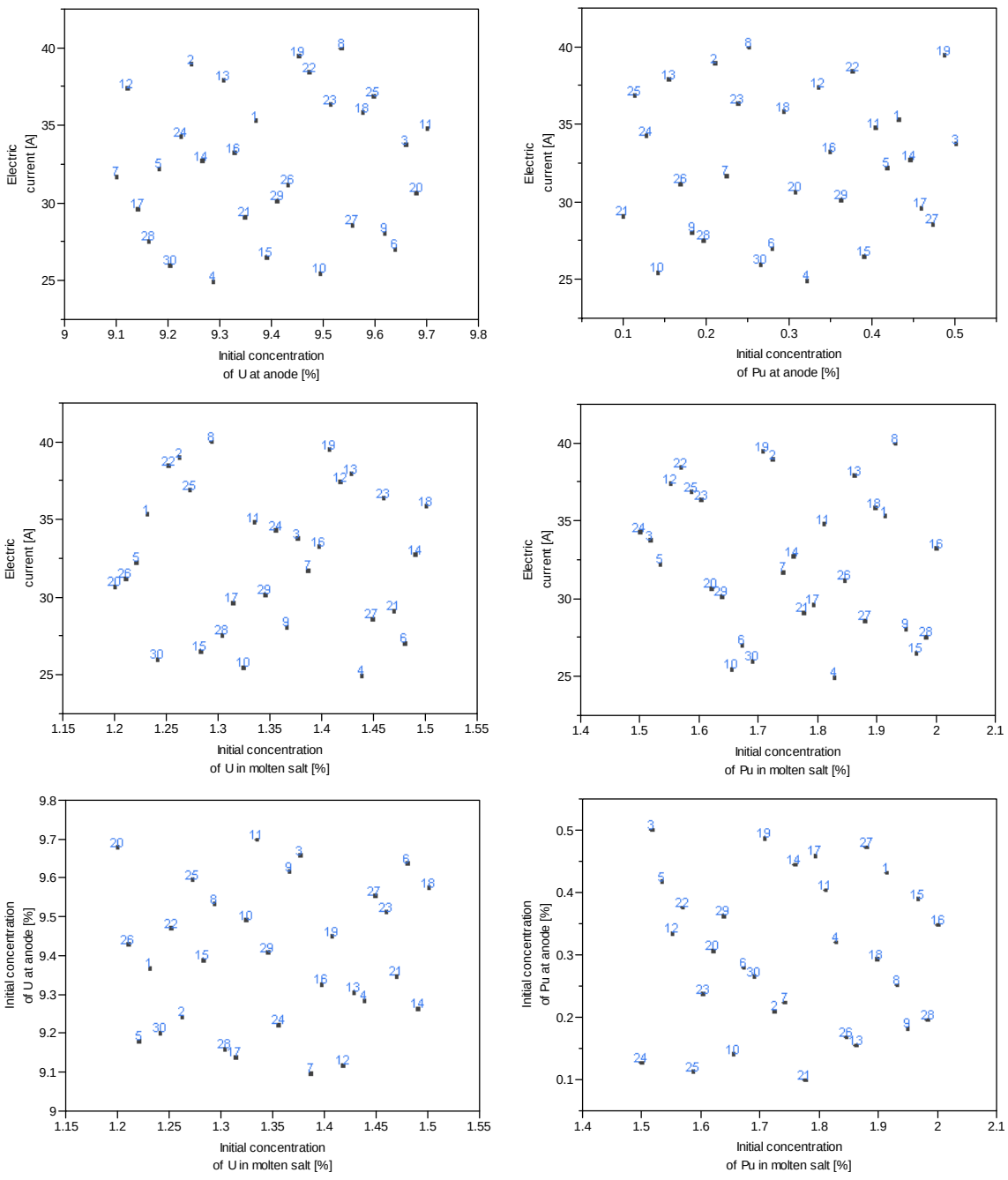

Figure 4.3 – Latin Hypercube design with optimal spacing

4.2 Three dimensional CFD Modeling

The goal of performing the CFD simulation using ANSYS CFX-11.0 is to solve the mass and momentum transfer in the bulk solution in order to determine the diffusion layer thickness. Flow velocity profiles and chemical concentration distribution of elements in the electrolyte are determined through three dimensional CFD modeling. In the bulk solution, the mass transfer is governed mostly by forced convection. The thickness of the diffusion layer is calculated based on element concentration profiles in the molten salt. Diffusion layer thickness determined using ANSYS CFX-11.0 is used as input for the electrochemical study. The approach used to solve the mass transfer in both bulk solution and diffusion layer is illustrated in Figure 4.4.

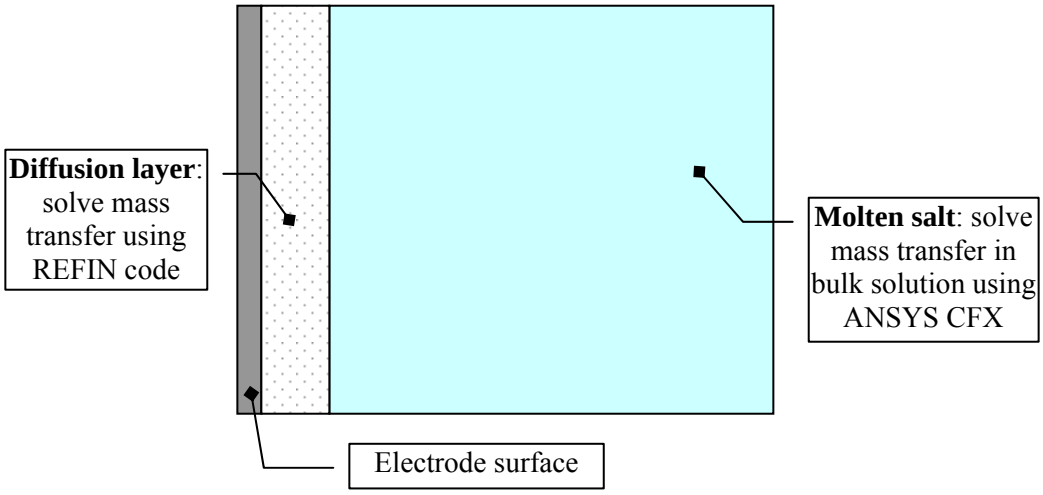

Figure 4.4 – REFIN and ANSYS CFX coupling

4.2.1 Electrorefiner Geometry and Mesh

The geometry of the continuous electrorefiner, described in Section 4.1.1, has been created using Autodesk Inventor Professional 2008. The geometry file created with this 3D CAD software can be exported in a suitable format for generating the mesh.

Several options have been investigated for the electrochemical cell design. Each approach provided useful insight on phenomena of interest and suggested improvements that were incorporated in subsequent designs.

Simulations for the design presented in Figure 4.5.a) have shown that insufficient uranium and molten salt mixing is achieved and a diffusion layer of desired characteristics does not develop at the cathode – molten salt interface. A stirrer design that ensures uniform flow field for the entire cathode height has to be further pursued. Consequently, this enhancement has been built in the second design which is presented in Figure 4.5.b). While this solution is capable of delivering desired flow patterns, the magnitude of its influence on the cathode – molten salt interface still does not yield a complete diffusion layer development. This is a direct result of relatively short stirrer blades and inadequate operating parameters, mainly stirrer rotational velocity. Further design refinement resulted in the final electrochemical cell geometry shown in Figure 4.5.c). Fine tuning of operating parameters, cathodes and stirrer direction and rotational velocity, as well as increased stirrer dimensions have a beneficial effect on the flow distribution and mixing of uranium and molten salt. As a result, the positive impact on the diffusion layer is quantified through a decrease in thickness

which is suitable for the simulation of continuous electrochemical deposition using REFIN. The final electrorefiner geometry is presented in Figure 4.6.

Based on the electrorefiner geometry, the mesh is obtained using ANSYS ICEM CFD. This is capable of creating several types of mesh, such as multiblock structured, unstructured hexahedral, unstructured tetrahedral, hybrid meshes consisting of hexahedral, tetrahedral, pyramidal and prismatic elements, triangular and quadrilateral surface meshes. In this study, the unstructured tetrahedral mesh has been employed for solving the electrochemical cell due to its high compatibility with ANSYS CFX. An important observation accentuates that the result precision of the CFD model and the solution convergence depend strongly on the quality of the mesh.

Prior to generating the mesh, the geometry has to be verified to represent a closed volume. The meshing algorithm will be unable to complete the mesh generation if there are any holes in geometry larger than the local tetras.

A very important aspect of meshing process is to assign a proper tetra size to surfaces and curves in accordance with their importance. Inadequate assignment may result in a coarse mesh in areas of interest whereas elements of minor importance have a finer mesh. The consequence would be a poor representation of the studied phenomena.

The method used to create the tetra mesh is Octree mesh. This is based on the spatial subdivision algorithm which uses larger elements of mesh where it is possible, to save computation time, but also ensuring a mesh refinement in areas of interest.

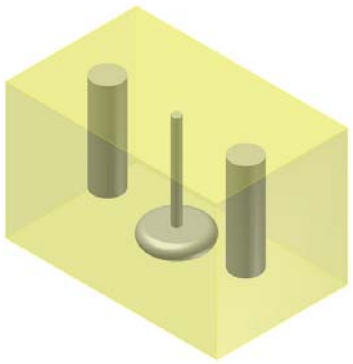

a) First design

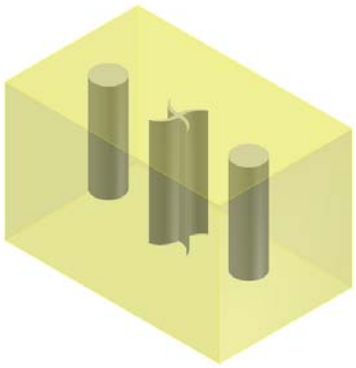

b) Second design

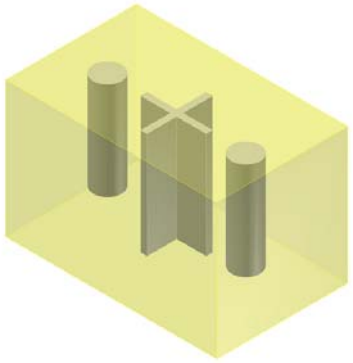

c) Final design

Figure 4.5 – Different electrochemical cell designs

a) Stirrer

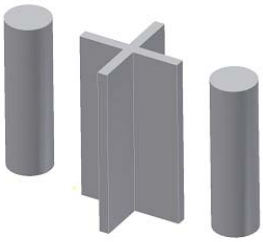

b) Stirrer and cathodes

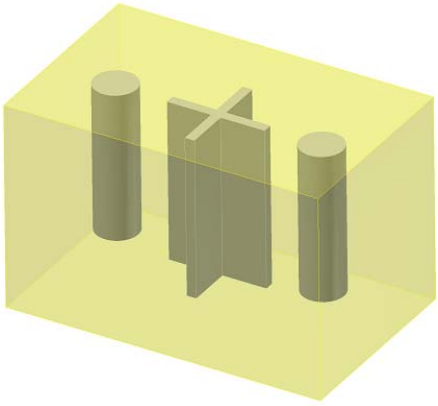

c) Electrochemical cells

Figure 4.6 – Final electrochemical cell geometry

The tetrahedral mesh for molten salt is characterized by a maximum tetra size of 10 mm, an initial tetra height of 3.5 mm and a height ratio of 1.5. For cathodes and stirrer, the tetrahedral mesh characteristics are: a maximum tetra size of 4.5 mm, an initial tetra height of 2 mm and a height ratio of 1.5.

Particular to the phenomena of interest, electrochemical deposition, special meshing features have been used. In order to represent the development of diffusion layer at molten salt – cathode interface a number of 75 prism layers have been grown from cathode wall into the molten salt for a total height of 0.9825 mm. The height of the first prism layer is 0.002 mm, the growth law is linear and the height ratio is 1.15. This approach allows computation at a very discrete level for variables of interest, mainly the variation of uranium concentration in molten salt. Figure 4.7 presents representative electrorefiner mesh details.

Table 4.9 provides a summary of the mesh characteristics for the electrorefiner.

Table 4.9 – Electrorefiner mesh characteristics

Domain	**Element type**			
	Nodes	**Tetrahedrons**	**Prisms**	**Faces**
Molten Salt	695347	583057	1159350	64250
Left Cathode	11754	57566	-	7704
Right Cathode	11766	57560	-	7754
Stirrer	36286	179058	-	25414
Total	755153	877241	1159350	105120

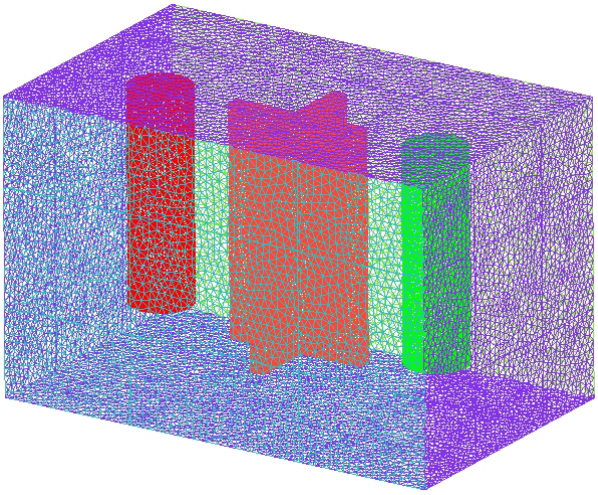

a) Electrochemical cell surface mesh

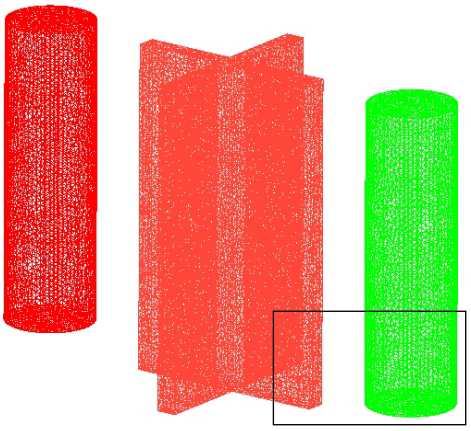

b) Stirrer and cathode surface mesh

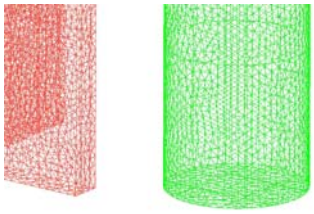

c) Surface mesh detail

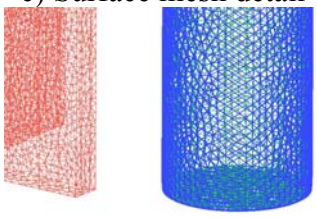

d) Cathode prism layers

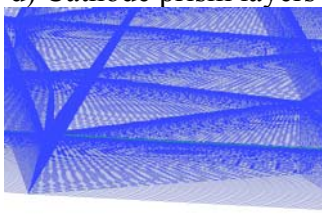

e) Prism layer detail

Figure 4.7 – Electrochemical cell mesh

4.2.2 Component Model

For this model, two components have been defined in ANSYS CFX: molten salt and uranium. Several physical characteristics have been specified for each of them, as shown in Tables 4.10 and 4.11.

Table 4.10 – Molten salt data [25]

Parameter	Value
Density [g/cm^3]	1.551
Dynamic viscosity [N·s/m^2]	0.00123
Operating temperature [K]	773

Table 4.11 – Uranium data [26]

Parameter	Value
Density [g/cm^3]	18.75
Dynamic viscosity [N·s/m^2]	0.0063
Conductivity [W/m·K]	46.3
Specific heat [J/kg·K]	146
Molar mass [g/mol]	238.03
Concentration [wt.%]	1.43

The turbulence model employed in this study is the homogeneous k-ε model. In order to determine the concentration profile of uranium in molten salt for diffusion layer thickness calculation, the volume fractions of uranium and molten salt have been specified. These were obtained from the optimum combination of element weight percent provided by the design of experiment sensitivity study.

CFD simulation solution convergence can be quantified using the Root Mean Square residual. A residual measures the difference between the left-hand-side and the right-hand-side of the equation for the investigated phenomena, at any point in space. The Root Mean Square residual is obtained by squaring all the residuals throughout the domain, calculating the mean, and then taking the square root of the mean. The maximum Root Mean Square residual for this study was less than $5 \cdot 10^{-5}$, to ensure reasonable numerical accuracy for the results.

4.2.3 Rotational Model

A sensitivity study has been performed to determine the optimum direction and magnitude of stirrer and cathode rotational velocities to ensure a uniform and very thin diffusion layer is obtained. The cathode rotational velocity considered in this study ranges between 10 rpm and 20 rpm. Also, simulations have been performed for different stirrer rotational velocities from 30 rpm to 120 rpm. The results for the combination that yielded the minimum thickness of the diffusion layer at cathode – molten salt interface are presented in Chapter 5.

4.2.4 Determination of Diffusion Layer Thickness

The goal of the CFD modeling and simulation is to accurately determine the thickness of the diffusion layer for the continuous electrorefiner. As described in Section 2.1.5, the method for determining the thickness of diffusion layer is based on the intersection of the tangent to the true uranium concentration profile at the electrode surface and the straight line extension of uranium concentration in the bulk solution. First step in implementing this method is to determine the equation of the tangent to the uranium concentration profile obtained from ANSYS CFX, near the cathode surface. Next, the uranium concentration in the bulk solution is calculated as the mean of the five uranium concentrations in the molten salt where a constant profile is achieved. Finally, the diffusion layer thickness is obtained from the intersection of the tangent with the mean value of the concentration.

Chapter 5 Results and Discussion

This chapter, divided into five parts, presents the simulation results for the continuous electrochemical processing. First part of the chapter illustrates the electrochemical modeling results obtained using REFIN code. Based on these findings the second part will elaborate on the design of experiment outcomes. Next, the CFD simulation results are given for the optimum combination of the initial element concentration and electric current obtained from the design of experiment. The fourth part presents the final results for the continuous electrorefiner, based on the diffusion layer thickness developed using ANSYS CFX. Finally, an overview of the findings is provided in the fifth part.

5.1 Electrochemical Modeling Results

Using the electrochemical cell geometry and the process parameters presented in Section 4.1, a study has been conducted to investigate the initial element concentration at anode and molten salt suitable for continuous operation of the electrorefiner.

First combination investigated consists of more uranium than plutonium at anode and molten salt. This represents category 1 in Table 4.6. A representative case for this category is summarized in Table 5.1.

Table 5.1 – Initial electrorefiner inventory for uranium extraction stage – category 1

Parameter	Value
Anode	
Initial U concentration at anode [wt.%]	10.0
Initial U mass at anode [g]	8315.82
Initial Pu concentration at anode [wt.%]	0.05
Initial Pu mass at anode [g]	41.58
Molten salt	
Initial U concentration in molten salt [wt.%]	10.0
Initial U mass in molten salt [g]	3750.24
Initial Pu concentration in molten salt [wt.%]	3.25
Initial Pu mass in molten salt [g]	1218.83
Anode + Molten salt	
Total U mass in electrorefiner [g]	12066.06
Total Pu mass in electrorefiner [g]	1260.41

Figure 5.1 illustrates changes in mass inventory in electrorefiner. In Figure 5.2 the cathode potential for each element is represented during electrorefiner operation.

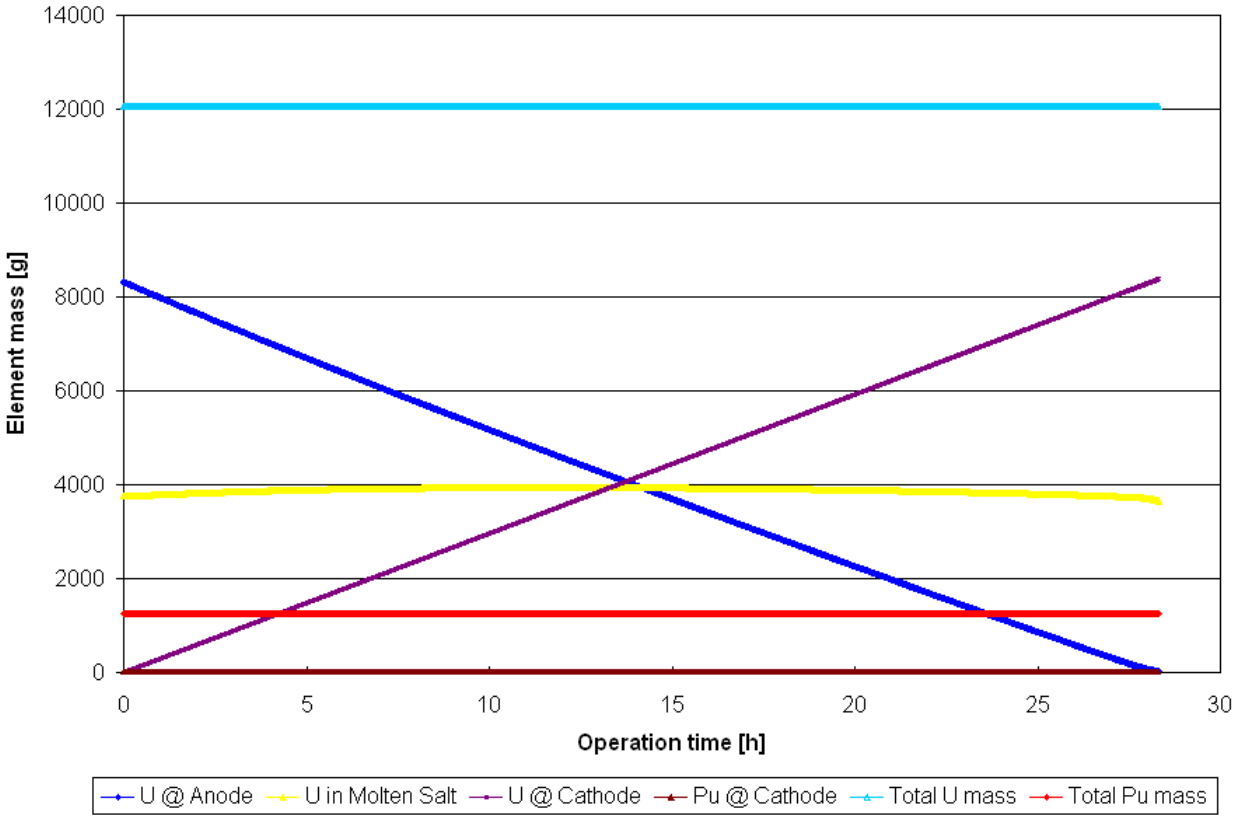

Figure 5.1 – Element mass in electrorefiner for uranium extraction stage – category 1

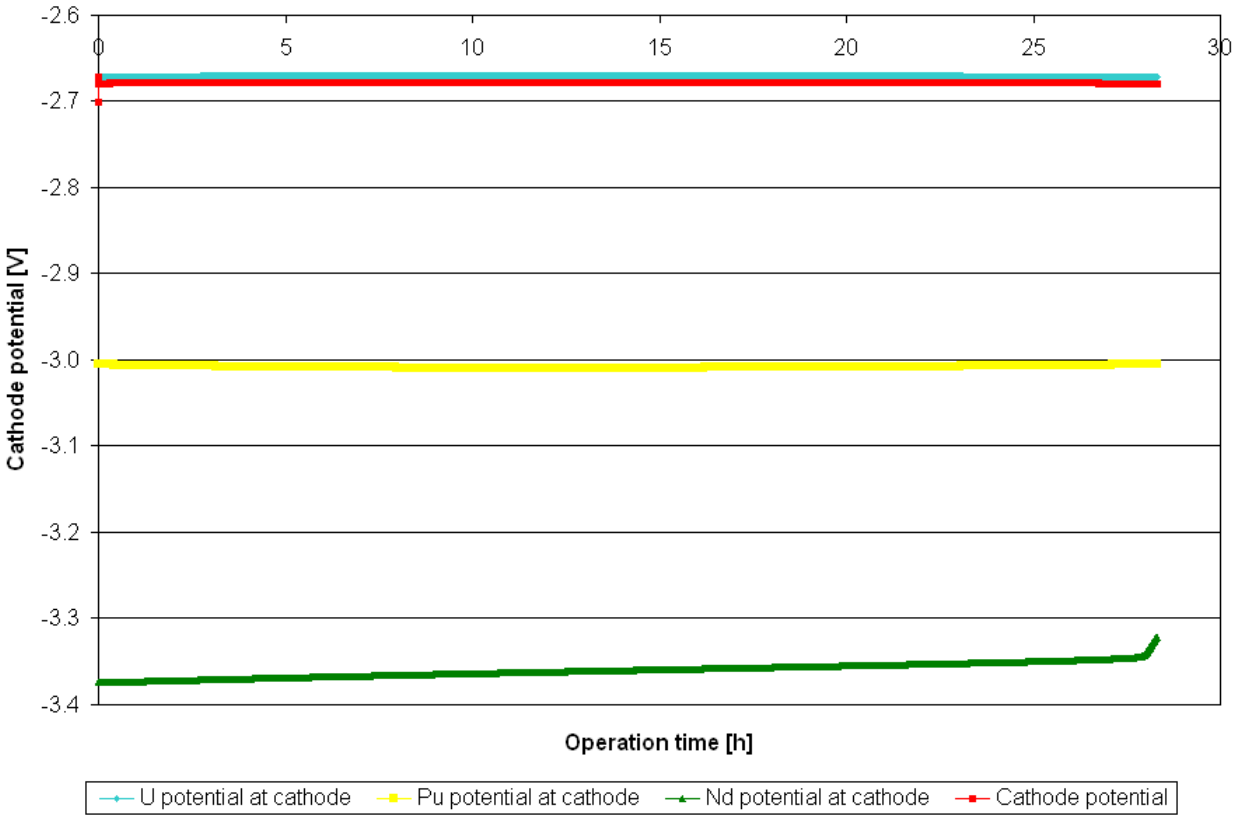

Figure 5.2 – Element cathode potential for uranium extraction stage – category 1

The results obtained for this representative case in category 1 are presented in Table 5.2.

Table 5.2 – Final electrorefiner data for uranium extraction stage – category 1

Parameter	Value
Anode	
Final U mass at anode [g]	31.63
Final Pu mass at anode [g]	10.18
Molten salt	
Final U mass in molten salt [g]	3654.24
Final Pu mass in molten salt [g]	1250.23
Cathode	
Final U mass at cathode [g]	8380.19
Final Pu mass at cathode [g]	0.0

As it can be seen from Figure 5.1 and Table 5.2 no plutonium is collected at the solid cathode during electrorefiner operation and it accumulates in molten salt. Uranium is deposited at cathode, with a rate of 2.96 g/A·h, mainly from anode and therefore the final uranium concentration in molten salt is much larger than plutonium concentration in molten salt. Figure 5.2 shows that only uranium potential at cathode is above the surface cathode potential and as a result only uranium is deposited at cathode. At the end of electrorefining operation there is still too much uranium mass in electrolyte to start plutonium deposition at cathode.

As a consequence, the operation of the electrorefiner can not be continued with plutonium extraction stage. Category 1 in Table 4.6 does not represent a feasible combination for continuous electrochemical processing.

The second combination studied has been uranium concentration at anode smaller than plutonium concentration at anode and uranium concentration in molten salt larger than plutonium concentration in molten salt. This combination represents category 2 in Table 4.6. A representative case for this category is shown in Table 5.3.

Table 5.3 – Initial electrorefiner inventory for uranium extraction stage – category 2

Parameter	**Value**
Anode	
Initial U concentration at anode [wt.%]	7.5
Initial U mass at anode [g]	6236.87
Initial Pu concentration at anode [wt.%]	10.0
Initial Pu mass at anode [g]	8315.82
Molten salt	
Initial U concentration in molten salt [wt.%]	3.25
Initial U mass in molten salt [g]	1218.83
Initial Pu concentration in molten salt [wt.%]	0.05
Initial Pu mass in molten salt [g]	18.75
Anode + Molten salt	
Total U mass in electrorefiner [g]	7455.69
Total Pu mass in electrorefiner [g]	8334.57

Figures 5.3 and 5.4 present the mass inventory changes and the element cathode potential variation during electrorefiner operation for the case illustrated in Table 5.3.

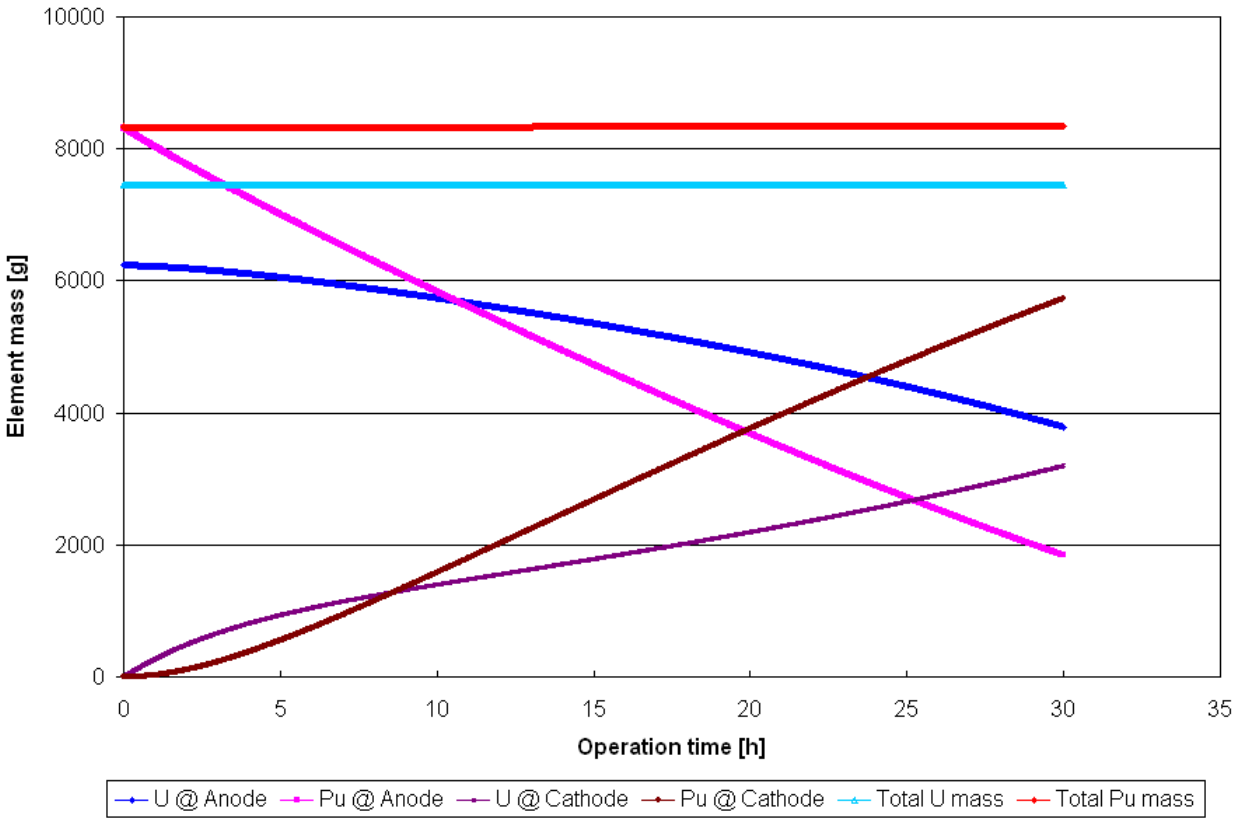

Figure 5.3 – Element mass in electrorefiner for uranium extraction stage – category 2

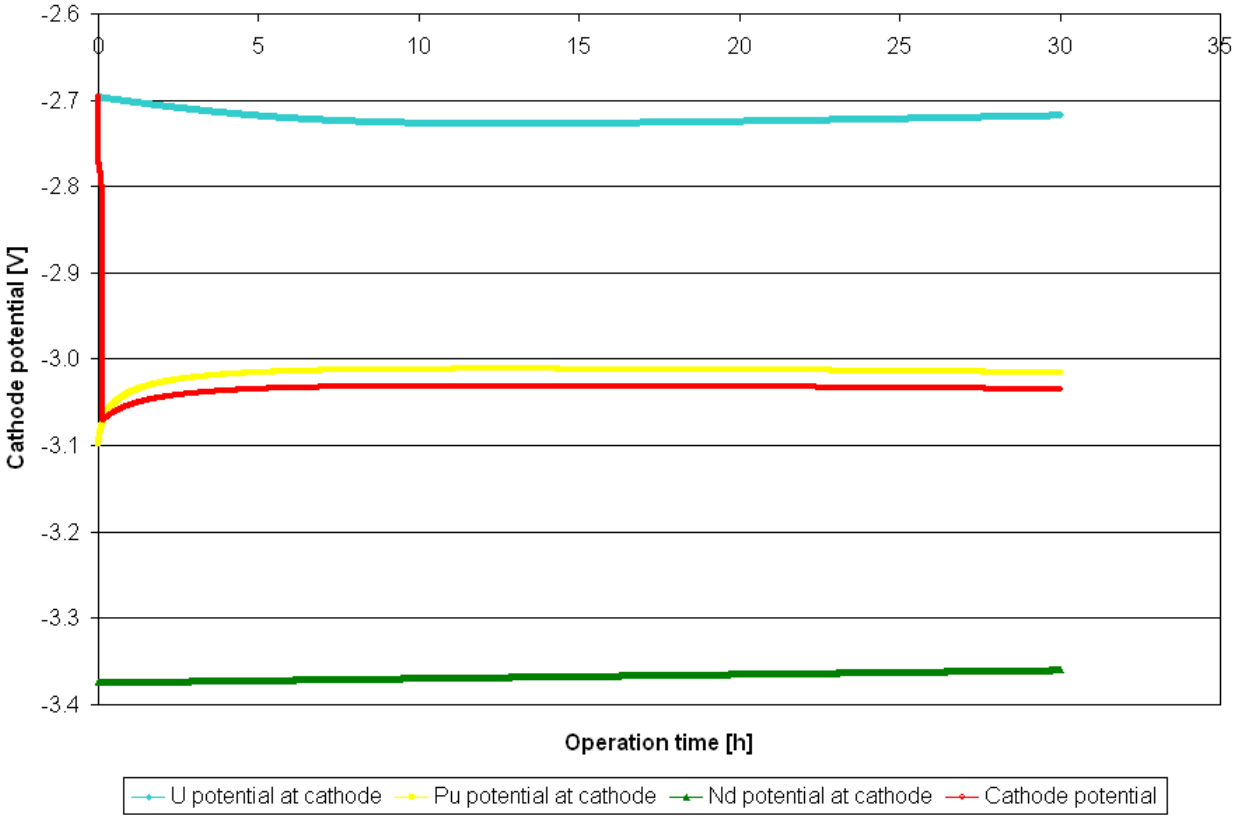

Figure 5.4 – Element cathode potential for uranium extraction stage – category 2

Table 5.4 shows the outcomes for this representative case for category 2.

Table 5.4 – Final electrorefiner data for uranium extraction stage – category 2

Parameter	Value
Anode	
Final U mass at anode [g]	3787.08
Final Pu mass at anode [g]	1838.66
Molten salt	
Final U mass in molten salt [g]	468.98
Final Pu mass in molten salt [g]	767.45
Cathode	
Final U mass at cathode [g]	3199.63
Final Pu mass at cathode [g]	5728.46

From Figure 5.3 and Table 5.4 it can be noticed that there is not enough uranium at anode, primary source of material for electrotransport and cathode deposition, to self maintain the level of electric current and thus the cathode surface potential decreases to the equilibrium potential of plutonium. This phenomenon is illustrated in Figure 5.4. As a result, plutonium deposition is initiated at solid cathode. As discussed in Chapter 2 plutonium deposition is not desired at solid cathode due to the deposit morphology. Consequently, the combinations in category 2 in Table 4.6 do not represent a feasible solution for continuous electrochemical processing.

The next combination of initial element concentrations examined has been uranium concentration at anode smaller than plutonium concentration at anode and uranium concentration in molten salt smaller than plutonium concentration in molten salt. This type of combination forms category 3 in Table 4.6. Table 5.5 summarizes a representative case for this category. Mass inventory changes and element cathode potential variation during electrorefiner operation for this case are shown in Figures 5.5 and 5.6.

Table 5.5 – Initial electrorefiner inventory for uranium extraction stage – category 3

Parameter	**Value**
Anode	
Initial U concentration at anode [wt.%]	7.5
Initial U mass at anode [g]	6236.87
Initial Pu concentration at anode [wt.%]	10.0
Initial Pu mass at anode [g]	8315.82
Molten salt	
Initial U concentration in molten salt [wt.%]	3.25
Initial U mass in molten salt [g]	1218.83
Initial Pu concentration in molten salt [wt.%]	7.5
Initial Pu mass in molten salt [g]	2812.68
Anode + Molten salt	
Total U mass in electrorefiner [g]	7455.69
Total Pu mass in electrorefiner [g]	11128.50

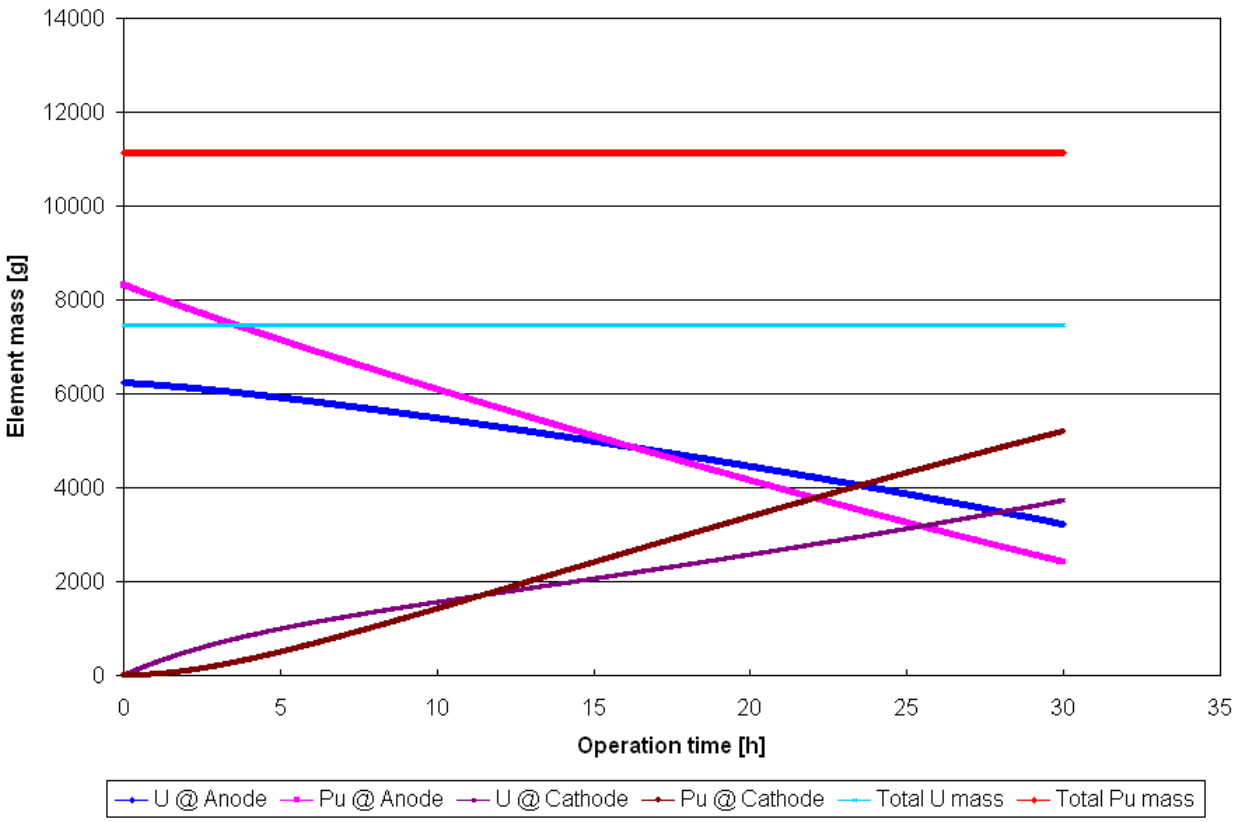

Figure 5.5 – Element mass in electrorefiner for uranium extraction stage – category 3

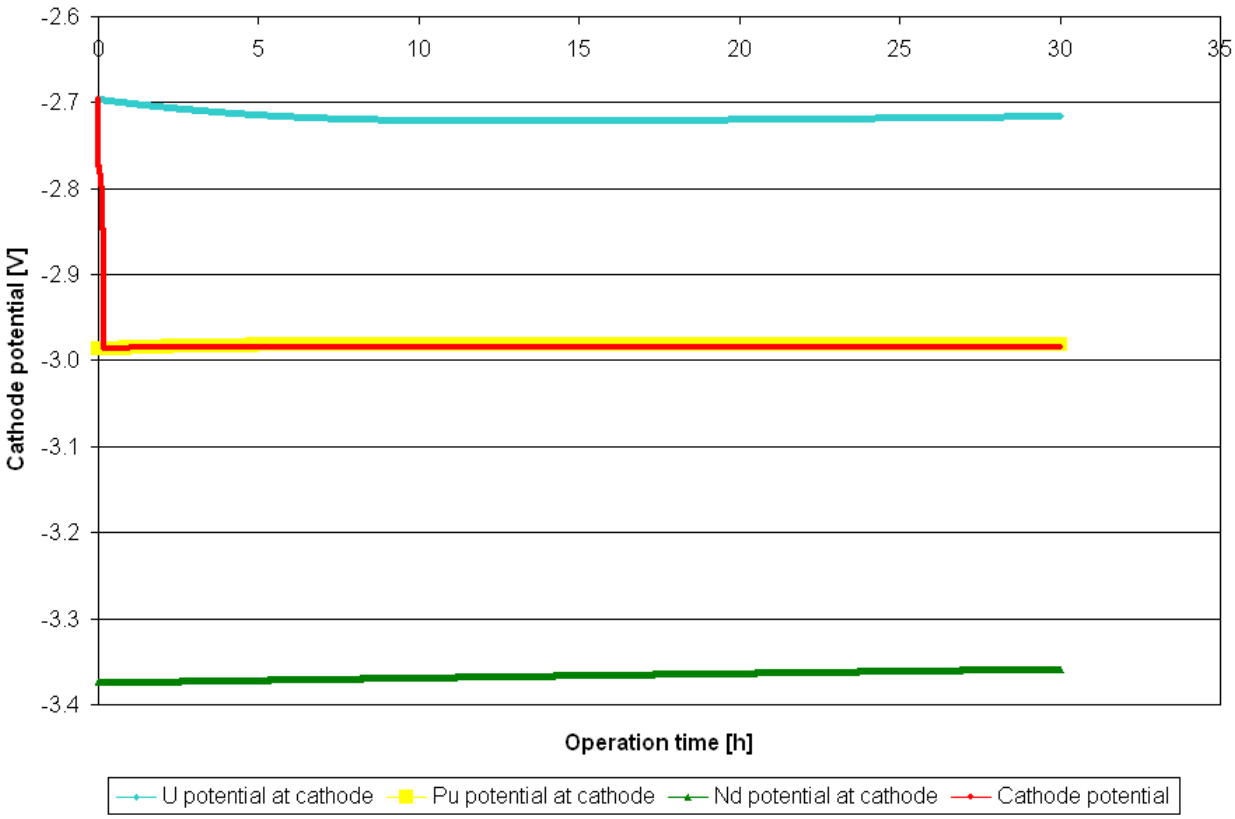

Figure 5.6 – Element cathode potential for uranium extraction stage – category 3

The findings for this case are provided in Table 5.6. Similar with the previous case investigated, the mass of uranium at anode is not sufficient to keep the level of electric current in the electrorefiner and accordingly the cathode surface potential decreases to the equilibrium potential of plutonium. This fact is shown in Figure 5.6.

Table 5.6 – Final electrorefiner data for uranium extraction stage – category 3

Parameter	**Value**
Anode	
Final U mass at anode [g]	3218.52
Final Pu mass at anode [g]	2412.83
Molten salt	
Final U mass in molten salt [g]	504.92
Final Pu mass in molten salt [g]	3524.23
Cathode	
Final U mass at cathode [g]	3732.25
Final Pu mass at cathode [g]	5191.44

As explained in the previous case, combinations in category 3 in Table 4.6 do not represent a viable answer for continuous electrochemical processing operation.

Another combination of initial element concentrations explored in this study has been a higher uranium concentration at anode than plutonium concentration and uranium concentration in molten salt lower than plutonium concentration in molten salt.

This combination exhibits the closest resemblance with the anode charge composition presented in Table 4.5 and represents category 4 in Table 4.6. Because this combination of initial element concentration has proven to be suitable for continuous electrochemical operation during the sensitivity study performed on 36 different concentrations, a further refinement was performed on both element concentration and electric current to ensure continuous electrochemical operation is achieved. This is presented in Table 5.7.

Table 5.7 – Initial electrorefiner inventory for uranium extraction stage – category 4

Parameter	**Value**
Anode	
Initial U concentration at anode [wt.%]	9.1
Initial U mass at anode [g]	7567.40
Initial Pu concentration at anode [wt.%]	0.1
Initial Pu mass at anode [g]	83.16
Molten salt	
Initial U concentration in molten salt [wt.%]	1.2
Initial U mass in molten salt [g]	450.03
Initial Pu concentration in molten salt [wt.%]	1.5
Initial Pu mass in molten salt [g]	562.54
Anode + Molten salt	
Total U mass in electrorefiner [g]	8017.43
Total Pu mass in electrorefiner [g]	645.70
Electric current [A]	30.0

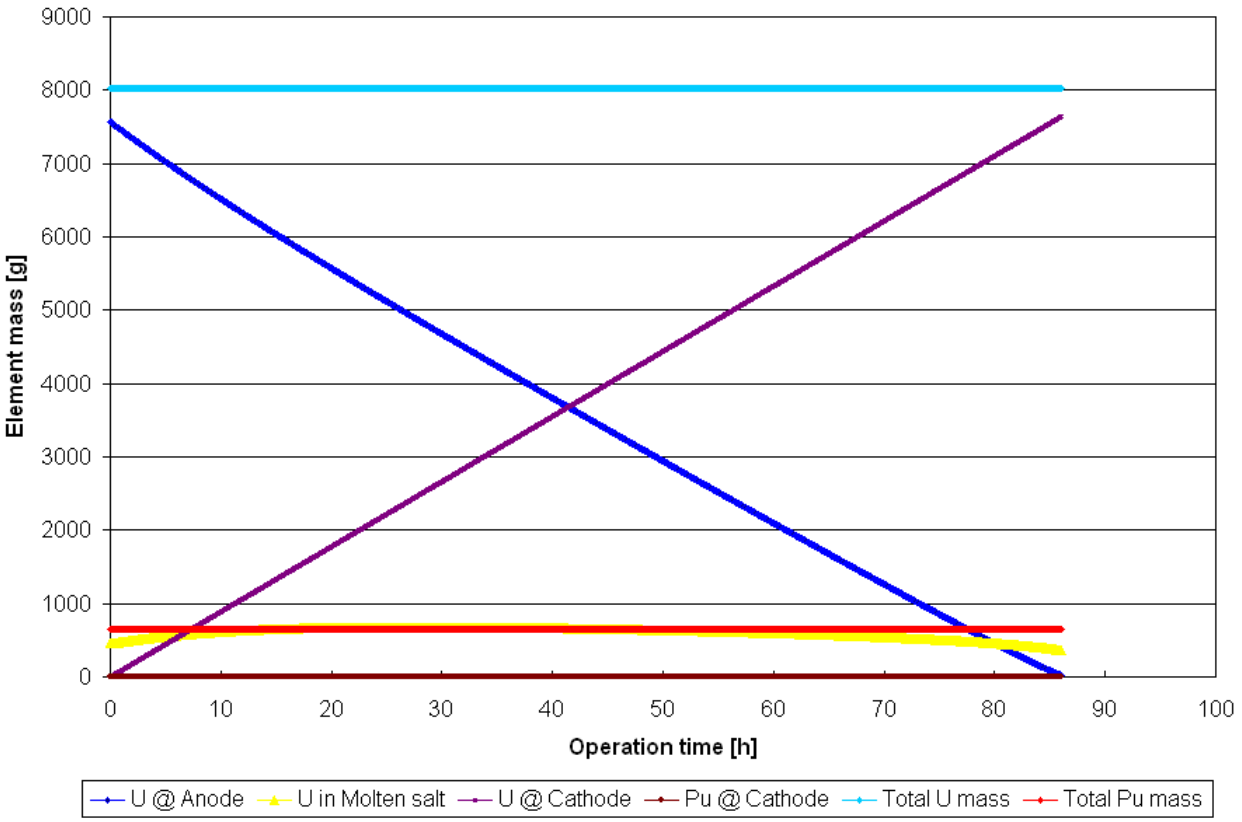

Figure 5.7 – Element mass in electrorefiner for uranium extraction stage – category 4

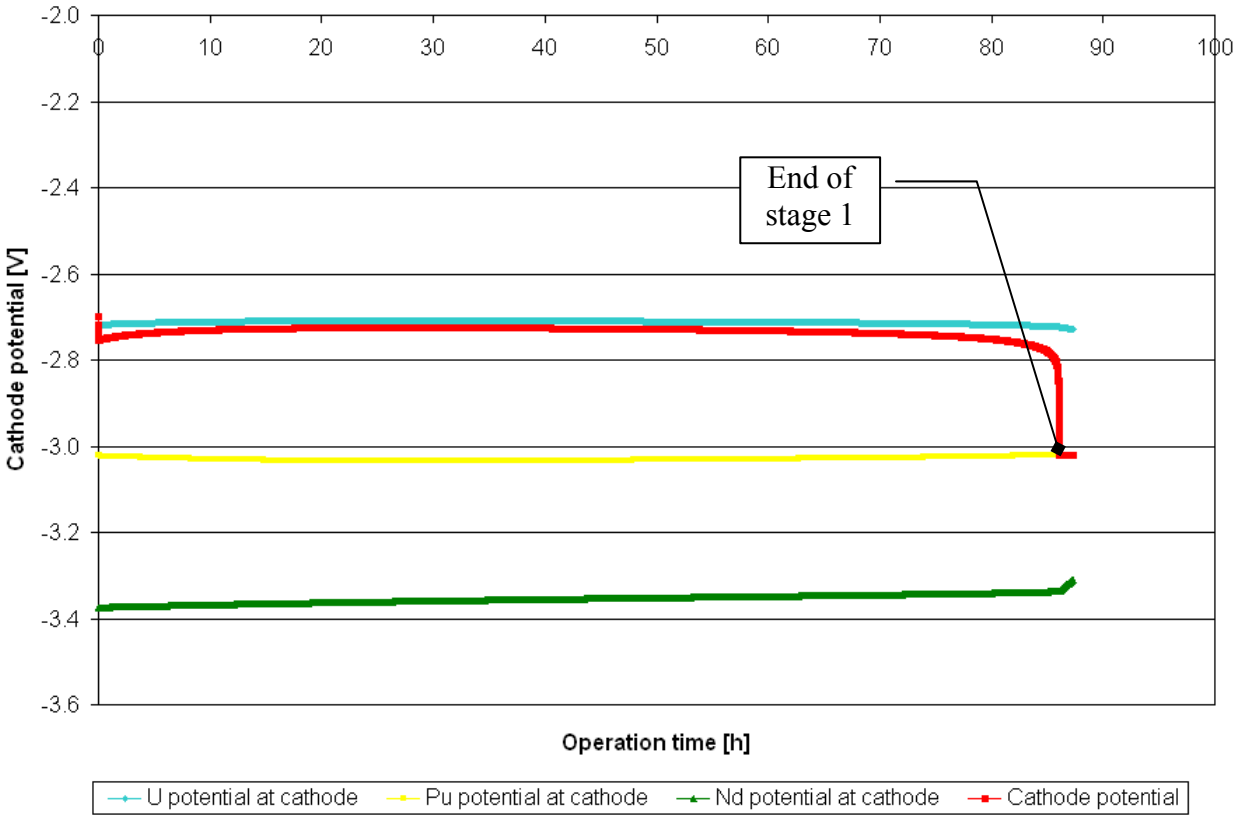

Figure 5.8 – Element cathode potential for uranium extraction stage – category 4

As it can be seen in Figure 5.8, only uranium cathode potential is above the surface cathode potential and therefore only uranium is extracted at solid cathode in first stage. This phenomenon is also illustrated in Figure 5.7 (brown line is zero). At the end of first stage simulation the mass of uranium at the anode is not sufficient to keep the level of electric current and thus the surface cathode potential decreases to the equilibrium potential of plutonium. This moment represents the end of the uranium extraction stage. As shown in Table 5.7, this simulation was performed for initial element concentration lower than other cases presented in this section and consequently the level of the applied electric current is also lower.

Another important observation represents the fact that uranium concentration in molten salt (yellow line in Figure 5.7) at the end of first stage is below the plutonium concentration in molten salt at end of first stage (red line in Figure 5.7). Quantitatively, uranium mass in molten salt is 357.3 g whereas plutonium mass in molten salt is 626.66 g. This allows simultaneous extraction of plutonium and uranium at liquid cadmium cathode in the second stage. Uranium and plutonium extraction stage is built on the final data obtained from the first stage, as seen in Table 5.8.

In the second stage, the mass of uranium at liquid anode is given by the amount of material dropped of the solid cathode mandrel during the first stage. The small amount of plutonium in the liquid cathode results from the role of intermediate electrode of cadmium pool during the operation of first stage. Consequently, the level of electric current is low, in equilibrium with the mass of material at anode.

As presented in Figure 5.9 both uranium and plutonium are recovered at liquid cadmium cathode (violent and brown lines). Moreover, Figure 5.10 illustrates that no pure plutonium is collected at cathode but a mixture of elements. The cathode surface potential (red line in Figure 5.10) decreases immediately below the equilibrium potential of neodymium, uranium and plutonium.

Table 5.8 – Initial electrorefiner data for uranium and plutonium extraction stage

Parameter	**Value**
Anode	
Initial U mass at anode [g]	83.16
Initial Pu mass at anode [g]	16.63
Molten salt	
Initial U mass in molten salt [g]	357.30
Initial Pu mass in molten salt [g]	626.66
Anode + Molten salt	
Total U mass in electrorefiner [g]	440.46
Total Pu mass in electrorefiner [g]	643.29
Electric current [A]	2.0

This simulation points out that an initial uranium concentration higher than plutonium at anode and an initial plutonium concentration in molten salt higher than uranium represents a functional combination for continuous electrorefiner operation. This is further refined to improve recovery efficiency and operation time.

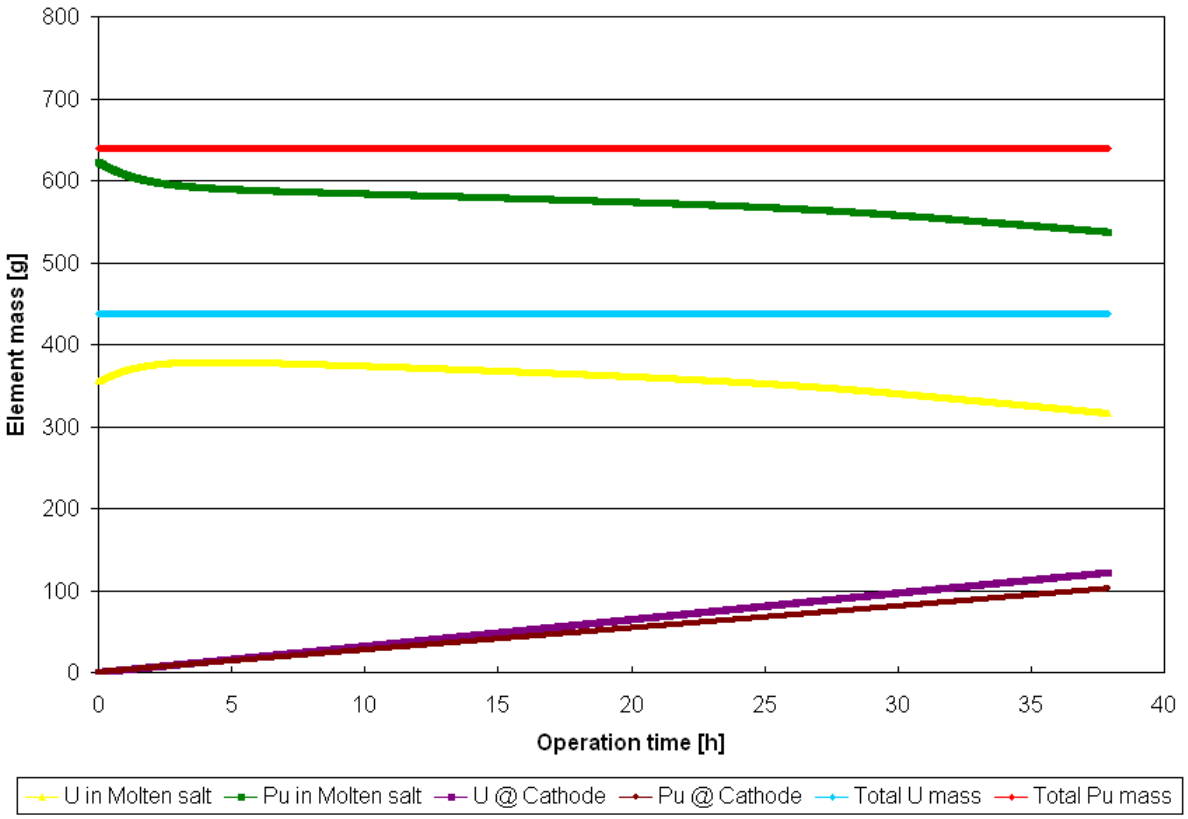

Figure 5.9 – Element mass in electrorefiner for uranium and plutonium extraction stage – category 4

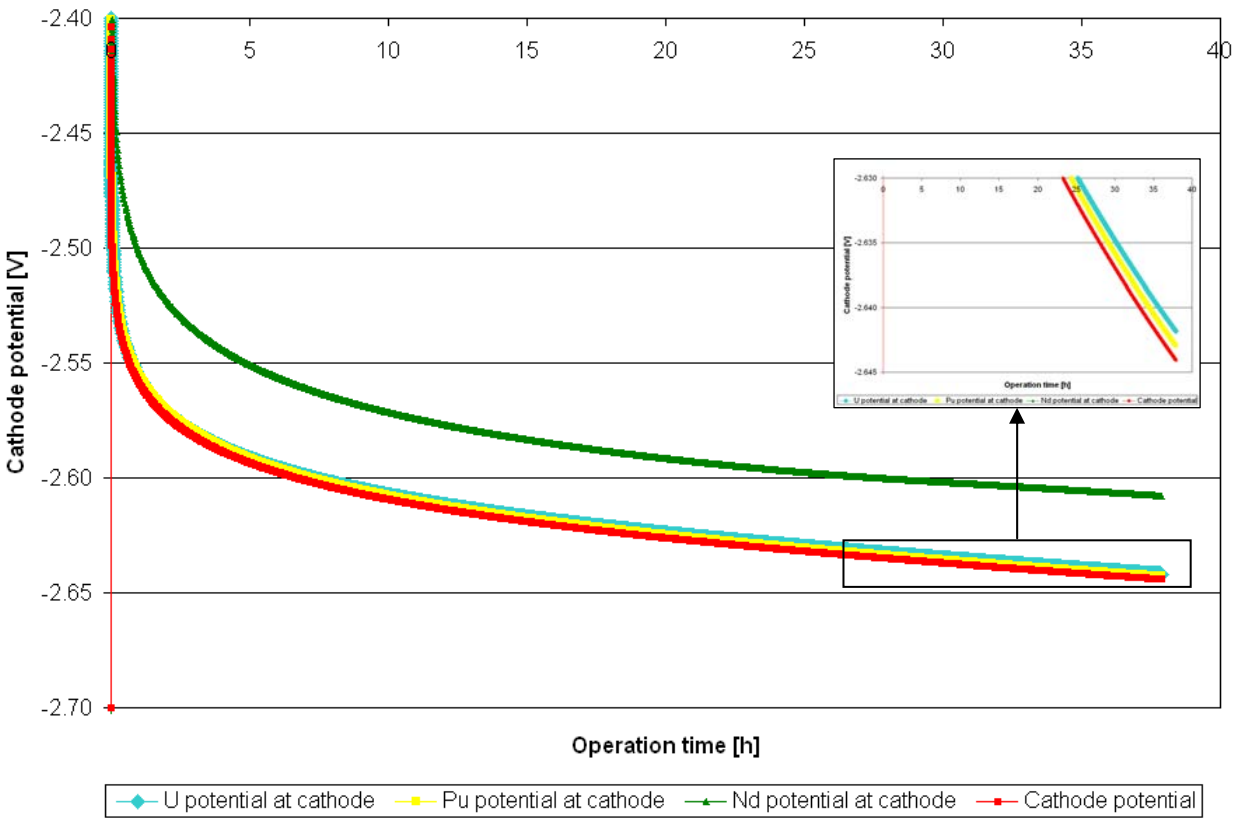

Figure 5.10 – Element cathode potential for uranium and plutonium extraction stage – category 4

5.2 Design of Experiment Results

A design of experiment was performed using the functional combination of initial element concentrations at anode and molten salt obtained from the electrochemical study presented in the previous section. The input variable space that respects this combination was presented in Table 4.7. The detailed results for the Latin Hypercube design with 30 runs presented in Table 4.8 are provided in Tables A.1, A.2 and A.3 in Appendix A. Table A.1 contains the results for the first stage of extraction and Table A.2 gives the results for the second stage. Table A.3 provides the recovery efficiencies and operation time for all 30 runs. A discussion of the results is provided below.

As presented in Chapter 2, the mass of material transported from anode to cathode is directly proportional to the electric current. As electric current increases more mass is deposited at cathode per hour. At the same time, recovery efficiency decreases as the electric current increases. Consequently, a balance between the operation time and recovery efficiency has to be achieved. Figure 5.11 shows the influence of electric current and element concentration on the operation time and recovery efficiency for the first stage. Next, Figure 5.12 illustrates total operation time and total recovery efficiency as function of electric current and element concentration.

Figure 5.11 shows that operation time for first stage is minimized for higher electric current values while the uranium recovery efficiency reaches its maximum for lower values of electric current.

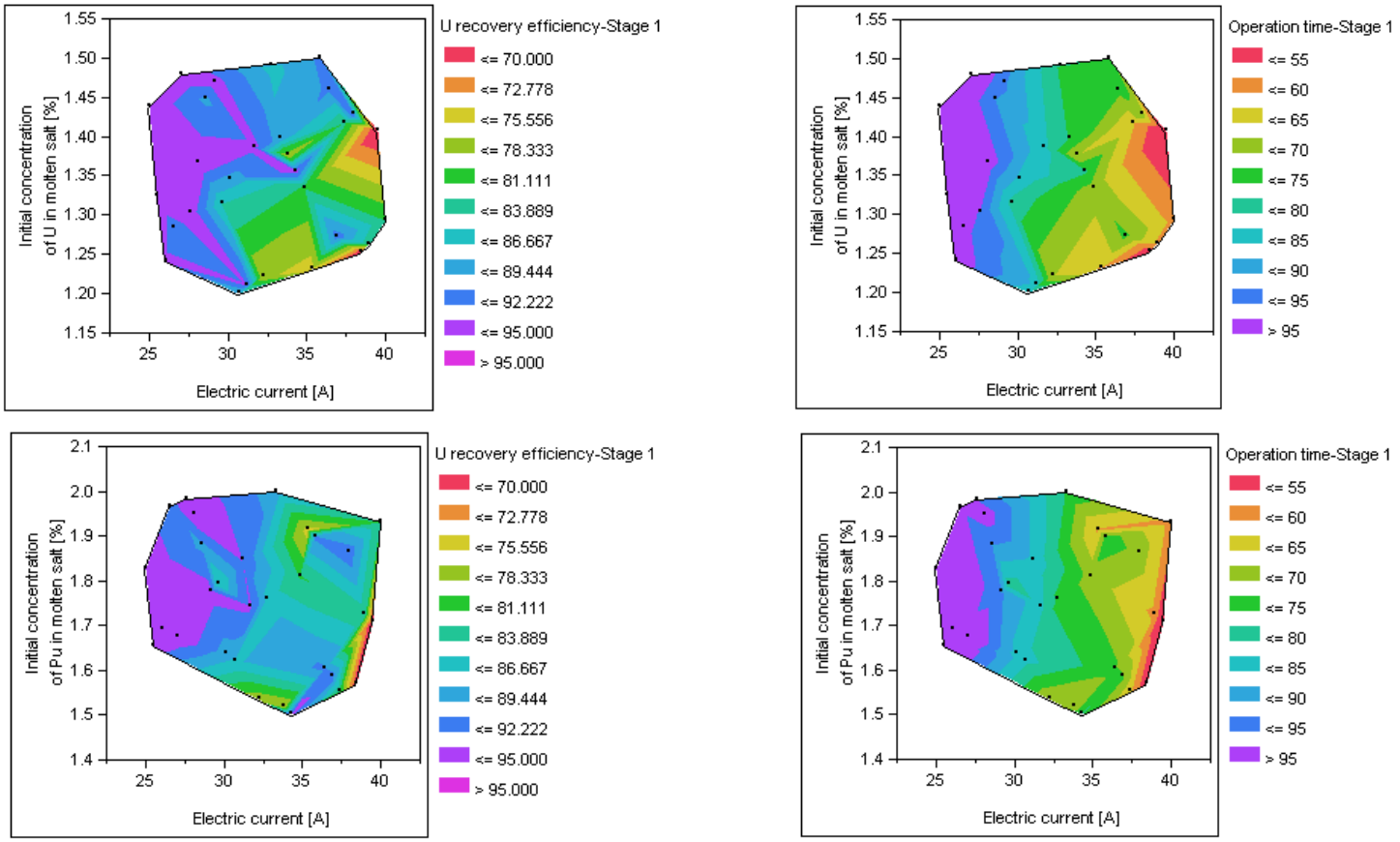

Figure 5.11 – First stage recovery efficiency and operation time as function of electric current and element concentration

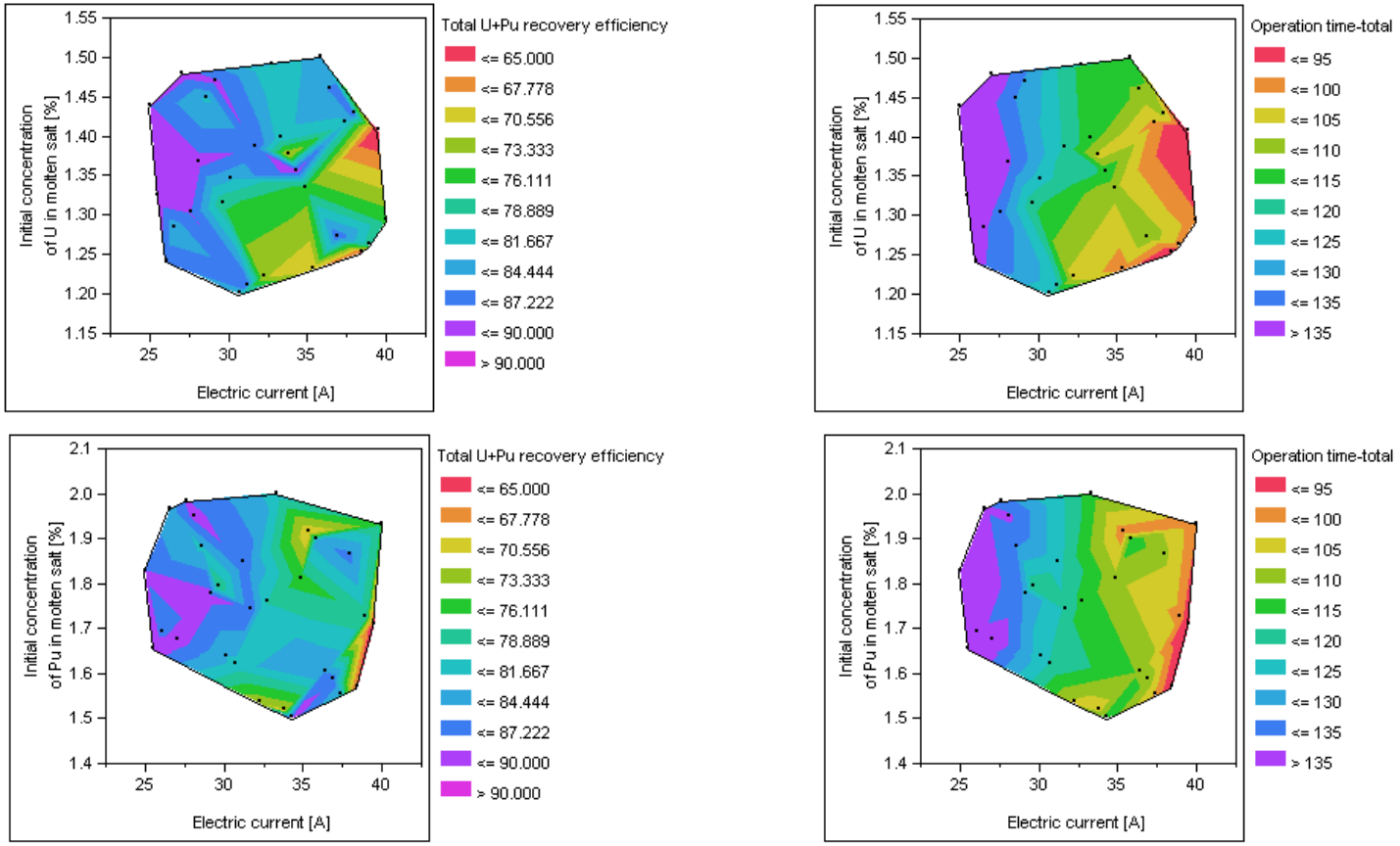

Figure 5.12 – Overall recovery efficiency and operation time as function of electric current and element concentration

Similarly, total operation time and overall recovery efficiency increase when electric current decreases, as seen in Figure 5.12. The optimum combination of initial concentrations and electric current has to reach equilibrium between operation time and efficiency. This is illustrated in Figure 5.13 for first stage and Figure 5.14 for overall operation.

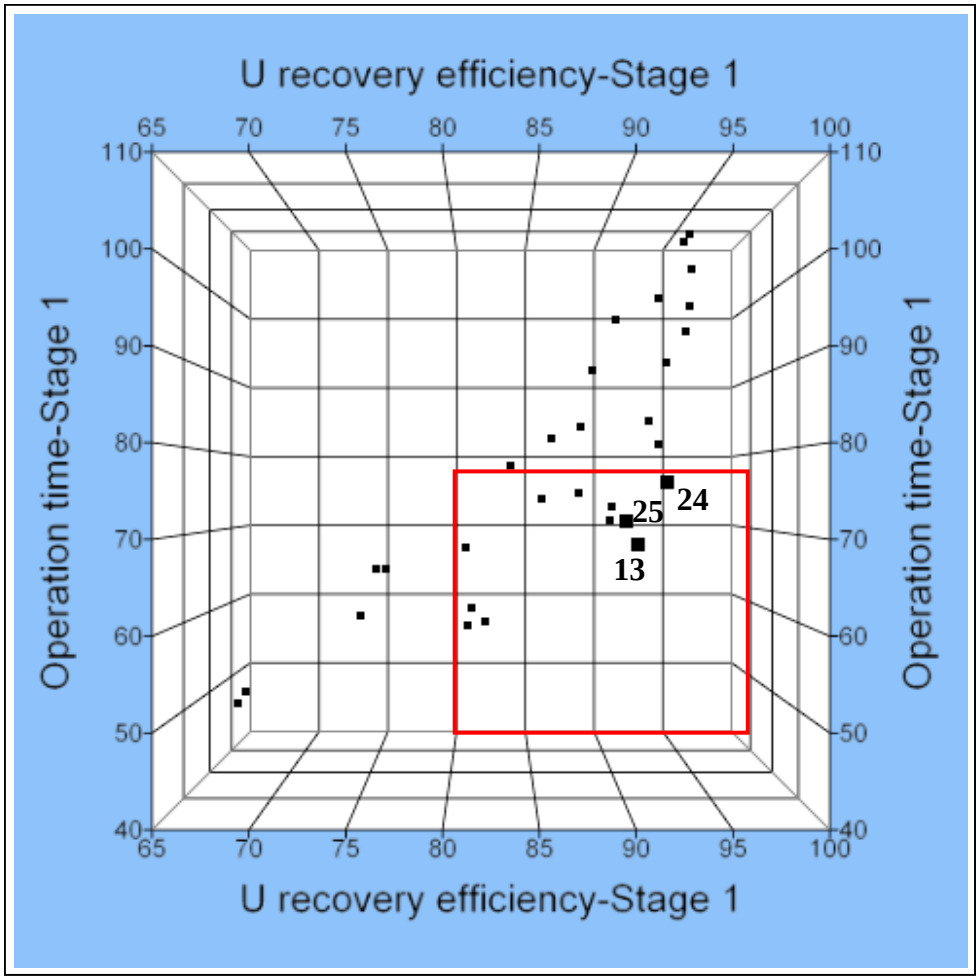

Figure 5.13 – First stage recovery efficiency vs. operation time

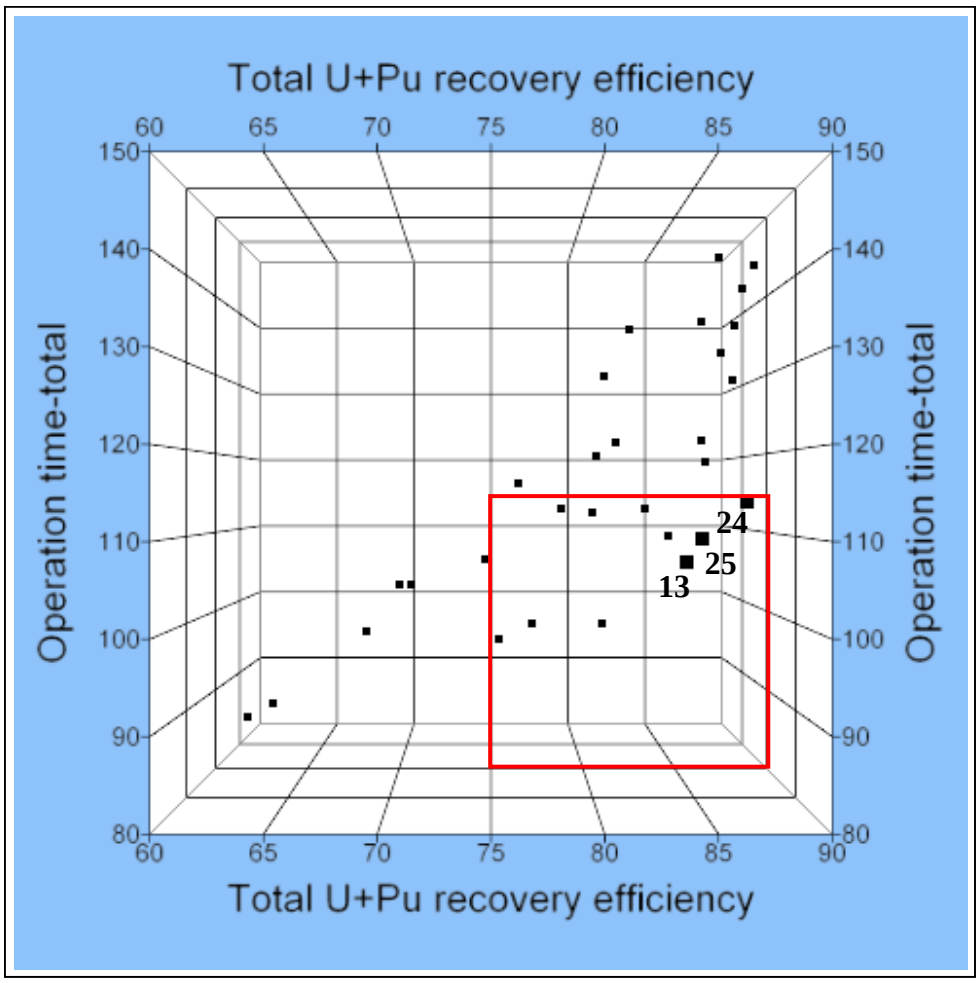

Figure 5.14 – Global recovery efficiency vs. total operation time

As it can be observed in Figures 5.13 and 5.14 the most favorable combinations of the design of experiment that minimize the operation time and maximize the recovery efficiency are given by runs 13, 24 and 25 from Table 4.8. Table 5.9 summarizes these results. Detailed results are provided in Appendix A.

Table 5.9 – Results summary for design of experiment

Run	U recovery efficiency for stage 1 [%]	Operation time for stage 1 [h]	Total U+Pu recovery efficiency [%]	Total operation time [h]
13	91.6	68.26	85.7	106.3
24	93.4	76.01	88.9	114.0
25	90.9	71.16	86.5	109.1

Based on these results, it is observed that run 13 has the minimum operation time, both for total operation and first stage. For the first stage, recovery efficiency of run 13 is 2 % less than the efficiency of run 24 but the operation time is 11 % shorter than the operation time of run 24. For the overall operation, run 13 efficiency is 4 % lower than the efficiency of case 24 but the operation time is 7 % shorter than that of run 24.

5.3 CFD Modeling Results

Several stirrer designs have been investigated to develop a minimum diffusion layer thickness uniformly distributed around the cathode surface. These designs have been illustrated in Figure 4.5. As described in Section 4.2.1, first stirrer design has not provided sufficient forced convection for molten salt and uranium and a diffusion layer of preferred characteristics does not develop at the cathode surface. Results for this case are shown in Figure 5.15.

a) First stirrer design

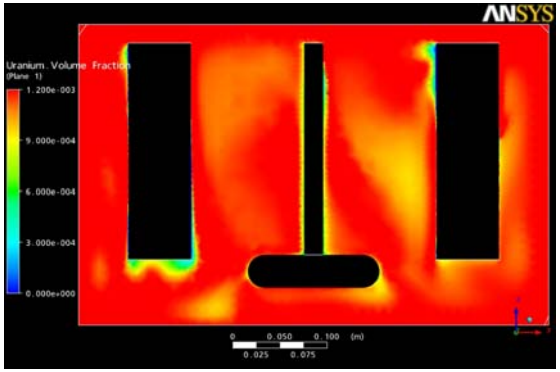

b) U volume fraction in molten salt

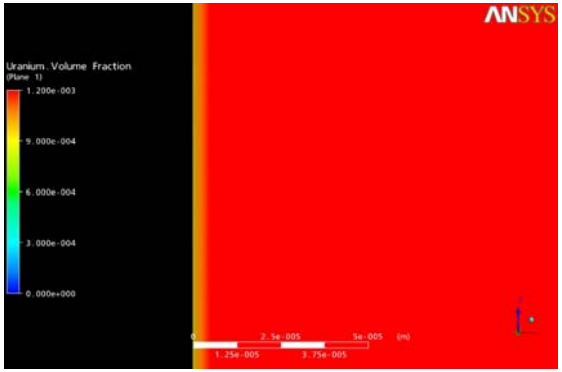

c) U volume fraction at left cathode – molten salt interface

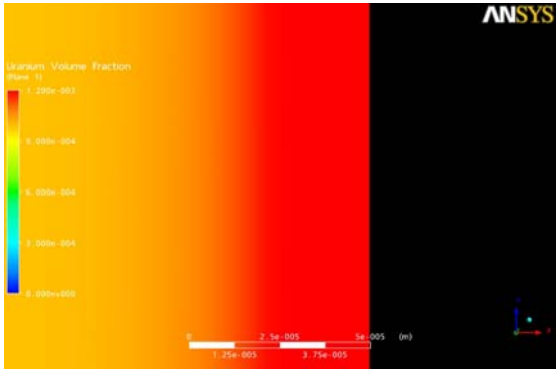

d) U volume fraction at right cathode – molten salt interface

Figure 5.15 – U volume fraction in molten salt for first stirrer design

Figure 5.15.b) illustrates uranium volume fraction in molten salt. The red color represents the maximum uranium concentration in the bulk solution. Uranium concentration at the cathode – molten salt interface is presented in Figures 5.15.c) and 5.15.d). It is observed that uranium concentration at cathode surface is equal to the value in the bulk solution and thus no diffusion layer is developed at cathode – molten salt interface.

Another stirrer design was developed to achieve a better mixing and diffusion layer. This was presented in Table 4.5.b). The CFD results for this design are given in Figure 5.16. For this case, uranium concentration in bulk solution does not reach a constant value as seen in Figure 5.16.b). The acceleration due to stirrer rotational velocity establishes areas depleted of uranium at the top and bottom of the cathodes. Development of the diffusion layer in these areas is impeded.

A further refinement on the stirrer design and parameters has been performed to achieve the desired diffusion layer thickness. Different rotational velocities, from 30 rpm to 120 rpm, have been applied to the final stirrer design, shown in Figure 4.5.c). The results for the stirrer rotational velocity of 30 rpm are presented in Figures 5.17. Next, Figure 5.18 illustrates the findings for 120 rpm stirrer rotational velocity. Two REFIN cells (left and right) have been simulated simultaneously using ANSYS CFX to ensure a minimum diffusion layer thickness is obtained for both cathodes.

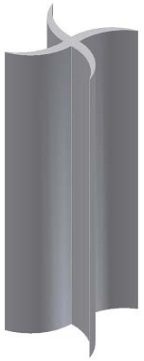

a) Second stirrer design

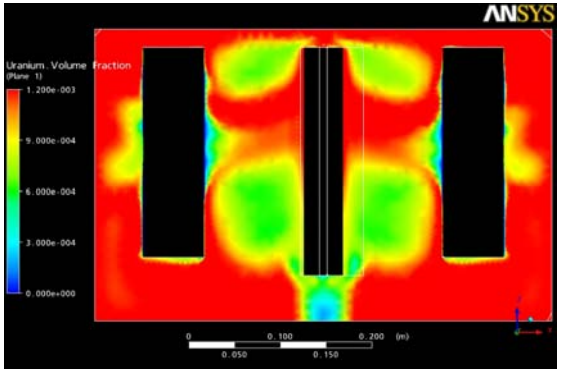

b) U volume fraction in molten salt

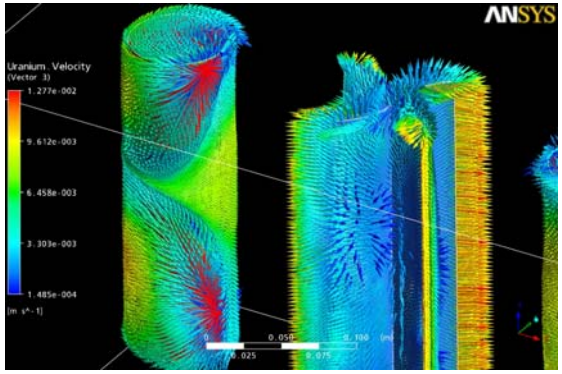

c) U velocity on left cathode – molten salt interface

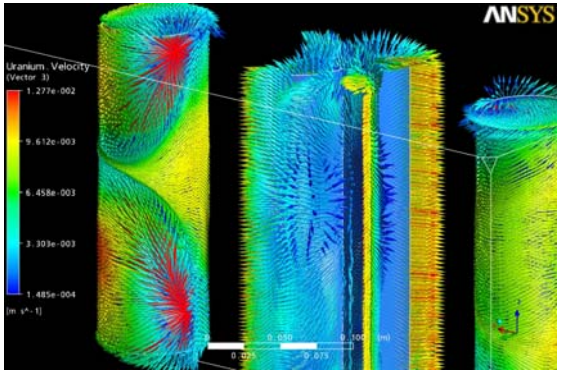

d) U velocity on right cathode – molten salt interface

Figure 5.16 – U volume fraction in molten salt for second stirrer design

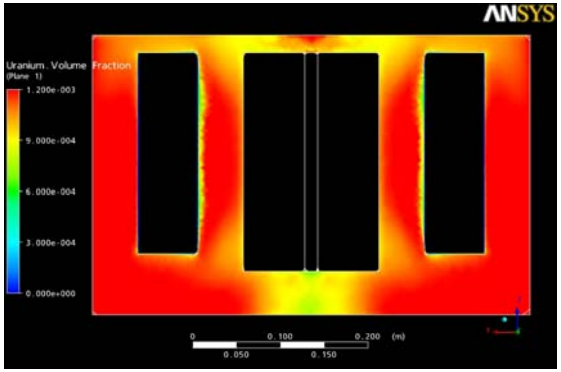

a) U volume fraction in molten salt

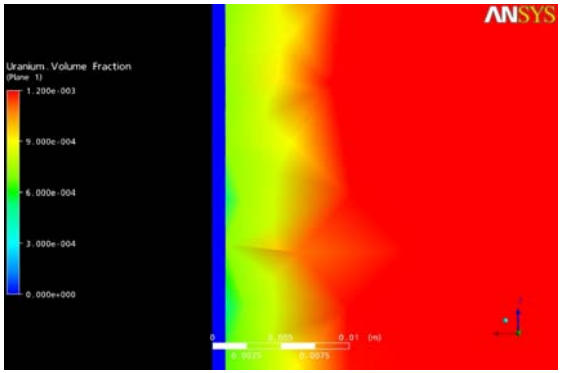

b) U volume fraction at left cathode for 30 rpm

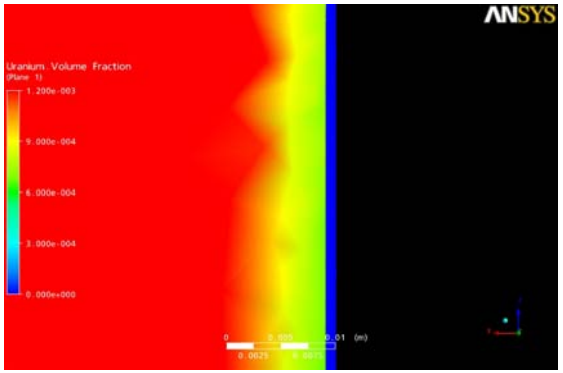

c) U volume fraction at right cathode for 30 rpm

Figure 5.17 – U volume fraction in molten salt for final stirrer design at 30 rpm

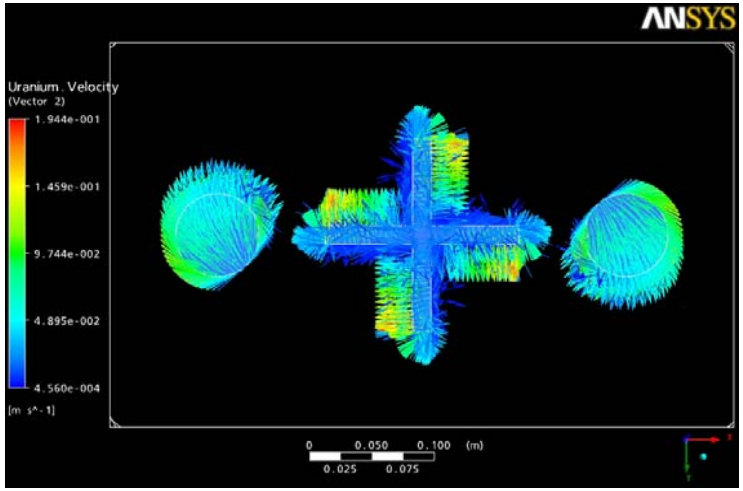

a) U velocity on cathodes and stirrer – bottom view

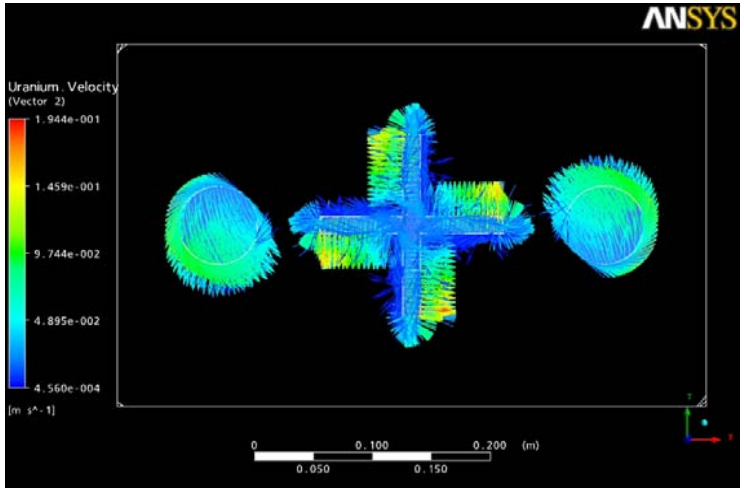

b) U velocity on cathodes and stirrer – top view

Figure 5.18 – U velocity on cathodes and stirrer for final stirrer design at 120 rpm

A rotational velocity of 30 rpm for stirrer does not provide adequate forced convection and therefore the diffusion layer developed at cathode – molten salt interface is inherently large. This phenomenon can be seen in Figure 5.17.b) and c). For the stirrer rotational velocity of 120 rpm a better mixing is achieved for uranium and molten salt. However, the molten salt is accelerated by the stirrer and this results in areas depleted of uranium along the cathode height. This fact is illustrated in Figure 5.18 by plotting uranium velocity at cathode – molten salt interface. This analysis indicates that a balance between the strong forced convection needed to develop a very thin diffusion layer at cathode – molten salt interface and a moderate stirrer rotational velocity that allows suppressing areas of depleted uranium on cathodes has to be reached.

As a consequence, a clockwise rotational velocity of 60 rpm has been employed for the stirrer. The cathodes are rotated counterclockwise at 20 rpm. The CFD results for this case are presented in the following figures. A strong forced convection is insured by stirrer and cathodes, as seen in Figure 5.19.b), which creates adequate hydraulic conditions for the electrochemical cell. The uranium concentration in bulk solution is constant and equal to its maximum value but at the electrode surface the uranium concentration decreases to zero.

Thus, a very thin diffusion layer, approximately 0.02 mm, is obtained at cathode – molten salt interface. This is illustrated in Figure 5.20 for left cathode and Figure 5.21 for right cathode.

A precise determination of the diffusion layer thickness has been performed for various points along the cathode height, using the method described in Section 4.2.4. Besides a very thin diffusion layer, this design also provides a uniform uranium velocity at cathode surfaces which suppresses the depleted uranium areas, as illustrated in Figure 5.22.

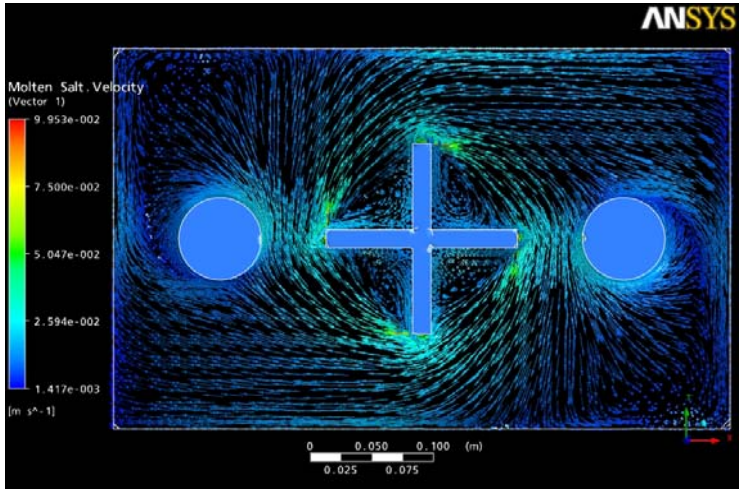

a) Molten salt velocity vector profile

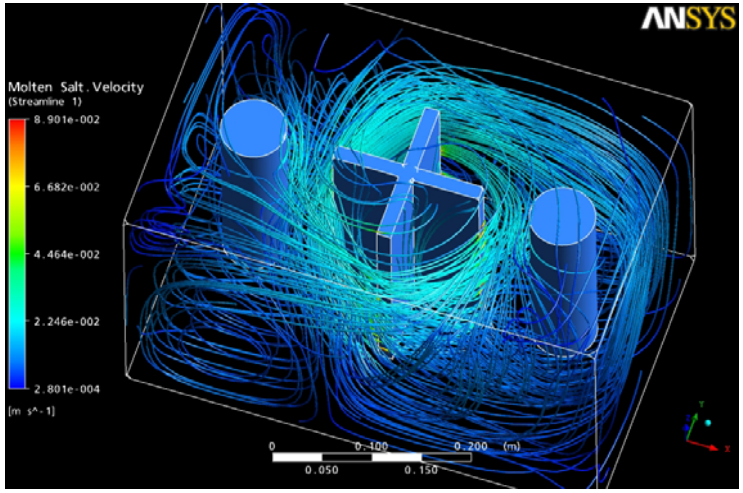

b) Molten salt velocity streamlines

Figure 5.19 – Molten salt velocity profile for final stirrer design at 60 rpm stirrer rotational velocity

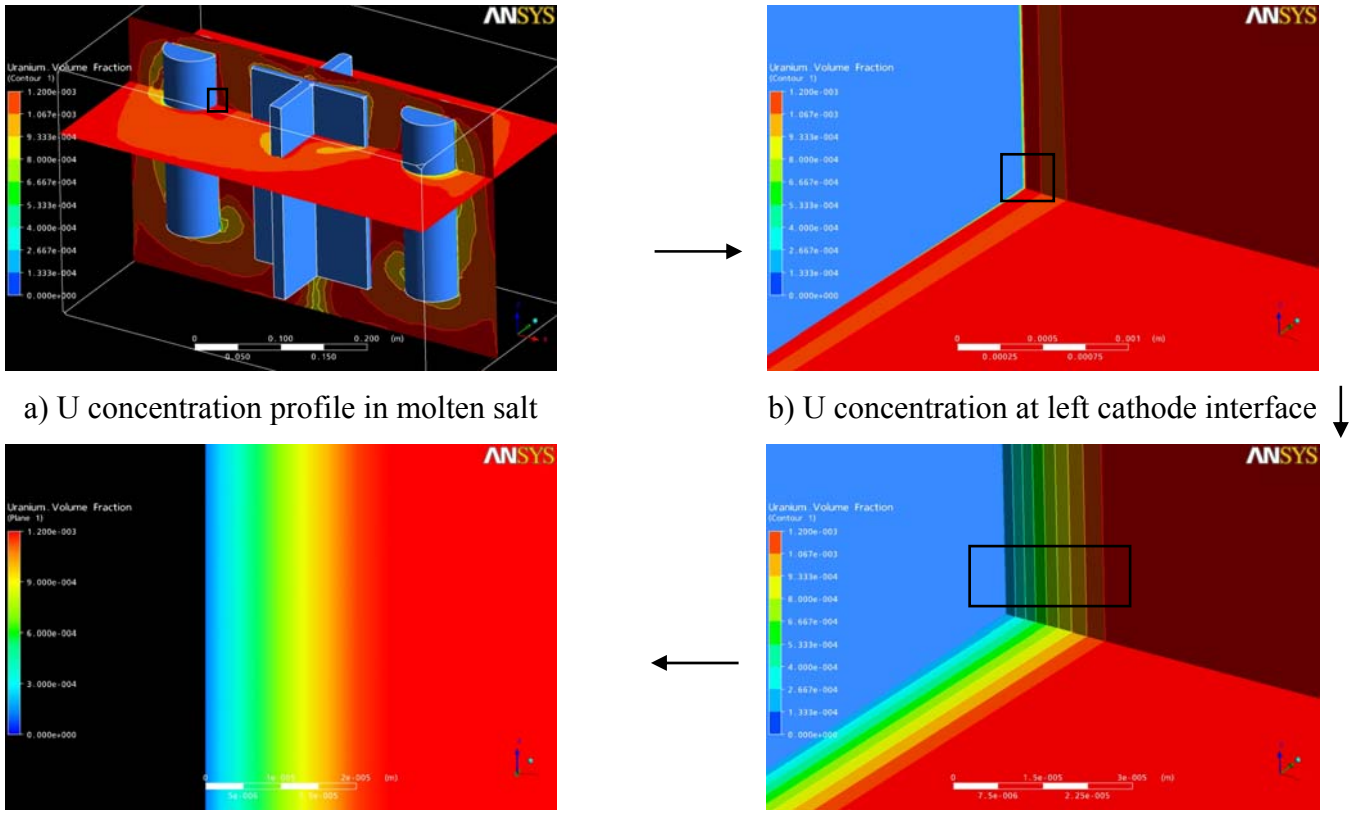

a) U concentration profile in molten salt

b) U concentration at left cathode interface

d) Diffusion layer at left cathode

c) U concentration at left cathode interface - detail

Figure 5.20 – Diffusion layer at left cathode for 60 rpm stirrer rotational velocity

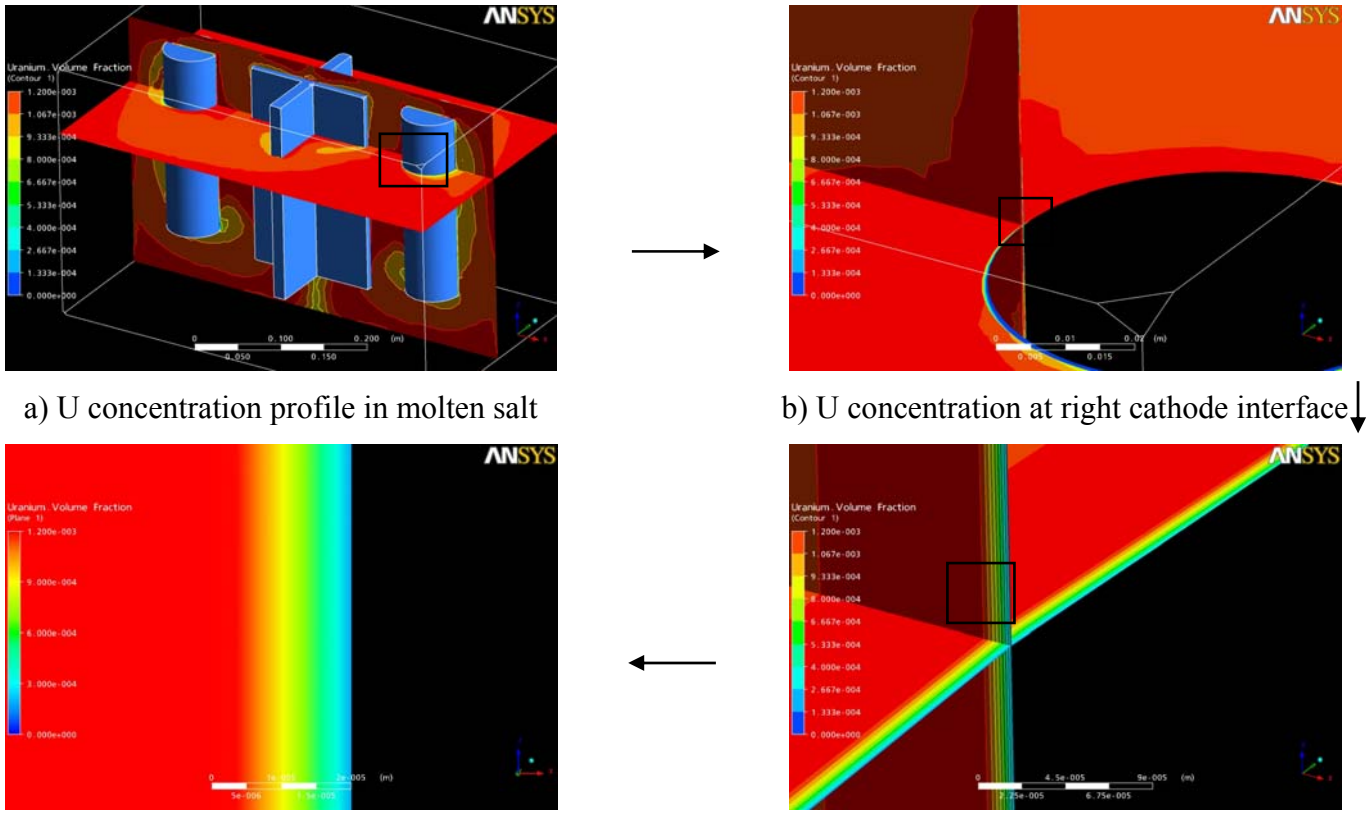

a) U concentration profile in molten salt

b) U concentration at right cathode interface

d) Diffusion layer at right cathode

c) U concentration at right cathode interface - detail

Figure 5.21 – Diffusion layer at right cathode for 60 rpm stirrer rotational velocity

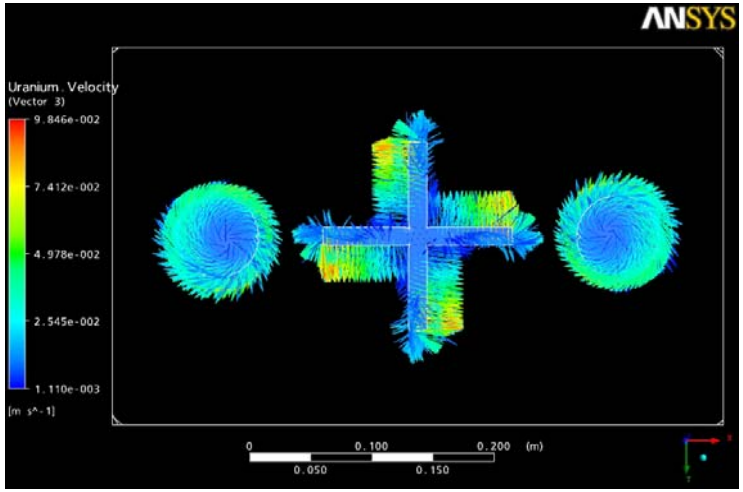

a) U velocity vector profile - bottom

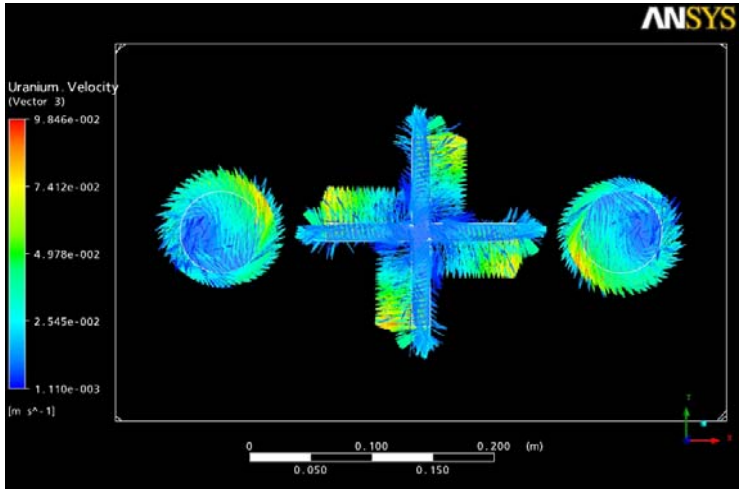

b) U velocity vector profile - top

Figure 5.22 – U velocity for final stirrer design at 60 rpm stirrer rotational velocity

The calculated diffusion layer thicknesses for final design of electrorefiner at different locations along cathode height are given in Tables 5.10 and 5.11 for left and right cathode.

Table 5.10 – Diffusion layer thickens for left cathode – molten salt interface

Location on left cathode [cm]	**Diffusion layer thickness [mm]**
3.8	0.0362
5.0	0.0241
5.5	0.0254
6.0	0.0278
6.5	0.0323
13.5	0.0268
14.2	0.0188
16.2	0.0148
16.5	0.0185
16.8	0.0187
17.0	0.0148
17.1	0.0132
18.9	0.0113
19.0	0.0117
19.5	0.0131
20.0	0.0141
20.5	0.0277
22.7	0.0681
Average diffusion layer thickness	**0.0232**

Table 5.11 – Diffusion layer thickens for right cathode – molten salt interface

Location on right cathode [cm]	**Diffusion layer thickness [mm]**
3.4	0.0655
5.0	0.0189
5.5	0.0194
6.5	0.0235
12.7	0.0411
14.5	0.0170
14.7	0.0145
15.0	0.0152
15.2	0.0156
15.4	0.0159
15.6	0.0156
15.8	0.0154
16.0	0.0164
17.5	0.0163
19.0	0.0118
19.5	0.0190
20.4	0.0134
22.5	0.0497
Average diffusion layer thickness	**0.0225**

A representative illustration of the uranium concentration profile at left and right cathode surface is provided in Figure 5.23.

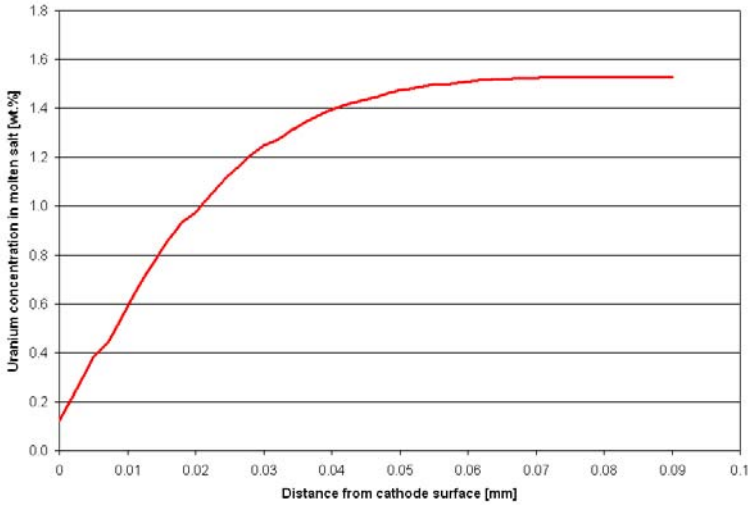

a) Left cathode

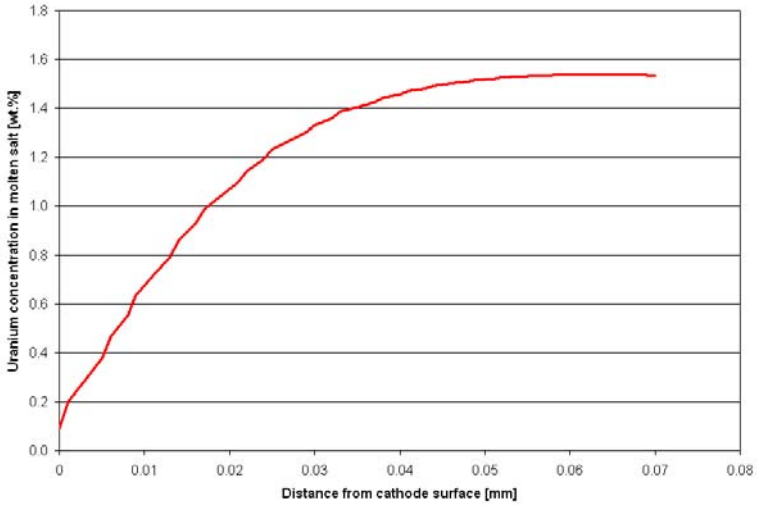

a) Right cathode

Figure 5.23 – U concentration profile at left and right cathode surfaces

The final rotational model employed in ANSYS CFX to determine the diffusion layer thickness is summarized in Table 5.12. The positive sign indicates a clockwise rotational velocity.

Table 5. 12 – Final rotational model for stirrer and cathodes

Rotational velocity [rpm]		
Right Cathode	**Stirrer**	**Left Cathode**
20	-60	20

The final diffusion layer thickness is calculated as the average of the right and left cathode diffusion layer thickness. This outcome is summarized in Table 5.13 and is used as input for electrochemical simulation performed with REFIN code.

Table 5.13 – Final diffusion layer thickness for electrorefiner

Average diffusion layer thickness for left cathode [cm]	**Average diffusion layer thickness for right cathode [cm]**	**Final diffusion layer thickness [cm]**
$2.32 \cdot 10^{-3}$	$2.25 \cdot 10^{-3}$	$2.28 \cdot 10^{-3}$

5.4 Final Electrochemical Results

The diffusion layer thickness for cathode – molten salt interface determined with ANSYS CFX is used as input data for run 13 from design of experiment. The value of molten salt – solid electrode diffusion layer thickness in Table 4.3 is updated to $2.28 \cdot 10^{-3}$ cm and the rest of the values for diffusion layer thickness are unchanged. The input files for both extraction stages are provided in Appendix B. The changes in mass inventory and the element cathode potential variation for first and second stage of extraction are illustrated in Figures 5.24 to 5.27.

As presented in Figure 5.24 only uranium is collected at solid cathode (violet line), mainly from the anode (blue line). By controlling the cathode potential we can obtain a pure uranium deposit at solid cathode in the first stage of operation.

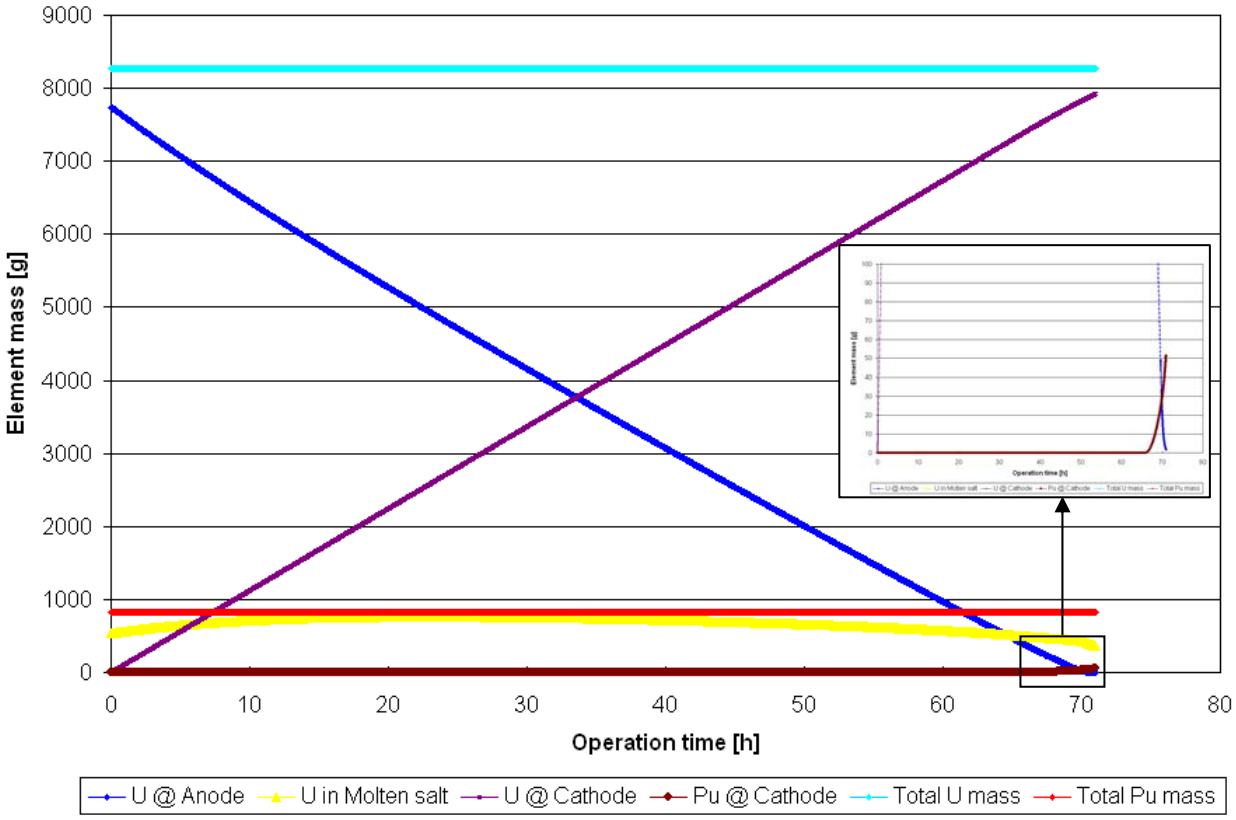

Figure 5.24 – Change in element mass per cell per stage for uranium extraction stage – optimum case

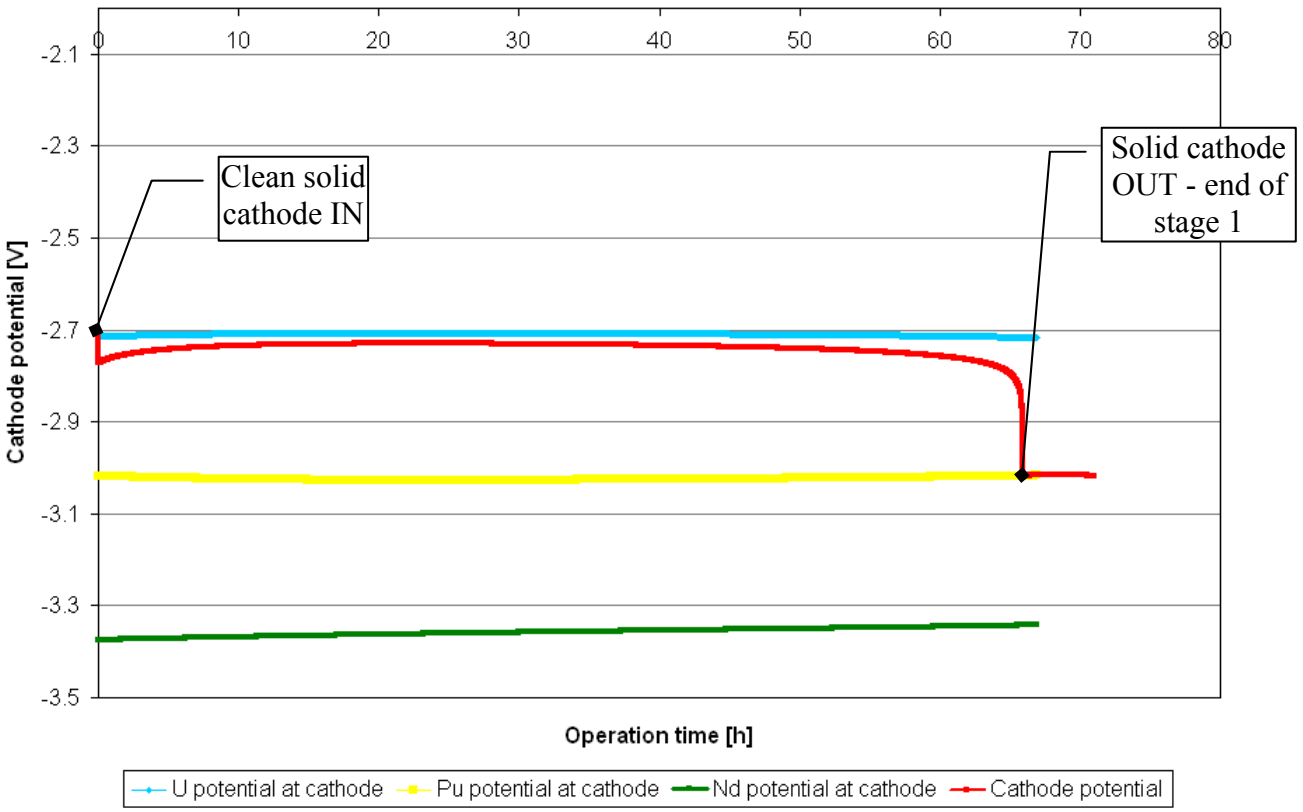

Figure 5.25 – Element cathode potential variation per cell per stage for uranium extraction stage – optimum case

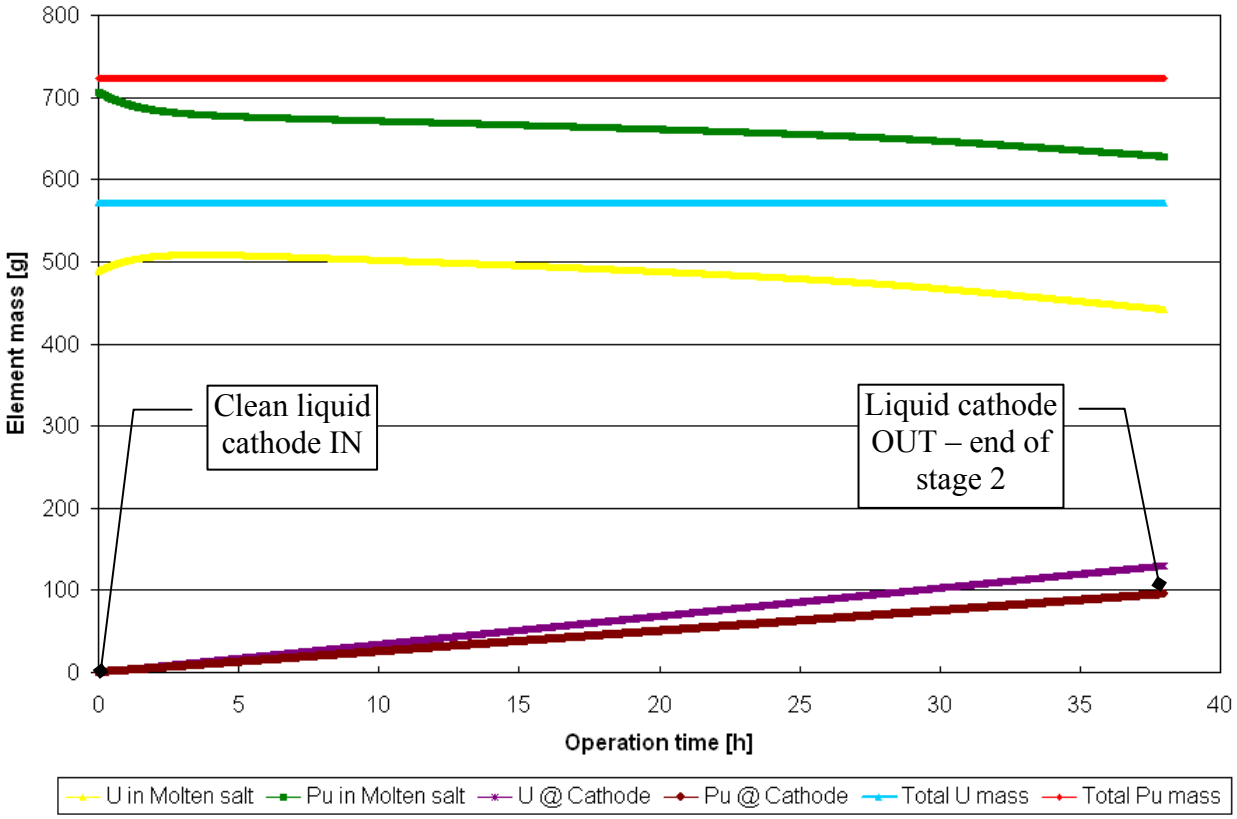

Figure 5.26 – Change in element mass per cell per stage for uranium and plutonium extraction stage – optimum case

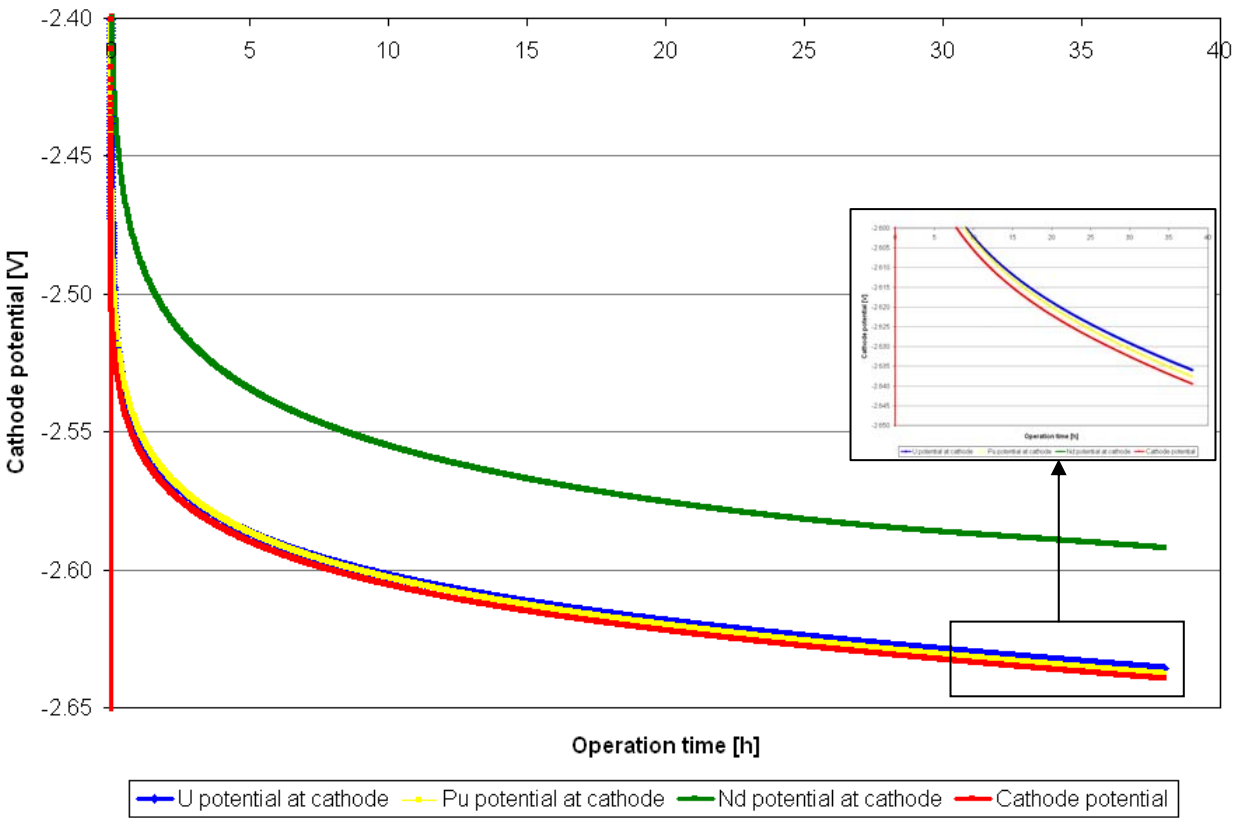

Figure 5.27 – Element cathode potential variation per cell per stage for uranium and plutonium extraction stage – optimum case

After several hours of operation the amount of uranium in electrorefiner is not sufficient to self maintain the electric current level and thus the cathode surface potential decreases sharply, as seen in Figure 5.25, to the equilibrium potential of plutonium. This is the end of the first stage where only a uranium deposition is desired. During the second stage of operation a liquid cathode is employed and a mixture of uranium, plutonium and other actinides are collected. This is clearly illustrated in Figure 5.27 where the surface cathode potential (red line) is below the cathode potential of uranium, plutonium and neodymium. Consequently, they are extracted together at liquid cathode during the second stage. This represents a major advantage for this technology compared to other aqueous processes.

A mass of 7316.88 g of pure uranium is deposited on each solid mandrel cathode during operation of first stage which requires 65.9 hours. No plutonium is recovered in the first stage. A mixture of 129.87 g of uranium and 95.19 g of plutonium is collected at the liquid cadmium cathode in the second stage of the electrorefiner. The operation of second stage takes 38.0 hours. Final results of mass inventory per cathode (per stage) are summarized in Table 5.14. The mass of uranium deposited at solid cathode in the first stage, presented in Table 5.14, does not include the amount of uranium assumed to fall from the solid mandrel (about 1 %) into the liquid cadmium pool during operation of first stage. This is recovered in the second stage when liquid cadmium cathode is employed. Also, the small amount of plutonium that remains in the cadmium pool during first stage of operation is recovered during the second stage.

Table 5.14 – Material balance per cathode and operation time for optimum case

Material IN	
Initial U mass at anode [g]	7742.03
Initial Pu mass at anode [g]	133.05
Initial U mass in molten salt [g]	536.28
Initial Pu mass in molten salt [g]	697.54
Material OUT (per stage)	
First stage final U mass at solid cathode [g]	7316.88
First stage final Pu mass at solid cathode [g]	0.0
Second stage final U mass at liquid cathode [g]	129.87
Second stage final Pu mass at liquid cathode [g]	95.19
Operation time (per stage)	
First stage operation time per cathode [h]	65.9
Second stage operation time per cathode [h]	38.0

Recirculation of the molten salt can be employed as there is still enough useful material (UCl_3 and $PuCl_3$) in the electrolyte at the end of the second stage. To lower the heat generated in the electrorefiner, the concentrations of alkali, alkali earths and rare earth fission products must be reduced at some point.

For the first stage a total of 10 anode baskets have been considered (10 REFIN cells), 5 anodes on each side of the first stage channel. For the second stage a number of 6 cells are considered, 3 on each side of the second stage channel. The length of the first stage is about 160 cm and the length of the second stage is 120 cm.

A graphical representation of this arrangement was given in Figure 3.2. Two clean solid cathodes and respectively two clean liquid cadmium cathodes enter the system every 13.18 hours ($\frac{65.9}{5}$ hours). Similarly, two solid cathodes and two liquid cathodes with deposit are extracted from the electrorefiner every 13.18 hours.

An annual capacity factor of 80 % was assumed for the electrorefiner and based on this the total yearly throughput was determined. The total throughput of the system is directly proportional to the considered capacity factor.

Total number of operation hours per year for an assumed annual capacity factor of 80% for the electrorefiner is given by:

$$T_{operation} = 365\frac{days}{year} \cdot 24\frac{hours}{day} \cdot 0.80 = 7008\frac{hours}{year}$$

The total number of solid mandrel cathodes employed per year in first stage is obtained as follows. At the beginning of the first stage operation, five cathode assemblies, each consisting of two solid mandrels (as seen in Figure 3.3), are placed into the molten salt.

During the first 65.9 hours, cathode assembly number 1 (Figure 3.2) operates for $\frac{65.9}{5} \cdot 1$ hours, cathode assembly number 2 operates for $\frac{65.9}{5} \cdot 2$ hours, cathode assembly number 3 operates for $\frac{65.9}{5} \cdot 3$ hours, cathode assembly number 4 operates for $\frac{65.9}{5} \cdot 4$ hours and cathode assembly number 5 operates for $\frac{65.9}{5} \cdot 5$ hours.

After first 65.9 operation hours, a cathode assembly (two cathode mandrels) is extracted every 13.18 hours from first stage of electrorefiner. Total number of solid cathode mandrels extracted per year from the first stage is given by:

$$N_{\text{Stage 1}}^{\text{Solid cathodes}} = 2 \cdot \left(\frac{5}{5} + \frac{4}{5} + \frac{3}{5} + \frac{2}{5} + \frac{1}{5} \right) + 2 \cdot \left(\frac{7008 - 65.9}{13.18} \right) = 2 \cdot 3 + 2 \cdot 526 = 1058 \text{ solid cathodes}$$

First term represents the number of solid cathode mandrels that operate during the first 65.9 hours of operation and the second term represents the number of solid cathode mandrels operating for the rest of 6942.1 hours per year.

The first two liquid cadmium cathodes are extracted from the second stage after (65.9+38.0) hours. Two liquid cathodes are removed from this stage every 13.18 hours, given a total number of liquid cadmium cathodes per year of:

$$N_{\text{Stage 2}}^{\text{Liquid cathodes}} = 2 \cdot \left(\frac{7008 - 65.9 - 38.0}{13.18} \right) = 2 \cdot 523 = 1046 \text{ liquid cathodes}$$

Final results for continuous electrorefiner performance are summarized in Table 5.15.

Table 5.15 – Continuous electrorefiner performance

First stage operation time per cathode [h]	65.9
Second stage operation time per cathode [h]	38.0
U recovery efficiency (stage 1) [%]	88.4
Total U+Pu recovery efficiency (stage 1 and 2) [%]	83.0
Annual capacity factor (assumed) [%]	80.0
Total operation time per year [h]	7008
Total number of solid cathodes extracted from stage 1 per year	1058
Total pure U output (from stage 1) [kg/year]	7741.2
Total number of liquid cathodes extracted from stage 2 per year	1046
Total U+Pu output (from stage 2) [kg/year]	235.4

5.5 Results Overview

The sensitivity study performed using REFIN code pointed out a feasible combination of initial element concentrations at anode and molten salt for continuous electrochemical processing. This is characterized by a higher concentration of uranium than plutonium at anode and a lower concentration of uranium than plutonium in molten salt.

Further refinement of this initial concentration combination through a design of experiment study yielded 9.31 wt.% U and 0.16 wt.% Pu for anode and 1.43 wt.% U and 1.86 wt.% Pu for molten salt as the best final combination which strikes an optimum balance between recovery efficiency and operation time.

CFD simulations using ANSYS CFX has given an average diffusion layer thickness at cathode – molten salt interface of $2.28 \cdot 10^{-3}$ cm for a clockwise stirrer rotational velocity of 60 rpm and a counterclockwise cathode rotational velocity of 20 rpm.

Electrochemical simulations using the final concentration combination and diffusion layer thickness have shown that an overall recovery efficiency of 83 % is achieved for the continuous operation concept. Assuming an electrorefiner annual capacity factor of 80 %, the total pure uranium output for first stage is 7741.2 kg/year and the mass of plutonium and uranium mixture extracted at the liquid cathode in the second stage is 235.4 kg/year. Every cell in the first stage operates at 37.9 A electric current and each cell in second stage operates at 2 A electric current.

A complete pass of a solid cathode through the first stage requires 65.9 hours while 38.0 hours are necessary for a liquid cathode to go through the second stage. The continuous electrorefiner operation necessitates that two clean cathodes are introduced in each stage every 13.18 hours and, consequently, two loaded cathodes are removed from each stage every 13.18 hours.

Chapter 6 Conclusions and Future Work Recommendations

6.1 Conclusions

The investigation of continuous electrochemical processing concept using computer based simulations has shown potential for development of an improved reprocessing technology for spent nuclear fuel. Larger throughput and reduction in mass balance uncertainties are important characteristics that offer advantages over current electrochemical processing technology. A particular concept feature consists of simultaneous operation of solid and liquid cathodes in distinct extraction stages. Additionally, no pure plutonium separation occurs providing an important advantage over conventional aqueous processing.

The research work found that the electrochemical transport strongly depends on the applied electric current and diffusion layer thickness and it is influenced by the initial concentration of elements at the anode and in the molten salt. The factors which have the most influence on the electric current are anode potential, salt resistance, distance between electrodes and area of electrodes. A higher electric current is needed to deposit more mass of metal at cathode per hour.

This can be achieved by increasing the anode potential (limited by the increase in electrochemical dissolution at anode of undesirable elements), decreasing the salt resistance, keeping a minimum distance between electrodes and increasing the area of electrodes. A strong forced convection is also necessary to provide a minimum diffusion layer thickness for the electrochemical processing.

A functional combination of initial element concentrations at the anode and in the molten salt suitable for continuous operation was identified as a result of an ample screening study over a wide range of values for the involved parameters. This is given by an initial concentration of uranium higher than plutonium at anode and a lower initial uranium concentration than plutonium in molten salt.

Further refinement of study results using design of experiment technique for computers provided a set of initial process conditions which increases the recovery efficiency and decreases the operation time, thus, maximizing the total system throughput. From this study it has been observed that the electrorefiner operation time is minimized for higher electric current values while the recovery efficiency reaches its maximum for lower values of the electric current.

Diffusion layer thickness and element concentration distribution in molten salt have been determined using three dimensional CFD simulations. Several stirrer designs, values and directions of the stirrer and cathode rotational velocity have been analyzed to attain a minimum diffusion layer thickness at the cathode – molten salt interface.

Beside this, the study focused on achieving a uniform uranium velocity at cathode surface. Both left and right cathodes have been modeled using three dimensional CFD simulations. This modeling approach provided a valuable insight on mixing and flow phenomena associated with the electrorefiner cell operation. Employment of three dimensional CFD simulation provides significant benefits in terms of reducing the design evaluation time and associated costs.

6.2 Future Work Recommendations

The work presented in this thesis created the opportunity for a broad range of research subjects to be further investigated which will result in a complete image of the spent nuclear fuel continuous electrochemical processing.

Among those worthy to be mentioned are improving REFIN code to allow simulation of solid anode and also defining more elements of interest in the code, experimental studies to verify the conceptual design, investigations of developing scale-up designs and assessment of process safeguardability.

Adding the capability to model a solid anode and thus having a complete code able to simulate several electrochemical processes (anodic dissolution, direct transport and deposition) would be an important improvement of REFIN code. Moreover, introducing additional elements (neptunium and others) to be considered in the electrochemical transport would also be of further research interest.

By scaling-up the design, more material can be fed into the system and also the electrode surface area and the electric current can be increased. Thus, a larger throughput of the system can be achieved.

Also, a large tray where liquid cadmium is flowing can be used to collect uranium and plutonium mixture in the second stage instead of separate cylindrical vessels in order to increase the liquid cathode surface area for the uranium and plutonium extraction stage.

Continuous increase of uranium deposit on solid cathode as a result of electrochemical process may influence the diffusion layer thickness. Consequently, further CFD simulations using increased cathode radial dimensions may be used to evaluate this phenomenon.

REFERENCES

[1] Rodriguez, C., and Baxter, A. (2000). "Transmutation of Nuclear Waste Using Gas-Cooled Reactor Technologies," *Proc. 8th. International Conference on Nuclear Engineering*, Baltimore, MD.

[2] Benedict, M., Pigford, T.H., and Levi, H.W. (1981). "Nuclear Chemical Engineering," McGraw-Hill Book Company, 2nd Edition.

[3] Laidler, J.J., Battles, J.E., Miller, W.E., Ackerman, J.P., and Carls, E.L. (1997). "Development of Pyroprocessing Technology," *Progress in Nuclear Energy*, Vol. 31, No. ½, pp. 131-140.

[4] Schurhammer, R., and Wipff, G. (2005). "Effect of the TBP and Water on the Complexation of Uranyl Nitrate and the Dissolution of Nitric Acid into Supercritical CO_2. A Theoretical Study," *Journal of Physical Chemistry*, Vol. 109, pp. 5208-5216.

[5] Nagarajan, K., Subramanian, T., Prabhakara Reddy, B., Vasudeva Rao, P.R., and Raj, B. (2008). "Current Status of Pyrochemical Reprocessing Research in India," *Nuclear Technology*, Vol. 162, pp. 259-263.

[6] Yamana, H. (2003). "Pyrochemical Reprocessing Developments in Japan – Overview and Some Topics," *Proc. of INSAC-2003*, India.

[7] Herceg, et al. (2006). "Continuous Process Electrorefiner," U.S. Patent No. 7,097,747 B1.

[8] Aryaeinejad, R., Cole, J.D., Drigert, M.W., Vaden D.E. (2006). "Safeguards and Non-proliferation Issues as Related to Advanced Fuel Cycle and Advanced Fast Reactor Development with Processing of Reactor Fuel," *2006 IEEE Nuclear Science Symposium Conference*, N14-189, pp. 529-534.

[9] Park, B.G. (1999). "A Time-Dependent Simulation of Molten Salt Electrolysis for Nuclear Waste Transmutation," Ph.D. dissertation, Seoul National University, Korea.

[10] Nawada, H.P., Bhat, N.P. (1995). "Thermochemical Modeling of Electrorefining Process for Reprocessing Spent Metallic Fuel," *Journal of NUCLEAR SCIENCE and TECHNOLOGY*, 32 [11], pp. 1127-1137.

[11] Tomczuk, Z. et al. (1992). "Uranium Transport to Solid Electrodes in Pyrochemical Reprocessing of Nuclear Fuel," *J. Electrochem. Soc.*, Vol. 139, No. 12, pp. 3523-3528.

[12] Simpson M. (2008). "Electrochemical Spent Fuel Processing Short Course," INL, U.S.A.

[13] Koyama T., Iizuka M., Shoji Y., Fujita R., Tanaka H., Kobayashi T., and Tokiwai M. (1997). "An Experimental Study of Molten Salt Electrorefining of Uranium Using Solid Iron Cathode and Liquid Cadmium Cathode for Development of Pyrometallurgical Reprocessing," *Journal of Nuclear Science and Technology*, Vol. 34, No. 4, pp. 384-393.

[14] Li, S.X. (2008). "Experimental Observations on the Roles of the Cadmium Pool in Mark-IV Electrorefiner," *Nuclear Technology*, Vol. 162, pp. 144-152.

[15] Ackerman, J.P. (1991). "Chemical Basis for Pyrochemical Reprocessing of Nuclear Fuel," *Ind. Eng. Chem.*, Vol. 30, pp. 141-145.

[16] Newman, J., and Thomas-Alyea, K.E. (2004). "Electrochemical Systems," JOHN WILEY & SONS, 3rd Edition, New Jersey, U.S.A.

[17] Compendium of Chemical Terminology (1997). 2nd Edition.

[18] Bockris J.O'M., Reddy A.K. (1973). "Modern Electrochemistry: An Introduction to an Interdisciplinary Area," Springer, Vol. 2, 1st Edition.

[19] Hamann C.H., Hamnett A., Vielstich W. (2007). "Electrochemistry," Wiley-VCH, 2nd Edition.

[20] Santner T.J., Williams, B.J., and Notz, W.I. (2003). "The Design and Analysis of Computer Experiments," Springer, 1st Edition.

[21] Fang, K.T., Li, R., Sudjianto, A. (2005). "Design and Modeling for Computer Experiments," Chapman & Hall/ CRC, 1st Edition.

[22] SAS Institute (2007). "Design of Experiments Guide," JMP Design of Experiment, Release 7.

[23] ANSYS Inc. (2006). "ANSYS CFX-Solver Theory Guide", ANSYS CFX Release 11.0.

[24] Ahluwalia, R., Hua, T.Q., and Geyer, H.K. (1999). "Behavior of Uranium and Zirconium in Direct Transport Tests with Irradiated ERB-II Fuel," *Nuclear Technology*, Vol. 126, pp. 289-302.

[25] Bae, J., Yi, K.W., Park, B.G., Hwang, I.S., and Lee, H.W. (2005). ”Development of an Electrochemical-Hydrodynamic Model for Electrorefining Process,” *Proc. of GLOBAL 2005*, Paper No. 302, Japan.

[26] Korzekwa, D., and Dunn, P. (1994). “A Combined Experimental and Modeling Approach to Uranium Casting,” *Symposium on Liquid Metal Processing and Casting*. Santa Fe, NM.

APPENDICES

APPENDIX A. Design of Experiment Detailed Results

The detailed results for Latin Hypercube design with 30 runs are presented in the following tables. Table A.1 shows the results for the uranium extraction stage. Table A.2 presents the electrochemical results for the second stage of operation. In Table A.3 the recovery efficiencies and operation time are detailed for both stages.

Table A.1 – Design of experiment results-uranium extraction stage

	Run	Operation time [h]	U mass at anode [g]	Pu mass at anode [g]	U mass in molten salt [g]	Pu mass in molten salt [g]	U mass at cathode [g]	Pu mass at cathode [g]
Input	1	59.47	7791.93	357.58	461.3	716.3	0.0	0.0
Output			1611.02	315.07	420.5	742.1	6138.8	0.0
Input	2	58.79	7683.83	174.63	472.5	645.0	0.0	0.0
Output			910.7	165.98	463.4	637.0	6699.4	0.0
Input	3	65.25	8033.1	415.8	517.5	570.0	0.0	0.0
Output			1619.3	298.87	402.3	670.3	6446.3	0.0
Input	4	106.96	7725.4	266.1	540.0	686.3	0.0	0.0
Output			52.3	36.04	298.0	899.5	7833.1	0.0
Input	5	65.31	7633.9	349.26	457.5	573.8	0.0	0.0
Output			1474.6	274.39	383.8	632.0	6150.3	0.0
Input	6	102.66	8016.46	232.84	555.0	626.3	0.0	0.0
Output			23.53	12.96	322.6	829.3	8143.4	0.0
Input	7	80.91	7567.4	182.94	521.3	652.5	0.0	0.0
Output			113.76	46.87	377.7	771.8	7514.9	0.0

Table A.1 (continued)

	Run	Operation time [h]	U mass at anode [g]	Pu mass at anode [g]	U mass in molten salt [g]	Pu mass in molten salt [g]	U mass at cathode [g]	Pu mass at cathode [g]
Input	8	58.26	7924.98	207.89	483.8	723.8	0.0	0.0
Output			1034.8	199.83	475.6	715.2	6815.6	0.0
Input	9	98.04	7999.82	149.6	513.8	731.3	0.0	0.0
Output			10.7	0.02	348.3	864.0	8072.7	0.0
Input	10	106.05	7891.7	116.4	495.0	622.5	0.0	0.0
Output			12.7	0.11	362.8	721.9	7929.2	0.0
Input	11	67.99	8066.35	332.63	498.8	678.8	0.0	0.0
Output			1140.85	248.67	414.5	746.0	6927.1	0.0
Input	12	60.36	7584.03	274.4	532.5	581.3	0.0	0.0
Output			987.4	186.54	445.0	652.4	6601.3	0.0
Input	13	68.26	7742.03	133.053	536.3	697.5	0.0	0.0
Output			162.46	53.42	451.2	706.4	7582.2	0.0
Input	14	73.95	7708.7	365.9	558.8	660.0	0.0	0.0
Output			705.7	198.97	390.0	810.0	7089.3	0.0

Table A.1 (continued)

	Run	Operation time [h]	U mass at anode [g]	Pu mass at anode [g]	U mass in molten salt [g]	Pu mass in molten salt [g]	U mass at cathode [g]	Pu mass at cathode [g]
Input	15	96.26	7808.56	324.3	480.0	738.8	0.0	0.0
Output			407.19	167.27	316.4	879.0	7482.7	0.0
Input	16	74.79	7758.6	291.05	525.0	750.0	0.0	0.0
Output			516.6	165.54	396.2	858.8	7285.5	0.0
Input	17	78.09	7600.6	382.5	491.3	671.3	0.0	0.0
Output			882.6	246.36	353.3	790.7	6773.4	0.0
Input	18	73.10	7966.56	241.16	562.5	712.5	0.0	0.0
Output			342.03	109.57	426.7	827.3	7678.0	0.0
Input	19	48.60	7858.45	407.47	528.8	641.3	0.0	0.0
Output			2234	343.63	469.5	688.4	5600.7	0.0
Input	20	81.66	8049.7	257.8	450.0	607.5	0.0	0.0
Output			715.9	176.76	365.5	671.8	7335.8	0.0
Input	21	91.10	7775.3	83.158	551.3	667.5	0.0	0.0
Output			14.9	0.03	453.8	733.8	7775.8	0.0

Table A.1 (continued)

	Run	Operation time [h]	U mass at anode [g]	Pu mass at anode [g]	U mass in molten salt [g]	Pu mass in molten salt [g]	U mass at cathode [g]	Pu mass at cathode [g]
Input	22	49.99	7875.1	316	468.8	588.8	0.0	0.0
Output			2196.3	300.57	457.3	587.5	5607.3	0.0
Input	23	71.37	7908.4	199.6	547.5	600.0	0.0	0.0
Output			336.8	88.97	432.8	693.9	7603.7	0.0
Input	24	76.01	7667.2	108.1	510.0	562.5	0.0	0.0
Output			48.78	14.79	408.3	639.0	7637.7	0.0
Input	25	71.16	7983.2	91.47	476.3	596.3	0.0	0.0
Output			247.66	59.54	438.9	611.5	7690.3	0.0
Input	26	83.8	7841.8	141.37	453.8	690.0	0.0	0.0
Output			182.07	66.77	371.7	747.9	7659.5	0.0
Input	27	90.04	7949.9	390.8	543.8	705.0	0.0	0.0
Output			524.95	192.81	341.1	886.3	7545.4	0.0
Input	28	94.84	7617.3	166.3	487.5	742.5	0.0	0.0
Output			30.83	19.31	328.7	872.7	7663.1	0.0

Table A.1 (continued)

	Run	Operation time [h]	U mass at anode [g]	Pu mass at anode [g]	U mass in molten salt [g]	Pu mass in molten salt [g]	U mass at cathode [g]	Pu mass at cathode [g]
Input	29	83.08	7825.2	299.3	502.5	615.0	0.0	0.0
Output			548.4	160.27	359.4	737.4	7337.5	0.0
Input	30	98.94	7650.5	224.5	465.0	633.8	0.0	0.0
Output			182.24	78.67	310.2	762.8	7540.9	0.0

Table A.2 – Design of experiment results-uranium and plutonium extraction stage

	Run	Operation time [h]	U mass at anode [g]	Pu mass at anode [g]	U mass in molten salt [g]	Pu mass in molten salt [g]	U mass at cathode [g]	Pu mass at cathode [g]
Input	1	38.00	83.158	16.63	420.5	742.1	0.0	0.0
Output			0.04	0.04	376.3	646.9	122.0	102.5
Input	2	39.61	83.158	16.63	463.4	637.0	0.0	0.0
Output			0.002	0.002	402.0	551.5	138.6	95.3
Input	3	38.01	83.158	16.63	402.3	670.3	0.0	0.0
Output			0.038	0.036	356.9	580.5	124.6	100.0
Input	4	37.97	83.158	16.63	298.0	899.5	0.0	0.0
Output			0.031	0.05	278.6	776.8	98.1	126.3
Input	5	38.06	83.158	16.63	383.8	632.0	0.0	0.0
Output			0.035	0.032	338.9	544.4	125.2	99.6
Input	6	38.22	83.158	16.63	322.6	829.3	0.0	0.0
Output			0.026	0.036	295.8	715.3	105.7	120.1
Input	7	38.07	83.158	16.63	377.7	771.8	0.0	0.0
Output			0.035	0.039	340.4	669.4	115.6	109.3

Table A.2 (continued)

	Run	Operation time [h]	U mass at anode [g]	Pu mass at anode [g]	U mass in molten salt [g]	Pu mass in molten salt [g]	U mass at cathode [g]	Pu mass at cathode [g]
Input	8	38.13	83.158	16.63	475.6	715.2	0.0	0.0
Output			0.04	0.035	422.1	626.2	129.7	95.6
Input	9	38.13	83.158	16.63	348.3	864.0	0.0	0.0
Output			0.031	0.041	319.1	749.5	107.0	118.2
Input	10	37.99	83.158	16.63	362.8	721.9	0.0	0.0
Output			0.036	0.039	325.6	623.2	116.5	107.9
Input	11	38.50	83.158	16.63	414.5	746.0	0.0	0.0
Output			0.023	0.023	369.6	648.4	122.7	104.8
Input	12	38.07	83.158	16.63	445.0	652.4	0.0	0.0
Output			0.04	0.033	392.8	567.9	130.57	94.3
Input	13	37.99	83.158	16.63	451.2	706.4	0.0	0.0
Output			0.044	0.042	403.2	662.8	124.3	100.2
Input	14	39.10	83.158	16.63	390.0	810.0	0.0	0.0
Output			0.008	0.009	349.6	702.0	117.9	113.1

Table A.2 (continued)

	Run	Operation time [h]	U mass at anode [g]	Pu mass at anode [g]	U mass in molten salt [g]	Pu mass in molten salt [g]	U mass at cathode [g]	Pu mass at cathode [g]
Input	15	39.52	83.158	16.63	316.4	879.0	0.0	0.0
Output			0.002	0.003	289.2	755.5	105.8	127.8
Input	16	37.82	83.158	16.63	396.2	858.8	0.0	0.0
Output			0.047	0.056	360.5	750.0	112.2	111.3
Input	17	38.22	83.158	16.63	353.3	790.7	0.0	0.0
Output			0.028	0.034	320.1	683.8	112.0	113.9
Input	18	39.76	83.158	16.63	426.7	827.3	0.0	0.0
Output			0.001	0.001	379.6	718.8	123.2	111.7
Input	19	37.98	83.158	16.63	469.5	688.4	0.0	0.0
Output			0.046	0.038	416.3	602.4	130.4	94.1
Input	20	38.17	83.158	16.63	365.5	671.8	0.0	0.0
Output			0.03	0.03	324.9	578.1	120.6	104.9
Input	21	38.33	83.158	16.63	453.8	733.8	0.0	0.0
Output			0.03	0.028	403.4	641.2	127.0	99.3

Table A.2 (continued)

	Run	Operation time [h]	U mass at anode [g]	Pu mass at anode [g]	U mass in molten salt [g]	Pu mass in molten salt [g]	U mass at cathode [g]	Pu mass at cathode [g]
Input	22	38.30	83.158	16.63	457.3	587.5	0.0	0.0
Output			0.03	0.02	396.3	509.9	136.8	89.4
Input	23	38.12	83.158	16.63	432.8	693.9	0.0	0.0
Output			0.037	0.034	384.2	604.0	126.7	98.5
Input	24	38.00	83.158	16.63	408.3	639.0	0.0	0.0
Output			0.04	0.035	360.5	553.0	127.3	97.1
Input	25	37.97	83.158	16.63	438.9	611.5	0.0	0.0
Output			0.04	0.035	385.7	530.9	132.4	91.8
Input	26	38.03	83.158	16.63	371.7	747.9	0.0	0.0
Output			0.036	0.04	334.3	647.5	116.1	108.5
Input	27	39.73	83.158	16.63	341.1	886.3	0.0	0.0
Output			0.001	0.001	309.5	763.9	109.4	125.4
Input	28	38.00	83.158	16.63	328.7	872.7	0.0	0.0
Output			0.033	0.048	303.2	755.7	103.7	120.8

Table A.2 (continued)

	Run	Operation time [h]	U mass at anode [g]	Pu mass at anode [g]	U mass in molten salt [g]	Pu mass in molten salt [g]	U mass at cathode [g]	Pu mass at cathode [g]
Input	29	38.36	83.158	16.63	359.4	737.4	0.0	0.0
Output			0.024	0.027	322.5	635.9	116.2	110.4
Input	30	37.90	83.158	16.63	310.2	762.8	0.0	0.0
Output			0.034	0.045	283.3	655.0	106.9	117.1

Table A.3 – Design of experiment results-recovery efficiencies and operation time

Run	U recovery efficiency for stage 1 [%]	Operation time for stage 1 [h]	U recovery efficiency for stage 1 + 2 [%]	Total U+Pu recovery efficiency for stage 1 + 2 [%]	Total operation time [h]
1	74.4	59.5	75.9	68.2	97.5
2	82.1	58.8	83.8	77.2	98.4
3	75.4	65.3	76.8	70.0	103.3
4	94.8	107.0	96.0	87.4	144.9
5	76.0	65.3	77.6	70.7	103.4
6	95.0	102.7	96.2	88.7	140.9
7	92.9	80.9	94.3	86.7	119.0
8	81.1	58.3	82.6	75.4	96.4
9	94.8	98.04	96.1	88.3	136.2
10	94.5	106.05	95.9	89.3	144.0

Table A.3 (continued)

Run	U recovery efficiency for stage 1 [%]	Operation time for stage 1 [h]	U recovery efficiency for stage 1 + 2 [%]	Total U+Pu recovery efficiency for stage 1 + 2 [%]	Total operation time [h]
11	80.9	67.99	82.3	74.7	106.5
12	81.3	60.36	82.9	81.0	98.4
13	91.6	68.26	93.1	85.7	106.3
14	85.7	73.95	87.2	78.8	113.1
15	90.3	96.26	91.6	82.5	135.8
16	88.0	74.79	89.3	80.5	112.6
17	83.7	78.09	85.1	76.5	116.3
18	90.0	73.1	91.5	83.4	112.9
19	66.8	48.6	68.3	61.7	86.6
20	86.3	81.66	87.7	80.7	119.8

Table A.3 (continued)

Run	U recovery efficiency for stage 1 [%]	Operation time for stage 1 [h]	U recovery efficiency for stage 1 + 2 [%]	Total U+Pu recovery efficiency for stage 1 + 2 [%]	Total operation time [h]
21	93.4	91.1	94.9	88.2	129.4
22	67.2	49.99	68.8	63.1	88.3
23	89.9	71.37	91.4	84.6	109.5
24	93.4	76.01	95.0	88.9	114.0
25	90.9	71.16	92.5	86.5	109.1
26	92.3	83.8	93.7	86.4	121.8
27	88.8	90.04	90.1	81.1	129.8
28	94.6	94.84	95.8	87.5	132.8
29	88.1	83.08	89.5	81.8	121.4
30	92.9	98.94	94.2	86.5	136.8

APPENDIX B. REFIN Input files for optimum case

The REFIN input files of the optimum case resulted from the design of experiment study and ANSYS CFX analysis for first and second stage are presented herein.

REFIN Input file for uranium extraction stage:

```
Stage 1 - Continuous electorefining, uranium extraction: RB - 02.11.2009
&input1 nelemt=7, temp=773.d0,
 ename = 'Ur', 'Pu', 'Nd', 'Cd', 'Li', 'Ka', 'Cl',
 stde  = 2.394d0, 2.706d0, 2.944d0, 1.403d0, 3.578d0, 3.760d0, 0.d0,
 diffu1= 1.5d-5, 1.5d-5,  1.5d-5, 1.5d-5, 1.5d-5, 1.5d-5, 1.5d-5,
 diffu2= 6.8634d-6, 1.0829d-5, 1.2075d-5, 2.23d-5, 2.5d-5, 2.5d-5, 2.5d-5,
 curr0 = 0.5d0, 0.6d0, 0.5d0, 0.40d-9, 1.d-10,  1.d-10, 1.d-16,
 zi    = 3.0d0, 3.0d0, 3.0d0, 2.00d0, 1.0d0, 1.0d0, -1.0d0,
 tca   = 0.5d0, 0.5d0, 0.5d0, 0.50d0, 0.5d0, 0.5d0,  0.5d0,
 tcc   = 0.5d0, 0.5d0, 0.5d0, 0.13d0, 0.5d0, 0.5d0,  0.5d0,
 catp=-2.7d0,
 anop=-2.7d0,
 ipset=1,
 tset=  150.0d0,
 cmaxt= 37.93d0,
```

```
  aberr=1.d-15,
&
&input2
  del1=2.0d-3,
  del2=2.0d-2,
  del3=2.28d-3,
  del4=1.0d-4,
  dy=1.0d-4,
  area=961.0d0,484.0d0,
  vol =10661.3d0, 24179.5d0, 1.0d0,
&
&INPUT3
  ISTATE=1,
  ITASK=5,
  TADD=1.D-3,
  epslon=5.d-3,
  iopt=1,
  mxstep=1000,
  h0=1.d-5,
  jt=5,
  ml=13,
```

```
 mu=13,
 hmax=100.0d0,
 itol=1,
 rtoli=1.d-10,
 atoli=1.d-10,
 iprint=2,
&
&input4
 Can= 9.31d-2, 0.16d-2, 0.1d-2, 90.43d-2, 0.0d-15,  0.0d-15,  2.0d-12,
 Cms= 1.43d-2, 1.86d-2, 0.01d-2,  0.0d-16, 6.6d-2, 29.6d-2, 60.5d-2,
 Cca= 0.0d-1, 0.0d-15, 0.0d-15,  0.0d-15, 0.0d-15,  0.0d-15,  0.0d-15,
&
&input5
 mass=83158.2, 37502.4, 100.0,
 gatom=238.03,  240.0, 144.24, 112.41, 6.939, 39.1, 35.453,
&
```

REFIN input file for uranium and plutonium extraction stage:

```
Stage 2 - Continuous electorefining, uranium and plutonium extraction: RB - 02.11.2009
&input1 nelemt=7, temp=773.d0,
  ename = 'Ur', 'Pu', 'Nd', 'Cd', 'Li', 'Ka', 'Cl',
  stde  = 2.394d0, 2.706d0, 2.944d0, 1.403d0, 3.578d0, 3.760d0, 0.d0,
  diffu1= 1.5d-5, 1.5d-5,  1.5d-5, 1.5d-5, 1.5d-5, 1.5d-5, 1.5d-5,
  diffu2= 6.8634d-6, 1.0829d-5, 1.2075d-5, 2.23d-5, 2.5d-5, 2.5d-5, 2.5d-5,
  curr0 = 0.5d0, 0.6d0, 0.5d0, 0.40d-9, 1.d-10,  1.d-10, 1.d-16,
  zi    = 3.0d0, 3.0d0, 3.0d0, 2.00d0, 1.0d0, 1.0d0, -1.0d0,
  tca   = 0.5d0, 0.5d0, 0.5d0, 0.50d0, 0.5d0, 0.5d0,  0.5d0,
  tcc   = 0.5d0, 0.5d0, 0.5d0, 0.13d0, 0.5d0, 0.5d0,  0.5d0,
  catp=-2.7d0,
  anop=-2.7d0,
  ipset=1,
  tset=  100.0d0,
  cmaxt= 2.0d0,
  aberr=1.d-15,
&
&input2
  del1=2.0d-3,
```

```
 del2=2.0d-2,
 del3=2.0d-2,
 del4=2.0d-3,
 dy=1.0d-4,
 area=2000.0d0,1000.0d0,
 vol =10661.3d0, 24179.5d0, 2000.0d0,
&
&INPUT3
 ISTATE=1,
 ITASK=5,
 TADD=1.D-3,
 epslon=5.d-3,
 iopt=1,
 mxstep=1000,
 h0=1.d-5,
 jt=5,
 ml=13,
 mu=13,
 hmax=100.0d0,
 itol=1,
 rtoli=1.d-10,
```

```
 atoli=1.d-10,
 iprint=2,
&
&input4
 Can= 0.1d-2, 0.02d-2, 0.1d-2, 99.78d-2, 0.0d-15,  0.0d-15,  2.0d-12,
 Cms= 1.303d-2, 1.884d-2, 0.0414d-2,  8.45d-17, 6.502d-2, 29.16d-2, 61.108d-2,
 Cca= 0.0d-1, 0.0d-15, 0.0d-15,  1.0d-0, 0.0d-15,  0.0d-15,  0.0d-15,
&
&input5
 mass=83158.2, 37502.4, 15600.0,
 gatom=238.03,  240.0, 144.24, 112.41, 6.939, 39.1, 35.453,
&
```